Dominik Lang, BSc

A Study of Boundary Element Methods for Electrostatic Transmission Problems

MASTER'S THESIS

to achieve the university degree of

Master of Science

Master's degree programme: Mathematics

submitted to

Graz University of Technology

Supervisor

Assoc.Prof. Dipl.-Math. Dr.rer.nat. G. Of

Institute of Applied Mathematics

Graz, August 2019

Acknowledgements

To begin with, I would like to thank my supervisor Assoc.Prof. Dipl.-Math. Dr.rer.nat. Günther Of at the Technical University of Graz for his level of expertise in my area of research and his constructive support throughout the production of this master's thesis.

I would also like to express my deepest gratitude to my parents Helga Hagen and Anton Lang for providing me their unconditional support during my years of studying.

In addition, I would like to acknowledge all my friends and family members for their cheerful company in the last years and especially for their help and occasional distraction during the development of this thesis.

I am deeply thankful to my colleagues at the Nerox GmbH for their encouragement and the enduring of my repeated absences due to the work on my master's thesis.

Finally, I wish to thank Anna Stiftinger for her moral support and the wonderful days we spent in the time of writing this thesis.

Contents

Introduction

In many applications in engineering and industry the computation of a solution to Maxwell's equations for dielectric materials is necessary to understand occurring electromagnetic fields. Only in special cases analytic solutions are available, which motivates the research of numerical methods in this field. If the dependency on the time is neglected Maxwell's equations decouple and provide a system of equations for solving the magnetostatic and electrostatic field problems independently. The electrostatic transmission problem is discussed in [16]. Popular choices for solving partial differential equations numerically are the finite element method, see, e.g., [3, 6, 8, 36], and the boundary element method see, e.g., [5, 12, 32, 34]. In the finite element method the domain is decomposed into finite elements, which requires a discretization of the whole domain and special techniques for the exterior domain in transmission problems. This thesis focuses on the boundary element method, which has already been used for the numerical solution of transmission problems in, e.g., [1, 2, 15, 18]. With the boundary element method a partial differential equation on the domain is transformed to a boundary integral equation. This transformation reduces the dimension of the problem to the spatial dimension of the boundary. The reduction of the problem's spatial dimension yields system matrices with lower dimensions compared to the finite element method, since only the boundary has to be discretized. Another advantage of the boundary element method is the natural handling of unbounded exteriors of bounded domains in transmission problems. On the other hand the matrices obtained by the boundary element method are, unlike the matrices occurring in the finite element method, no longer sparse. Also the knowledge of an analytic fundamental solution for the problem is required, which restricts the class of problems where the boundary element method is applicable. Therefore both have their individual advantages and disadvantages depending on the type of partial differential equation.

The physical background of this thesis is mainly influenced by works on plasmon resonances of metallic nanoparticles, see, e.g., [7, 13, 37]. The foundations for this master's thesis were laid in the previous work [19], which was part of the project in Technomathematics at the Institute of Applied Mathematics at the University of Technology in Graz. The main ideas for the analytical background of the boundary element methods are given in [1, 2, 20, 34].

In this work we will derive the electrostatic transmission problem from Maxwell's equations by using a scalar potential ansatz. With the help of several boundary integral operators, such as the single layer potential and the double layer potential

operator, we will obtain three boundary integral equations for solving the electrostatic transmission problem. Furthermore we will obtain discrete versions of the variational formulations of this boundary integral equations by using the Galerkin method. The resulting linear systems will be used to solve the transmission problem numerically, where we use the fast multipole method, see, e.g., [11, 27], to increase the performance. The different formulations will be compared with respect to errors and computational times and several efforts will be made to increase the performance.

The thesis is structured as follows: In the first chapter we will state Maxwell's equations and we will reduce them to a decoupled system of electrostatics and magnetostatics by making some assumptions on the domain and the physical nature of the problem. For computations of the electric field we will see that we have to solve an electrostatic transmission problem with the Laplace equation.

In the second chapter we will derive three boundary integral equations by using suitable boundary integral operators following [1, 2, 20]: the single layer and double layer potential formulations and the Steklov–Poincaré interface equation. We will also investigate unique solvability and equivalence of these equations on the continuous level.

In the third chapter we will use the boundary element method to state discrete versions of the boundary integral formulations, we will provide an error analysis of the Steklov–Poincaré operator formulation and we will prove unique solvability of this discrete problem.

The fourth chapter is dedicated to the numerical investigation of the boundary element methods, where bounded domains with constant permittivities in the interior and the exterior are placed in an electric excitation. Two examples will be considered: a unit sphere and a microscopic cube with a given side length. Since we know an analytical solution of the transmission problem for the sphere it is suitable to test if the numerical methods yield the orders of convergence, which we would expect theoretically by the results we will have obtained in the third chapter. The cube on the other hand has a geometry, which is numerically more challenging and therefore more appropriate for testing how the methods would perform in real world applications. The electric field and other physical quantities, like the electric dipole moment, will be computed by several derived formulations and these methods will be compared with respect to computational time and accuracy.

After the first computation with the beforehand derived formulations several adaptions will be made to improve numerical performance in the last chapter. These adaptions include variations in the discretization, by using the collocation method, see, e.g., [31], or choosing graded meshes, which are characterized through a stronger refinement and therefore smaller boundary elements closer to singularities like edges and corners, see, e.g., [17, 29, 30]. We will also test alternative ansatz functions, which use Dirac like point sources. Finally we will find an alternative computation of the dipole moment for the double layer formulation.

1 Electrostatic Transmission Problem

In this chapter we will state Maxwell's equations, from which we will derive a decoupled system of two equations in the static case. For this purpose we will use scalar and vector potentials and a suitable gauge condition. The decoupled system allows us to compute the magnetic field and the electric field independently from each other. In this work we only consider electrostatics.

1.1 Maxwell's Equations

Let us now consider macroscopic Maxwell's equations in frequency space and Gaussian units with the free charge density ρ and the electric current density $\mathbf{j}$, see, e.g., [7, 16]:

$$\begin{aligned} \nabla \cdot \mathbf{B} &= 0, && \text{(Gauss's Law)} \\ \nabla \cdot \mathbf{D} &= 4\pi\rho, && \text{(Coulomb's Law)} \\ \nabla \times \mathbf{H} + ik\mathbf{D} &= \frac{4\pi}{c}\mathbf{j}, && \text{(Ampère's Circuital Law)} \\ \nabla \times \mathbf{E} - ik\mathbf{B} &= 0, && \text{(Faraday's Induction Law)} \end{aligned}$$

where c is the speed of light, ω is the frequency, $k = \frac{\omega}{c}$ is the wavenumber, $\mathbf{D} = \varepsilon\mathbf{E}$ is the dielectric displacement, $\mathbf{B} = \mu\mathbf{H}$ is the magnetic flux density, $\mathbf{E}$ is the electric field, and $\mathbf{H}$ is the magnetic field.

With Gauss's Law and Faraday's Induction Law we can conclude the existence of a vector potential $\mathbf{A}$ and a scalar potential Φ, see, e.g., [37, p. 40], with

$$\mathbf{B} = \nabla \times \mathbf{A}, \tag{1.1}$$

$$\mathbf{E} = -\nabla\Phi + ik\mathbf{A}. \tag{1.2}$$

Because of the invariance under divergence or gradient, respectively, we can choose $\mathbf{A}$ and Φ in such a way that they fulfill the Lorenz condition [21]

$$\nabla \cdot \mathbf{A} - ik\Phi = 0. \tag{1.3}$$

If we restrict our considerations to the microscopic form of Maxwell's equations, the Lorenz condition (1.3) in combination with Coulomb's Law and Ampère's Circuital

Law leads to two decoupled wave equations for $\mathbf{A}$ and Φ:

$$-\Delta\Phi - k^2\Phi = 4\pi\rho, \tag{1.4a}$$

$$-\Delta\mathbf{A} - k^2\mathbf{A} = \frac{4\pi}{c}\mathbf{j}. \tag{1.4b}$$

In this thesis we will only consider the solution to (1.4a) in the limit of small particles (compared to the wavelength $\lambda = \frac{1}{k}$). In this case we can put $k \approx 0$ and neglect all retardation effects [37, p. 42].
Therefore (1.4) simplifies to the decoupled system

$$-\Delta\Phi = 4\pi\rho, \qquad \text{(Poisson equation)}$$

$$-\Delta\mathbf{A} = \frac{4\pi}{c}\mathbf{j}.$$

We are interested in the computation of $\mathbf{E}$, which is why we have to solve only the Poisson equation. If there are no external charges present the Poisson equation reduces to the Laplace equation

$$-\Delta\Phi = 0. \qquad \text{(Laplace equation)}$$

1.2 Transmission Problem

Let $\Omega \subset \mathbb{R}^3$ be some bounded Lipschitz domain with $\varepsilon(x) = \varepsilon_1$ for $x \in \Omega$ and $\varepsilon(x) = \varepsilon_0$ for $x \in \Omega^{\text{ext}}$ with $\Omega^{\text{ext}} := \mathbb{R}^3 \setminus \overline{\Omega}$. We denote the boundary of the domain by $\Gamma := \partial\Omega$. We further request $0 < \varepsilon_0 < \varepsilon_1$.

For the solution of the Poisson equation we consider $\Phi = \Phi_{\text{hom}} + \Phi_{\text{part}}$, where Φ_{part} is a given solution to the Poisson equation.

Thus it remains to find Φ_{hom} as a solution of the Laplace equation with appropriate transmission conditions. We require $\Phi\big|_{\Omega}$ and $\Phi\big|_{\Omega^{\text{ext}}}$ to fulfill the transmission conditions given in [37]:

$$\Phi\big|_{\Omega}(x) = \Phi\big|_{\Omega^{\text{ext}}}(x) \quad \text{for } x \in \Gamma,$$

and

$$\varepsilon_1 \left(\frac{\partial}{\partial n}\Phi\big|_{\Omega}(x)\right) = \varepsilon_0 \left(\frac{\partial}{\partial n}\Phi\big|_{\Omega^{\text{ext}}}(x)\right) \quad \text{for } x \in \Gamma,$$

as well as the radiation condition for $\Phi\big|_{\Omega^{\text{ext}}}$

$$\Phi\big|_{\Omega^{\text{ext}}}(x) = \mathcal{O}\left(\frac{1}{|x|}\right) \quad \text{as } |x| \to \infty.$$

We define $\Phi_1 := \Phi_{\text{hom}}\big|_{\Omega}$ and $\Phi_0 := \Phi_{\text{hom}}\big|_{\Omega^{\text{ext}}}$ and obtain the transmission boundary value problem

$$-\Delta\Phi_1(x) = 0 \qquad \text{for } x \in \Omega, \tag{1.5a}$$

$$-\Delta\Phi_0(x) = 0 \qquad \text{for } x \in \Omega^{\text{ext}}, \tag{1.5b}$$

$$\Phi_1(x) = \Phi_0(x) \qquad \text{for } x \in \Gamma, \tag{1.5c}$$

$$\varepsilon_1 \left(\frac{\partial}{\partial n} \Phi_1(x) \right) - \varepsilon_0 \left(\frac{\partial}{\partial n} \Phi_0(x) \right) = (\varepsilon_0 - \varepsilon_1) \frac{\partial}{\partial n} \Phi_{\text{part}}(x) \qquad \text{for } x \in \Gamma, \tag{1.5d}$$

$$\Phi_0(x) = \mathcal{O}\left(\frac{1}{|x|} \right) \qquad \text{as } |x| \to \infty. \tag{1.5e}$$

This transmission problem differs to the one given in [1, 2] by the right hand side in (1.5d). In the following chapters we will discuss several approaches for the solution of this transmission problem.

2 Boundary Integral Equations

In this chapter we will consider three approaches to find a weak solution of the transmission problem (1.5), using different boundary integral formulations. Afterwards we will show that all three approaches yield equivalent solutions and that they are uniquely solvable on the continuous level.

For easier notation we will write Φ instead of Φ_{hom} in this chapter. Most of the representations and formulas are given in [1]. The herein used notations are similar to the notations in [34].

2.1 Single Layer Potential Formulation

At first we will consider an indirect single layer formulation. Let $w \in H^{-\frac{1}{2}}(\Gamma)$ be an unknown charge, we define the single layer potential as

$$\widetilde{V}w(x) := \int_\Gamma U^*(x,y)w(y)\,ds_y \quad \text{for } x \in \Omega \cup \Omega^{\text{ext}}, \tag{2.1}$$

with the fundamental solution for the Laplace equation $U^*(x,y) := \dfrac{1}{4\pi|x-y|}$.

If we choose $\Phi := \widetilde{V}w$ then continuity on the surface (1.5c) and the radiation condition (1.5e) are satisfied. By [34, p. 118] it also holds that Φ is a weak solution of the Laplace equation in $\Omega \cup \Omega^{\text{ext}}$ and therefore a weak solution of the Laplace equations (1.5a) and (1.5b). It remains to satisfy the Neumann transmission (1.5d). By [34, pp. 119-124] there holds for $w \in H^{-\frac{1}{2}}(\Gamma)$

$$\begin{aligned}\gamma_1^{\text{int}}\Phi_1 &= (\sigma I + K')\,w\\ \gamma_1^{\text{ext}}\Phi_0 &= ([\sigma-1]I + K')\,w\end{aligned}$$

in the sense of $H^{-\frac{1}{2}}(\Gamma)$, where

$$\begin{aligned}(K'w)(x) &:= \lim_{\delta\to 0} \int_{y\in\Gamma:\ |y-x|\geq\delta} \gamma_{1,x}^{\text{int}} U^*(x,y)w(y)\,ds_y && \text{for } x \in \Gamma,\\ \sigma(x) &:= \lim_{\delta\to 0} \frac{1}{4\pi\delta^2} \int_{y\in\Omega:\ |y-x|=\delta} ds_y && \text{for } x \in \Gamma,\end{aligned}$$

and $\gamma_0^{\text{int}}, \gamma_0^{\text{ext}}, \gamma_1^{\text{int}}, \gamma_1^{\text{ext}}$ are the interior and exterior trace operators and conormal derivatives. From (1.5d) and the fact that $\sigma(x) = \frac{1}{2}$ for almost every (f.a.e.) $x \in \Gamma$ we conclude that

$$\left(\frac{1}{2}\frac{\varepsilon_1 + \varepsilon_0}{\varepsilon_1 - \varepsilon_0} I + K'\right) w = -\gamma_1^{\text{int}} \Phi_{\text{part}} \quad \text{on } \Gamma. \tag{2.2}$$

This is the boundary integral equation for which we wish to find a unique solution later in this chapter.

2.2 Steklov–Poincaré Operator Formulation

The next boundary integral formulation, which we will derive, is the Steklov–Poincaré operator formulation. The interior and exterior representation formulas will be used to obtain this formulation.

2.2.1 Interior Steklov–Poincaré Operator

A solution of the interior Laplace equation in (1.5a) is given by the representation formula, see, e.g., [34, p. 96],

$$\Phi_1(x) = \left(\widetilde{V}\gamma_1^{\text{int}}\Phi_1\right)(x) - (W\gamma_0^{\text{int}}\Phi_1)(x) \quad \text{for } x \in \Omega, \tag{2.3}$$

where for $v \in H^{\frac{1}{2}}(\Gamma)$

$$(Wv)(x) := \int_\Gamma \gamma_{1,y}^{\text{int}} U^*(x,y) v(y)\, ds_y \quad \text{for } x \in \Omega \cup \Omega^{\text{ext}}$$

is the double layer potential. For the limit $x \to \Gamma$ in (2.3) we obtain by [34, pp. 125-127]

$$\gamma_0^{\text{int}}\Phi_1 = \left(V\gamma_1^{\text{int}}\Phi_1\right) - ([-1+\sigma]I + K)\gamma_0^{\text{int}}\Phi_1$$

where $V := \gamma_0^{\text{int}}\widetilde{V}$ and

$$(Kv)(x) := \lim_{\delta \to 0} \int_{y \in \Gamma:\ |y-x| \geq \delta} U^*(x,y) v(y)\, ds_y \quad \text{for } x \in \Gamma.$$

Rewriting this yields the following boundary integral equation

$$\left(V\gamma_1^{\text{int}}\Phi_1\right) = \left(\frac{1}{2}I + K\right)\gamma_0^{\text{int}}\Phi_1. \tag{2.4}$$

By [4] all operators are bounded. If we use the fact that the single layer potential V is invertible [34, p. 139] we obtain the interior Steklov–Poincaré operator S_1 and the interior Dirichlet to Neumann map

$$\gamma_1^{\text{int}}\Phi_1 = V^{-1}\left(\frac{1}{2}I + K\right)\gamma_0^{\text{int}}\Phi_1 =: (S_1\gamma_0^{\text{int}}\Phi_1). \tag{2.5}$$

2.2.2 Exterior Steklov–Poincaré Operator

Similarly to the interior representation formula (2.3) we can write the solution to the exterior Laplace equation as

$$\Phi_0(x) = -\left(\widetilde{V}\gamma_1^{\text{ext}}\Phi_0\right)(x) + (W\gamma_0^{\text{ext}}\Phi_0)(x) \quad \text{for } x \in \Omega^{\text{ext}}, \tag{2.6}$$

and conclude for $v \in H^{\frac{1}{2}}(\Gamma)$

$$\left(V\gamma_1^{\text{ext}}\Phi_0\right) = \left(-\frac{1}{2}I + K\right)\gamma_0^{\text{ext}}\Phi_0, \tag{2.7}$$

which leads to the exterior Steklov–Poincaré operator S_0 and the exterior Dirichlet to Neumann map

$$\gamma_1^{\text{ext}}\Phi_0 = -V^{-1}\left(\frac{1}{2}I - K\right)\gamma_0^{\text{ext}}\Phi_0 =: -(S_0\gamma_0^{\text{ext}}\Phi_0). \tag{2.8}$$

2.2.3 Steklov–Poincaré Boundary Integral Equation

By using the Dirichlet to Neumann maps (2.5) and (2.8) and the Dirichlet transmission condition $\gamma_0^{\text{ext}}\Phi_0(x) = \gamma_0^{\text{int}}\Phi_1(x) = \Phi(x)$ for $x \in \Gamma$ we can rewrite the Neumann transmission condition (1.5d) to

$$\varepsilon_1(S_1\Phi)(x) + \varepsilon_0(S_0\Phi)(x) = (\varepsilon_0 - \varepsilon_1)\gamma_1^{\text{int}}\Phi_{\text{part}}(x) \quad \text{for } x \in \Gamma. \tag{2.9}$$

By applying the Dirichlet to Neumann maps (2.5) and (2.8) once more, and using the representation formulas (2.3) and (2.6) we can compute Φ on Ω.

2.3 Double Layer Potential Formulation

For the double layer potential we would like to find a formulation that is derived analogously to the single layer potential formulation. For this purpose we reformulate the transmission problem (1.5) similar to [1]. We define ψ such that

$$\begin{aligned} -\Delta\psi(x) &= 0 && \text{for } x \in \Omega, \\ \gamma_1^{\text{int}}\psi(x) &= -\gamma_1^{\text{int}}\Phi_{\text{part}}(x) =: g(x) && \text{for } x \in \Gamma, \end{aligned} \tag{2.10}$$

where the solvability condition

$$\int_\Gamma g(x)ds_x = 0 \tag{2.11}$$

has to be fulfilled. ψ can be obtained by using the first boundary integral equation

$$\left(\frac{1}{2}I + K\right)\psi = Vg. \tag{2.12}$$

The solution ψ to the variational formulation of the Neumann boundary value problem (2.10) is only unique up to an additive constant, see, e.g., [34, p. 67], which is why we use a modified variational problem with the scaling condition

$$\int_\Gamma \psi(x) ds_x = 0.$$

We denote by

$$H_{**}^{\frac{1}{2}}(\Gamma) := \left\{ v \in H^{\frac{1}{2}}(\Gamma) : \langle v, 1\rangle_\Gamma = 0 \right\}$$

the space of $H^{\frac{1}{2}}(\Gamma)$-functions which satisfy this condition. We also define

$$H_{*}^{\frac{1}{2}}(\Gamma) := \left\{ v \in H^{\frac{1}{2}}(\Gamma) : \langle v, w_{\text{eq}}\rangle_\Gamma = 0 \right\},$$

where $w_{\text{eq}} = V^{-1}1 \in H^{-\frac{1}{2}}(\Gamma)$ is the natural density given in [34, p. 142]. Since the single layer potential $V^{-1} : H^{\frac{1}{2}}(\Gamma) \to H^{-\frac{1}{2}}(\Gamma)$ is bounded and $H^{-\frac{1}{2}}(\Gamma)$-elliptic ([34, p. 178]), we can define

$$\langle w, v\rangle_{V^{-1}} := \langle V^{-1}w, v\rangle_\Gamma \quad \text{for all } w, v \in H^{\frac{1}{2}}(\Gamma)$$

to be an inner product in $H^{\frac{1}{2}}(\Gamma)$. The variational formulation then is to find $\psi \in H_{*}^{\frac{1}{2}}(\Gamma)$ such that

$$\left\langle \left(\frac{1}{2}I + K\right)\psi, v \right\rangle_{V^{-1}} = \langle Vg, v\rangle_{V^{-1}} \quad \text{for all } v \in H_{*}^{\frac{1}{2}}(\Gamma), \tag{2.13}$$

which is, since $V : H_{*}^{-\frac{1}{2}}(\Gamma) \to H_{*}^{\frac{1}{2}}(\Gamma)$ is isomorphic ([34, p. 144]), equivalent to finding $\psi \in H_{*}^{\frac{1}{2}}(\Gamma)$ such that

$$\left\langle \left(\frac{1}{2}I + K\right)\psi, w \right\rangle_\Gamma = \langle Vg, w\rangle_\Gamma \quad \text{for all } w \in H_{*}^{-\frac{1}{2}}(\Gamma), \tag{2.14}$$

where

$$H_{*}^{-\frac{1}{2}}(\Gamma) := \left\{ w \in H^{-\frac{1}{2}}(\Gamma) : \langle w, 1\rangle_\Gamma = 0 \right\}.$$

Since (2.13) is uniquely solvable ([34, p. 178]) (2.14) is also uniquely solvable. We consider the modified variational formulation to find $\psi^* \in H^{\frac{1}{2}}_{**}(\Gamma)$ such that

$$\left\langle \left(\frac{1}{2}I + K\right)\psi^*, w \right\rangle_\Gamma = \langle Vg, w\rangle_\Gamma \quad \text{for all } w \in H_*^{-\frac{1}{2}}(\Gamma). \tag{2.15}$$

Since the solvability condition (2.11) is satisfied, there holds that $Vg \in H^{\frac{1}{2}}_*(\Gamma)$. The map $\left(\frac{1}{2}I + K\right) : H^{\frac{1}{2}}_{**}(\Gamma) \to H^{\frac{1}{2}}_*(\Gamma)$ is surjective, since for the solution $\psi \in H^{\frac{1}{2}}_*(\Gamma)$ of (2.14) there holds that $\psi^* = \psi + \beta 1 \in H^{\frac{1}{2}}_{**}(\Gamma)$, with $\beta = -\frac{\langle \psi, 1\rangle_\Gamma}{|\Gamma|}$, is a solution of (2.15). It is also injective since

$$(1 - \tilde{c}_K)\|u^*\|_{V^{-1}} \leq \| \left(\frac{1}{2}I + K\right) u^* \|_{V^{-1}} \quad \text{for all } u^* \in H^{\frac{1}{2}}_{**}(\Gamma),$$

with

$$\tilde{c}_K = \frac{1}{2} + \sqrt{\frac{1}{4} - c_1^V \tilde{c}_1^D},$$

where c_1^V and $\tilde{c}_1^D$ are the ellipticity constants of the single layer boundary integral operator V and of the hypersingular boundary integral operator $D := -\gamma_1^{\text{int}} W$, respectively. This can be shown analogous to [34, p. 149, Thm. 6.26]. Therefore the modified variational formulation (2.15) again defines a unique solution of (2.10).

Next we provide a formulation which defines another solution of the Neumann problem (2.10) but is easier to solve numerically than (2.15).

Lemma 2.1. *The problem* (2.15) *is equivalent to the problem of finding* $\widetilde{\psi} \in H^{\frac{1}{2}}(\Gamma)$ *such that*

$$\left\langle \left(\frac{1}{2}I + K\right)\widetilde{\psi}, w \right\rangle_\Gamma + \langle \widetilde{\psi}, 1\rangle_\Gamma \langle w, 1\rangle_\Gamma = \langle Vg, w\rangle_\Gamma \quad \textit{for all } w \in H^{-\frac{1}{2}}(\Gamma), \tag{2.16}$$

with

$$(\widetilde{\psi} + \alpha 1) = \psi^* \in H^{\frac{1}{2}}_{**}(\Gamma),$$

where $\alpha = \frac{\gamma}{|\Gamma|^2}$, $\gamma = -\langle Vg, 1\rangle_\Gamma + \langle (\frac{1}{2}I + K)\psi^*, 1\rangle_\Gamma = -\langle Vg, 1\rangle_\Gamma + \langle (\frac{1}{2}I + K)\widetilde{\psi}, 1\rangle_\Gamma$.

Proof. First we observe that $\left(\frac{1}{2}I + K\right)\widetilde{\psi} = \left(\frac{1}{2}I + K\right)\psi^*$, since $\left(\frac{1}{2}I + K\right)1 = 0$.

Let $\psi^* \in H^{\frac{1}{2}}_{**}(\Gamma)$ be a solution of (2.15) and let $w \in H^{-\frac{1}{2}}(\Gamma)$ be arbitrary. Then $w = w^* + \beta 1$ with $w^* \in H_*^{-\frac{1}{2}}(\Gamma)$ and $\beta = \frac{1}{|\Gamma|}\langle w, 1\rangle$. Therefore it is sufficient to show

(2.16) for $w \in H_*^{-\frac{1}{2}}(\Gamma)$ and for $w = 1$. For $w \in H_*^{-\frac{1}{2}}(\Gamma)$ there holds $\langle w, 1\rangle_\Gamma = 0$ and therefore (2.16). For $w = 1$ we have for $\psi^* \in H_{**}^{\frac{1}{2}}(\Gamma)$ that

$$\begin{aligned} 0 = |\Gamma|\langle \psi^*, 1\rangle_\Gamma &= \langle 1, 1\rangle_\Gamma \langle \widetilde{\psi}, 1\rangle_\Gamma + \alpha \langle 1, 1\rangle_\Gamma \langle 1, 1\rangle_\Gamma \\ &= \langle 1, 1\rangle_\Gamma \langle \widetilde{\psi}, 1\rangle_\Gamma + \gamma \\ &= \langle 1, 1\rangle_\Gamma \langle \widetilde{\psi}, 1\rangle_\Gamma - \langle Vg, 1\rangle_\Gamma + \left\langle \left(\frac{1}{2} I + K\right) \widetilde{\psi}, 1 \right\rangle_\Gamma, \end{aligned}$$

which is equivalent to (2.16) for $w = 1$. In total we have shown (2.16) for $w \in H^{-\frac{1}{2}}(\Gamma)$.

Now let $\widetilde{\psi} \in H^{\frac{1}{2}}(\Gamma)$ be a solution of (2.16). Let $w \in H_*^{-\frac{1}{2}}(\Gamma)$, then $\langle w, 1\rangle_\Gamma = 0$ and we conclude from (2.16)

$$\langle Vg, w\rangle_\Gamma = \left\langle \left(\frac{1}{2} I + K\right) \widetilde{\psi}, w \right\rangle_\Gamma = \left\langle \left(\frac{1}{2} I + K\right) \psi^*, w \right\rangle_\Gamma.$$

It remains to show that $\psi^* \in H_{**}^{\frac{1}{2}}(\Gamma)$. For this purpose we insert $w = 1$ in (2.16) and obtain

$$\begin{aligned} 0 &= |\Gamma|\langle \widetilde{\psi}, 1\rangle_\Gamma + \left\langle \left(\frac{1}{2} I + K\right) \widetilde{\psi}, 1 \right\rangle_\Gamma - \langle Vg, 1\rangle_\Gamma \\ &= |\Gamma|\langle \widetilde{\psi}, 1\rangle_\Gamma + \gamma \\ &= |\Gamma| \left\langle \widetilde{\psi} + \frac{\gamma}{|\Gamma|^2} 1, 1 \right\rangle_\Gamma = |\Gamma|\langle \psi^*, 1\rangle_\Gamma. \end{aligned}$$

□

Since $\psi^* = (\widetilde{\psi} + \alpha 1)$, it is also a solution to the Neumann problem (2.10). Our next step is to consider the ansatz

$$\begin{aligned} \Phi_1(x) &:= \frac{1}{\varepsilon_1} \left(\widetilde{\Phi}_1(x) + (\varepsilon_1 - \varepsilon_0) \widetilde{\psi}(x) \right) && \text{for } x \in \Omega, \\ \Phi_0(x) &:= \frac{1}{\varepsilon_0} \widetilde{\Phi}_0(x) && \text{for } x \in \Omega^{\text{ext}}, \end{aligned} \tag{2.17}$$

where

$$-\Delta \widetilde{\Phi}_1(x) = 0 \qquad \text{for } x \in \Omega, \tag{2.18}$$

$$-\Delta \widetilde{\Phi}_0(x) = 0 \qquad \text{for } x \in \Omega^{\text{ext}}, \tag{2.19}$$

and therefore $\widetilde{\Phi}_1$ and $\widetilde{\Phi}_0$ satisfy the Laplace equations (1.5a) and (1.5b).
For the radiation condition (1.5e) we obtain

$$\widetilde{\Phi}_0(x) = \mathcal{O}\left(\frac{1}{|x|}\right) \quad \text{as } |x| \to \infty. \tag{2.20}$$

From the Neumann transmission condition (1.5d) we conclude for $x \in \Gamma$

$$\begin{aligned}\varepsilon_1 \gamma_1^{\text{int}} \Phi_1(x) - \varepsilon_0 \gamma_1^{\text{ext}} \Phi_0(x) &= \gamma_1^{\text{int}} \widetilde{\Phi}_1(x) + (\varepsilon_1 - \varepsilon_0) \gamma_1^{\text{int}} \widetilde{\psi}(x) - \gamma_1^{\text{ext}} \widetilde{\Phi}_0(x) \\ &= \gamma_1^{\text{int}} \widetilde{\Phi}_1(x) - \gamma_1^{\text{ext}} \widetilde{\Phi}_0(x) - (\varepsilon_1 - \varepsilon_0) \gamma_1^{\text{int}} \Phi_{\text{part}}(x).\end{aligned}$$

Hence we require for the new transmission problem the Neumann transmission condition

$$\gamma_1^{\text{int}} \widetilde{\Phi}_1 = \gamma_1^{\text{ext}} \widetilde{\Phi}_0. \tag{2.21}$$

For (1.5c) we have

$$\varepsilon_0 \widetilde{\Phi}_1 - \varepsilon_1 \widetilde{\Phi}_0 = (\varepsilon_0 - \varepsilon_1) \varepsilon_0 \widetilde{\psi}. \tag{2.22}$$

Altogether we have now obtained a new transmission problem (2.18)–(2.22). For this problem we proceed in the same way as for the single layer potential, but now we use the double layer ansatz for an unknown charge $v \in H^{\frac{1}{2}}(\Gamma)$:

$$\widetilde{\Phi}(x) := -(Wv)(x) \quad \text{for } x \in \Omega \cup \Omega^{\text{ext}}, \tag{2.23}$$

and use the restrictions $\widetilde{\Phi}_1 = \widetilde{\Phi}\big|_{\Omega}$ and $\widetilde{\Phi}_0 = \widetilde{\Phi}\big|_{\Omega^{\text{ext}}}$, which satisfy the Laplace equations (2.18), (2.19), the radiation condition (2.20), and the Neumann transmission condition (2.21). An application of the interior and exterior trace operators gives

$$\begin{aligned}\gamma_0^{\text{int}} \widetilde{\Phi}_1 &= -\left((\sigma - 1)I + K\right) v, \\ \gamma_0^{\text{ext}} \widetilde{\Phi}_0 &= -\left(\sigma I + K\right) v,\end{aligned}$$

in the sense of $H^{\frac{1}{2}}(\Gamma)$.

From the jump condition (2.22) we conclude the boundary integral equation , see, e.g., [1],

$$\left(\frac{1}{2}\frac{\varepsilon_1 + \varepsilon_0}{\varepsilon_1 - \varepsilon_0} I + K\right) v(x) = -\varepsilon_0 \widetilde{\psi}(x) \quad \text{on } \Gamma. \tag{2.24}$$

2.4 Equivalence of Formulations and Unique Solvability

In this section we will prove that all three formulations are equivalent and also uniquely solvable on the continuous level. The theorems and proofs are analogous to the proofs in [1].

Theorem 2.2 ([1, pp. 121–122])**.** *Let $w \in H^{-\frac{1}{2}}(\Gamma)$ be a solution of the single layer integral operator equation* (2.2)*, let $\Phi \in H^{\frac{1}{2}}(\Gamma)$ be a solution of the Steklov–Poincaré operator equation* (2.9)*, and let $v \in H^{\frac{1}{2}}(\Gamma)$ be a solution of the double layer integral operator equation* (2.24)*. Then there hold the following relations:*

$$\Phi(x) = (Vw)(x) = -\frac{1}{\varepsilon_0}\left(\frac{1}{2} I + K\right) v(x) \quad \textit{for } x \in \Gamma.$$

Proof. Let us first rewrite the single layer potential boundary integral equation (2.2) as

$$\varepsilon_1 \left(\frac{1}{2}I + K'\right) w(x) + \varepsilon_0 \left(\frac{1}{2}I - K'\right) w(x) = -(\varepsilon_1 - \varepsilon_0)\gamma_1^{\text{int}}\Phi_{\text{part}}(x) \quad \text{f.a.e. } x \in \Gamma,$$

and in the following, by using the identity $I = V^{-1}V$, as

$$\begin{aligned}\varepsilon_1 \left(\frac{1}{2}I + K'\right) V^{-1}Vw(x) + \varepsilon_0 \left(\frac{1}{2}I - K'\right) V^{-1}Vw(x)& \\ = -(\varepsilon_1 - \varepsilon_0)\gamma_1^{\text{int}}\Phi_{\text{part}}(x) \quad \text{f.a.e. } x \in \Gamma.&\end{aligned}$$

With the symmetry relation $VK' = KV$, see, e.g., [34, p. 138], we conclude $K'V^{-1} = V^{-1}K$ and therefore we obtain

$$\begin{aligned}\varepsilon_1 V^{-1}\left(\frac{1}{2}I + K\right) Vw(x) + \varepsilon_0 V^{-1}\left(\frac{1}{2}I - K\right) Vw(x)& \\ = -(\varepsilon_1 - \varepsilon_0)\gamma_1^{\text{int}}\Phi_{\text{part}}(x) \quad \text{f.a.e. } x \in \Gamma.&\end{aligned}$$

With the Steklov–Poincaré operators $S_1 = V^{-1}\left(\frac{1}{2}I + K\right)$ and $S_0 = V^{-1}\left(\frac{1}{2}I - K\right)$ we further obtain

$$\varepsilon_1 S_1 Vw(x) + \varepsilon_0 S_0 Vw(x) = -(\varepsilon_1 - \varepsilon_0)\gamma_1^{\text{int}}\Phi_{\text{part}}(x) \quad \text{f.a.e. } x \in \Gamma,$$

which shows the equivalence with the Steklov–Poincaré operator equation (2.9) when introducing $\Phi = Vw$.

Let us now consider the double layer integral operator equation (2.24), i.e.,

$$\varepsilon_1 \left(\frac{1}{2}I + K\right) v(x) + \varepsilon_0 \left(\frac{1}{2}I - K\right) v(x) + (\varepsilon_1 - \varepsilon_0)\varepsilon_0\widetilde{\psi}(x) = 0 \quad \text{f.a.e. } x \in \Gamma.$$

Recall, that $\widetilde{\psi}$ is a solution of the Neumann boundary value problem (2.10). Hence, by using the boundary integral equation (2.12) and by multiplying the double layer integral equation with $\left(\frac{1}{2}I + K\right)$ we obtain

$$\begin{aligned}\varepsilon_1 \left(\frac{1}{2}I + K\right)\left(\frac{1}{2}I + K\right) v(x) + \varepsilon_0 \left(\frac{1}{2}I + K\right)\left(\frac{1}{2}I - K\right) v(x)& \\ + (\varepsilon_1 - \varepsilon_0)\varepsilon_0 \left(\frac{1}{2}I + K\right)\widetilde{\psi}(x) = 0 \quad \text{f.a.e. } x \in \Gamma,&\end{aligned}$$

and therefore

$$\begin{aligned}\varepsilon_1 \left(\frac{1}{2}I + K\right)\left(\frac{1}{2}I + K\right) v(x) + \varepsilon_0 \left(\frac{1}{2}I + K\right)\left(\frac{1}{2}I - K\right) v(x)& \\ - (\varepsilon_1 - \varepsilon_0)\varepsilon_0 \left(V\gamma_1^{\text{int}}\Phi_{\text{part}}\right)(x) = 0 \quad \text{f.a.e. } x \in \Gamma.&\end{aligned}$$

Recall that

$$\varepsilon_0 \Phi(x) = \widetilde{\Phi}_0(x) = -\left(\frac{1}{2}I + K\right) v(x) \quad \text{f.a.e. } x \in \Gamma.$$

Hence we conclude

$$\varepsilon_1 \left(\frac{1}{2}I + K\right)[-\varepsilon_0 \Phi(x)] + \varepsilon_0 \left(\frac{1}{2}I - K\right)[-\varepsilon_0 \Phi(x)] \\ - (\varepsilon_1 - \varepsilon_0)\varepsilon_0 \left(V \gamma_1^{\text{int}} \Phi_{\text{part}}\right)(x) = 0 \quad \text{f.a.e. } x \in \Gamma,$$

and in the following

$$\varepsilon_1 \left(\frac{1}{2}I + K\right)\Phi(x) + \varepsilon_0 \left(\frac{1}{2}I + K\right)\Phi(x) \\ + (\varepsilon_1 - \varepsilon_0)\left(V \gamma_1^{\text{int}} \Phi_{\text{part}}\right)(x) = 0 \quad \text{f.a.e. } x \in \Gamma.$$

An application of the inverse single layer integral operator V^{-1} finally results in the Steklov–Poincaré operator equation (2.9). □

As a consequence of Theorem 2.2 we see that unique solvability of one formulation yields unique solvability of the others.

Theorem 2.3 ([1, p. 122])**.** *Let $0 < \varepsilon_0 \leq \varepsilon_1$. The operator*

$$\frac{1}{2}I + \frac{\varepsilon_1 - \varepsilon_0}{\varepsilon_1 + \varepsilon_0} K = I - \left(\frac{1}{2}I - \frac{\varepsilon_1 - \varepsilon_0}{\varepsilon_1 + \varepsilon_0} K\right) : H^{\frac{1}{2}}(\Gamma) \to H^{\frac{1}{2}}(\Gamma)$$

admits a unique inverse by the Neumann series

$$\left(\frac{1}{2}I + \frac{\varepsilon_1 - \varepsilon_0}{\varepsilon_1 + \varepsilon_0} K\right)^{-1} = \sum_{k=0}^{\infty} \left(\frac{1}{2}I - \frac{\varepsilon_1 - \varepsilon_0}{\varepsilon_1 + \varepsilon_0} K\right)^k,$$

i.e., the operator

$$\frac{1}{2}I - \frac{\varepsilon_1 - \varepsilon_0}{\varepsilon_1 + \varepsilon_0} K : H^{\frac{1}{2}}(\Gamma) \to H^{\frac{1}{2}}(\Gamma)$$

is a contraction satisfying

$$\left\| \left(\frac{1}{2}I - \frac{\varepsilon_1 - \varepsilon_0}{\varepsilon_1 + \varepsilon_0} K\right) v \right\|_{V^{-1}} \leq \frac{1}{2}\left(1 + \frac{\varepsilon_1 - \varepsilon_0}{\varepsilon_1 + \varepsilon_0}\right) \|v\|_{V^{-1}}$$

for all $v \in H^{\frac{1}{2}}(\Gamma)$.

Proof. For $v \in H^{\frac{1}{2}}(\Gamma)$ we use an equivalent norm which is induced by the inverse single layer boundary integral operator,

$$\|v\|_{V^{-1}} := \sqrt{\langle V^{-1} v, v \rangle_\Gamma}.$$

Note that we have, see, e.g.,[35, pp. 745–746] and [34, p. 151],

$$\left\| \left(\frac{1}{2} I - K \right) v \right\|_{V^{-1}} \leq \|v\|_{V^{-1}} \quad \text{for all } v \in H^{\frac{1}{2}}(\Gamma),$$

where the equality holds for all constant v. Then,

$$\begin{aligned}
\left\| \left(\frac{1}{2} I - \frac{\varepsilon_1 - \varepsilon_0}{\varepsilon_1 + \varepsilon_0} K \right) v \right\|_{V^{-1}} &= \left\| \frac{\varepsilon_1 - \varepsilon_0}{\varepsilon_1 + \varepsilon_0} \left(\frac{1}{2} I - K \right) v + \frac{1}{2} \left(1 - \frac{\varepsilon_1 - \varepsilon_0}{\varepsilon_1 + \varepsilon_0} \right) v \right\|_{V^{-1}} \\
&\leq \frac{\varepsilon_1 - \varepsilon_0}{\varepsilon_1 + \varepsilon_0} \left\| \left(\frac{1}{2} I - K \right) v \right\|_{V^{-1}} + \frac{1}{2} \left(1 - \frac{\varepsilon_1 - \varepsilon_0}{\varepsilon_1 + \varepsilon_0} \right) \|v\|_{V^{-1}} \\
&\leq \left[\frac{\varepsilon_1 - \varepsilon_0}{\varepsilon_1 + \varepsilon_0} + \frac{1}{2} \left(1 - \frac{\varepsilon_1 - \varepsilon_0}{\varepsilon_1 + \varepsilon_0} \right) \right] \|v\|_{V^{-1}} \\
&= \frac{1}{2} \left(1 + \frac{\varepsilon_1 - \varepsilon_0}{\varepsilon_1 + \varepsilon_0} \right) \|v\|_{V^{-1}} .
\end{aligned}$$

□

As a consequence of Theorem 2.2 together with Theorem 2.3 we conclude unique solvability of the three formulations (2.2), (2.9), and (2.24).

2.5 Evaluation of the Electric Field

In this section we show how to evaluate the electric field $\mathbf{E}$ on the continuous level. After computing the scalar potential Φ as the solution of the transmission problem (1.5) we can use the representation of the electric field as given in (1.2) with $k = 0$ to obtain

$$\mathbf{E}(x) = -\nabla \Phi_{\text{part}}(x) - \nabla \Phi(x) \quad \text{for } x \in \mathbb{R}^3. \tag{2.25}$$

For the single layer potential formulation (2.2) and the Steklov–Poincaré formulation (2.9) the evaluation in the general case follows directly from (2.25), i.e.

$$\mathbf{E}(x) = -\nabla \Phi_{\text{part}}(x) - \nabla (\widetilde{V} w)(x) \quad \text{for } x \in \mathbb{R}^3 \setminus \Gamma, \tag{2.26}$$

for the **single layer formulation** and

$$\mathbf{E}(x) = -\nabla \Phi_{\text{part}}(x) - \nabla \Phi_{\text{hom}}(x) \quad \text{for } x \in \mathbb{R}^3, \tag{2.27}$$

for the **Steklov–Poincaré formulation**, where Φ_{hom} is given by the representation formulas (2.3) and (2.6), respectively. For the evaluation in the case of the

double layer formulation we use the ansatz (2.17) to obtain

$$\begin{aligned}\mathbf{E}(x) = -\nabla\Phi_{\text{part}}(x) &+ \frac{1}{\varepsilon_1}\nabla(Wv)(x) \\ &- \frac{\varepsilon_1-\varepsilon_0}{\varepsilon_1}(\nabla(\widetilde{V}g)(x) - \nabla(W\widetilde{\psi})(x)) \quad \text{for } x \in \Omega, \\ \mathbf{E}(x) = -\nabla\Phi_{\text{part}}(x) &+ \frac{1}{\varepsilon_0}\nabla(Wv)(x) \qquad\qquad\qquad\qquad \text{for } x \in \Omega^{\text{ext}}.\end{aligned} \tag{2.28}$$

2.5.1 Simply Connected Domain

It is well known that, if Ω is simply connected,

$$\mathbf{E}(x) = -\nabla\Phi_{\text{part}}(x) - \nabla\Phi_1(x) \to 0 \quad \text{for } x \in \Omega \text{ as } \varepsilon_1 \to \infty.$$

In this case we are interested in a more robust computation of the electric field on the discrete level, since otherwise high values of ε_1 could cause troubles. Analogous to [1] we consider the same ansatz (2.17) as in the double layer potential formulation, where the interior solution was denoted by

$$\Phi_1(x) := \frac{1}{\varepsilon_1}\left(\widetilde{\Phi}_1(x) + (\varepsilon_1-\varepsilon_0)\widetilde{\psi}(x)\right) \quad \text{for } x \in \Omega,$$

and $\widetilde{\psi}$ is a solution to the Neumann boundary value problem (2.10). From the evaluation of the electric field by (2.25) we obtain

$$\begin{aligned}\varepsilon_1\mathbf{E}(x) &= \varepsilon_1\left(-\nabla\Phi_{\text{part}}(x) - \nabla\Phi(x)\right) \\ &= -\varepsilon_0\nabla\Phi_{\text{part}}(x) - \nabla\widetilde{\Phi}_1(x) + (\varepsilon_1-\varepsilon_0)\left(-\nabla\Phi_{\text{part}}(x) - \nabla\widetilde{\psi}(x)\right) \\ &= -\varepsilon_0\nabla\Phi_{\text{part}}(x) - \nabla\widetilde{\Phi}_1(x) \quad \text{for } x \in \Omega,\end{aligned}$$

since there holds

$$\nabla\widetilde{\psi} = -\nabla\Phi_{\text{part}}$$

by definition in (2.10).

By using this result we are able to compute alternative representations of the electric field. If Ω is simply connected we compute the electric field for the **single layer formulation** by

$$\mathbf{E}(x) = \nabla(\widetilde{V}w_j)(x) - \nabla(\widetilde{V}w)(x) \quad \text{for } x \in \Omega, \tag{2.29}$$

where $w_j \in H^{-\frac{1}{2}}(\Gamma)$ is a solution of

$$\left(\frac{1}{2}I + K'\right)w_j = -\gamma_1^{\text{int}}\Phi_{\text{part}} \quad \text{on } \Gamma. \tag{2.30}$$

Analogously to the derivation of the stabilized variational formulation (2.16) we can obtain a similar stabilized variational formulation for (2.30), where we want to find $\widetilde{w}_j \in H^{-\frac{1}{2}}(\Gamma)$ with

$$\left\langle \left(\frac{1}{2}I + K'\right)\widetilde{w}_j, v \right\rangle_\Gamma + \langle \widetilde{w}_j, 1\rangle_\Gamma \langle v, 1\rangle_\Gamma = \langle -\gamma_1^{\text{int}}\Phi_{\text{part}}, v\rangle_\Gamma \quad \text{for all } v \in H^{\frac{1}{2}}(\Gamma) \tag{2.31}$$

and $\nabla(\widetilde{V}w_j)(x) = \nabla(\widetilde{V}\widetilde{w}_j)(x)$.

For the **Steklov–Poincarè interface equation** we compute an alternative to the gradient of the particular solution by finding $\widetilde{\psi} \in H^{\frac{1}{2}}(\Gamma)$ with

$$\langle S_1\widetilde{\psi}, v\rangle_\Gamma + \langle \widetilde{\psi}, 1\rangle_\Gamma \langle v, 1\rangle_\Gamma = \langle -\gamma_1^{\text{int}}\Phi_{\text{part}}, v\rangle_\Gamma \quad \text{for all } v \in H^{\frac{1}{2}}(\Gamma),$$

and calculating the Neumann datum $t_j \in H^{-\frac{1}{2}}(\Gamma)$ by

$$\langle Vt_j, w\rangle_\Gamma = \left\langle \left(\frac{1}{2}I + K\right)\widetilde{\psi}, w \right\rangle_\Gamma \quad \text{for all } w \in H^{-\frac{1}{2}}(\Gamma).$$

Then we compute the electric field by

$$\mathbf{E}(x) = (\nabla(\widetilde{V}t_j(x) - \nabla(W\widetilde{\psi})(x)) - \nabla\Phi(x) \quad \text{for } x \in \Omega. \tag{2.32}$$

For the **double layer potential formulation** the evaluation in the domain changes from (2.28) to

$$\mathbf{E}(x) = -\frac{\varepsilon_0}{\varepsilon_1}\nabla\Phi_{\text{part}}(x) + \frac{1}{\varepsilon_1}\nabla(Wv)(x) \quad \text{for } x \in \Omega. \tag{2.33}$$

3 Boundary Element Methods

In this chapter we will discuss discrete formulations of the boundary integral formulations (2.2), (2.9), and (2.24). We will only concern ourselves with unique solvability and error analysis of the Steklov–Poincaré operator formulation, since the analysis of the other two formulations is more involved and would go beyond the scope of this work. We will use Galerkin variational formulations to obtain systems of linear equations and choose discrete spaces, which seem to be most convenient for implementation. For $\ell = 1, \ldots, N$ we define $h_\ell := \operatorname{diam} \tau_\ell$ and denote by $h := \max_{\ell \in \{1,\ldots,N\}} h_\ell$. For a function v we denote by v_h the discrete approximation and by $\underline{v}$ the corresponding vector in $\mathbb{R}^N$, if the discrete space is $\operatorname{span}\{\psi_\ell\}_{\ell=1}^N$, i.e.

$$v_h = \sum_{\ell=1}^{N} \psi_\ell \underline{v}_\ell.$$

3.1 Single Layer Potential Formulation

For the single layer potential formulation (2.2) we consider its equivalent variational formulation, which has a unique solution by Theorem 2.3, where we want to find $w \in H^{-\frac{1}{2}}(\Gamma)$ such that

$$\left\langle \left(\frac{1}{2} \frac{\varepsilon_1 + \varepsilon_0}{\varepsilon_1 - \varepsilon_0} I + K' \right) w, z \right\rangle_\Gamma = \left\langle -\gamma_1^{\text{int}} \Phi_{\text{part}}, z \right\rangle_\Gamma \quad \text{for all } z \in H^{\frac{1}{2}}(\Gamma).$$

The Galerkin variational formulation is to find a piecewise constant approximation $w_h \in S_h^0(\Gamma) = \operatorname{span}\{\psi_\ell^0\}_{\ell=1}^N$ such that

$$\left\langle \left(\frac{1}{2} \frac{\varepsilon_1 + \varepsilon_0}{\varepsilon_1 - \varepsilon_0} I + K' \right) w_h, z_h \right\rangle_\Gamma = \left\langle -\gamma_1^{\text{int}} \Phi_{\text{part}}, z_h \right\rangle_\Gamma \quad \text{for all } z_h \in S_h^0(\Gamma).$$

The corresponding linear system reads

$$\left(\frac{1}{2} \frac{\varepsilon_1 + \varepsilon_0}{\varepsilon_1 - \varepsilon_0} \widetilde{M}_h + \widetilde{K}'_h \right) \underline{w} = \underline{f}^0, \tag{3.1}$$

where for $k, \ell = 1, \ldots, N$

$$\widetilde{M}_h[k,\ell] = \langle \psi_\ell^0, \psi_k^0 \rangle_\Gamma, \quad \widetilde{K}'_h[k,\ell] = \langle K' \psi_\ell^0, \psi_k^0 \rangle_\Gamma, \quad f_k^0 = \langle -\gamma_1^{\text{int}} \Phi_{\text{part}}, \psi_k^0 \rangle_\Gamma.$$

By using the evaluation of the electric field (2.26) and inserting w_h instead of w we are able to compute a numerical approximation of the electric field by

$$\widetilde{\mathbf{E}}(x) = -\nabla\Phi_{\text{part}}(x) - \nabla(\widetilde{V}w_h)(x) \quad \text{for } x \in \mathbb{R}^3. \tag{3.2}$$

In the case of a simply connected domain we have to compute an approximation $w_{j,h} \in S_h^0(\Gamma)$ of $\widetilde{w}_j$ as given in the stabilized formulation (2.31). The linear system for this purpose is given by

$$\left(\frac{1}{2}\widetilde{M}_h + \widetilde{K}_h' + \underline{a}\,\underline{a}^\top\right)\underline{w}_j = \underline{f}^0,$$

where for $k = 1, \ldots, N$

$$a_k = \langle \psi_k^0, 1\rangle_\Gamma.$$

We evaluate the electric field as in (2.29) by

$$\widetilde{\mathbf{E}}(x) = \nabla\widetilde{V}(w_{j,h} - w_h)(x) \quad \text{for } x \in \Omega. \tag{3.3}$$

3.2 Steklov–Poincaré Operator Formulation

Now we consider a variational formulation of the Steklov–Poincaré operator formulation (2.9), where we aim to find $\Phi \in H^{\frac{1}{2}}(\Gamma)$ such that

$$\langle(\varepsilon_1 S_1 + \varepsilon_0 S_0)\,\Phi, z\rangle_\Gamma = \langle(\varepsilon_0 - \varepsilon_1)\gamma_1^{\text{int}}\Phi_{\text{part}}, z\rangle_\Gamma \quad \text{for all } z \in H^{\frac{1}{2}}(\Gamma). \tag{3.4}$$

For the discretization of (3.4) we use piecewiese linear and globally continuous basis functions, i.e. the space $S_h^1(\Gamma) = \operatorname{span}\{\psi_m^1\}_{m=1}^M$ and obtain a Galerkin variational formulation to find $\widehat{\Phi}_h \in S_h^1(\Gamma)$ such that

$$\langle(\varepsilon_1 S_1 + \varepsilon_0 S_0)\,\widehat{\Phi}_h, z_h\rangle_\Gamma = \langle(\varepsilon_0 - \varepsilon_1)\gamma_1^{\text{int}}\Phi_{\text{part}}, z_h\rangle_\Gamma \quad \text{for all } z_h \in S_h^1(\Gamma).$$

Since a direct discretization of the Steklov–Poincaré operators S_0 and S_1 is not possible in general, we will use symmetric approximations [34, p.284] instead.

For $v \in H^{\frac{1}{2}}(\Gamma)$ the interior and exterior Steklov–Poincaré operators are given by

$$S_1 v = Dv + \left(\frac{1}{2}I + K'\right)V^{-1}\left(\frac{1}{2}I + K\right)v = Dv + \left(\frac{1}{2}I + K'\right)w_1,$$
$$S_0 v = Dv + \left(\frac{1}{2}I - K'\right)V^{-1}\left(\frac{1}{2}I - K\right)v = Dv + \left(\frac{1}{2}I - K'\right)w_0,$$

where $w_1 = V^{-1}\left(\frac{1}{2}I + K\right)v \in H^{-\frac{1}{2}}(\Gamma)$ and $w_0 = V^{-1}\left(\frac{1}{2}I - K\right)v \in H^{-\frac{1}{2}}(\Gamma)$ are unique solutions of the variational problems

$$\langle Vw_1, \tau\rangle_\Gamma = \left\langle \left(\frac{1}{2}I + K\right)v, \tau \right\rangle_\Gamma \quad \text{for all } \tau \in H^{-\frac{1}{2}}(\Gamma),$$
$$\langle Vw_0, \tau\rangle_\Gamma = \left\langle \left(\frac{1}{2}I - K\right)v, \tau \right\rangle_\Gamma \quad \text{for all } \tau \in H^{-\frac{1}{2}}(\Gamma).$$

Approximations of S_1 and S_0 are defined by

$$\widetilde{S}_1 v = Dv + \left(\frac{1}{2}I + K'\right)w_{1,h}, \tag{3.5a}$$
$$\widetilde{S}_0 v = Dv + \left(\frac{1}{2}I - K'\right)w_{0,h}, \tag{3.5b}$$

where $w_{i,h} \in S_h^0(\Gamma)$ are the unique solutions of the variational problems

$$\langle Vw_{1,h}, \tau_h\rangle_\Gamma = \left\langle \left(\frac{1}{2}I + K\right)v, \tau_h \right\rangle_\Gamma \quad \text{for all } \tau_h \in S_h^0(\Gamma), \tag{3.6a}$$
$$\langle Vw_{0,h}, \tau_h\rangle_\Gamma = \left\langle \left(\frac{1}{2}I - K\right)v, \tau_h \right\rangle_\Gamma \quad \text{for all } \tau_h \in S_h^0(\Gamma). \tag{3.6b}$$

We obtain a perturbed variational formulation, where we want to find $\Phi_h \in S_h^1(\Gamma)$ such that

$$\left\langle \left(\varepsilon_1\widetilde{S}_1 + \varepsilon_0\widetilde{S}_0\right)\Phi_h, z_h \right\rangle_\Gamma = \left\langle (\varepsilon_0 - \varepsilon_1)\gamma_1^{\text{int}}\Phi_{\text{part}}, z_h \right\rangle_\Gamma \quad \text{for all } z_h \in S_h^1(\Gamma). \tag{3.7}$$

The corresponding Galerkin matrices are given by

$$S_{1,h} = D_h + \left(\frac{1}{2}M_h^\top + K_h^\top\right)V_h^{-1}\left(\frac{1}{2}M_h + K_h\right), \tag{3.8a}$$
$$S_{0,h} = D_h + \left(\frac{1}{2}M_h^\top - K_h^\top\right)V_h^{-1}\left(\frac{1}{2}M_h - K_h\right), \tag{3.8b}$$

where

$$D_h[m,n] = \langle D\psi_n^1, \psi_m^1\rangle_\Gamma, \qquad K_h[k,n] = \langle K\psi_n^1, \psi_k^0\rangle_\Gamma,$$
$$M_h[k,n] = \langle \psi_n^1, \psi_k^0\rangle_\Gamma, \qquad V_h[k,\ell] = \langle V\psi_\ell^0, \psi_k^0\rangle_\Gamma,$$

for $m,n = 1,\ldots,M$ and $k,\ell = 1,\ldots,N$.

From (3.7) we obtain the linear system

$$(\varepsilon_1 S_{1,h} + \varepsilon_0 S_{0,h})\,\underline{\Phi} = (\varepsilon_1 - \varepsilon_0)\underline{f}^1, \tag{3.9}$$

where for $k = 1, \ldots, M$

$$f_k^1 = \left\langle -\gamma_1^{\text{int}} \Phi_{\text{part}}, \psi_k^1 \right\rangle_\Gamma .$$

By using discrete versions of the boundary integral equations (2.4) and (2.7), i.e. by solving

$$V_h \underline{t}_1 = \left(\frac{1}{2} M_h + K_h \right) \underline{\Phi}, \tag{3.10a}$$

$$V_h \underline{t}_0 = \left(\frac{1}{2} M_h - K_h \right) \underline{\Phi}, \tag{3.10b}$$

we obtain discrete approximations $t_{1,h}$ and $t_{0,h}$ of the interior and exterior Neumann data $t_1 = \gamma_1^{\text{int}} \Phi$ and $t_0 = \gamma_1^{\text{ext}} \Phi$, respectively.

The evaluation of the electric field is done by using the representation formulas (2.3) and (2.6) on the discrete approximations Φ_h and $t_{i,h}$. On the transmission interface we use evaluation in the centers x_k of the triangles τ_k with normal direction n_k to get an approximation

$$\widetilde{\mathbf{E}}(x_k) = -\nabla \Phi_{\text{part}}(x_k) - \left(t_{i,k} n_k + \nabla_\Gamma \Phi_h(x_k) \right), \tag{3.11}$$

where ∇_Γ denotes the tangential derivative. In the case of a simply connected domain we replace $-\nabla \Phi_{\text{part}}$ as described in the modified evaluation (2.32):

$$\mathbf{E}(x_k) = \left(\nabla (\widetilde{V} t_{j,h})(x_k) - \nabla (W \widetilde{\psi}_h)(x_k) \right) - \left(t_{i,k} n_k + \nabla_\Gamma \Phi_h(x_k) \right). \tag{3.12}$$

3.2.1 Error Analysis

We would like to give error estimates for various quantities for which we are interested in the numerical computation. We start with estimating the $L^2(\Gamma)$-error of the solution $\Phi_h \in S_h^1(\Gamma)$ of the perturbed variational problem (3.7). For this purpose we need some other estimates beforehand.

Lemma 3.1 ([26, 28, 34])**.** *The approximate Steklov–Poincaré operators $\widetilde{S}_0, \widetilde{S}_1$ are bounded, i.e. $\widetilde{S}_i : H^{-\frac{1}{2}}(\Gamma) \to H^{-\frac{1}{2}}(\Gamma)$ satisfy*

$$\|\widetilde{S}_i v\|_{H^{-\frac{1}{2}}(\Gamma)} \leq c_2^{\widetilde{S}_i} \|v\|_{H^{\frac{1}{2}}(\Gamma)} \quad \text{for all } v \in H^{\frac{1}{2}}(\Gamma).$$

Moreover, $\widetilde{S}_1$ is $H^{\frac{1}{2}}(\Gamma)$-semi-elliptic,

$$\langle \widetilde{S}_1 v, v \rangle_\Gamma \geq c_1^D |v|^2_{H^{\frac{1}{2}}(\Gamma)} \quad \text{for all } v \in H^{\frac{1}{2}}(\Gamma),$$

$\widetilde{S}_0$ is $H^{\frac{1}{2}}(\Gamma)$-elliptic,

$$\langle \widetilde{S}_0 v, v \rangle_\Gamma \geq c \|v\|^2_{H^{\frac{1}{2}}(\Gamma)} \quad \text{for all } v \in H^{\frac{1}{2}}(\Gamma),$$

and they satisfy the error estimates

$$\|(S_i - \widetilde{S}_i)v\|_{H^{-\frac{1}{2}}(\Gamma)} \leq c \inf_{\tau_h \in S_h^0(\Gamma)} \|S_i v - \tau_h\|_{H^{-\frac{1}{2}}(\Gamma)}.$$

Remark 3.1. *Analogously to [34, Theorem 12.11] we can conclude boundedness and an error estimate for the approximate exterior Steklov–Poincaré operator $\widetilde{S}_0$. $\widetilde{S}_0$ is not only $H^{\frac{1}{2}}(\Gamma)$-semi-elliptic, but also $H^{\frac{1}{2}}(\Gamma)$-elliptic. A proof is given in [26] following the main idea of [28, Lemma 1.93].*

With the results for the interior and exterior operators in mind we can easily provide an approximation error for the operator $A := (\varepsilon_1 S_1 + \varepsilon_0 S_0)$, occurring in the Steklov–Poincaré formulation, by using triangle inequality.

Corollary 3.2. *The approximate operator $\widetilde{A} := (\varepsilon_1 \widetilde{S}_1 + \varepsilon_0 \widetilde{S}_0) : H^{-\frac{1}{2}}(\Gamma) \to H^{-\frac{1}{2}}(\Gamma)$ is bounded*

$$\|\widetilde{A}v\|_{H^{-\frac{1}{2}}(\Gamma)} \leq c_2^{\widetilde{A}} \|v\|_{H^{\frac{1}{2}}(\Gamma)} \quad \text{for all } v \in H^{\frac{1}{2}}(\Gamma).$$

Moreover, $\widetilde{A}$ is $H^{\frac{1}{2}}(\Gamma)$-elliptic,

$$\langle \widetilde{A}v, v \rangle_\Gamma \geq c \|v\|^2_{H^{\frac{1}{2}}(\Gamma)} \quad \text{for all } v \in H^{\frac{1}{2}}(\Gamma),$$

and satisfies the error estimate

$$\begin{aligned} &\|(A - \widetilde{A})v\|_{H^{-\frac{1}{2}}(\Gamma)} \\ &\qquad \leq c \left(\inf_{\tau_h \in S_h^0(\Gamma)} \|S_1 v - \tau_h\|_{H^{-\frac{1}{2}}(\Gamma)} + \inf_{\tau_h \in S_h^0(\Gamma)} \|S_0 v - \tau_h\|_{H^{-\frac{1}{2}}(\Gamma)} \right). \end{aligned} \tag{3.13}$$

Now we are able to prove a first error estimate for the solution $\Phi \in H^{\frac{1}{2}}(\Gamma)$ of the analytic Steklov–Poincaré variational formulation (3.4) and the solution $\Phi_h \in S_h^1(\Gamma)$ of the perturbed variational formulation (3.7).

Lemma 3.3. *Let $s \in [-\frac{1}{2}, 1]$, $S_i \Phi \in H^s_{\mathrm{pw}}(\Gamma)$, $\Phi \in H^{s+1}(\Gamma)$ and $\gamma_1^{int} \Phi_{\mathrm{part}} \in H^{-\frac{1}{2}}(\Gamma)$. Then there is a unique solution $\Phi_h \in S_h^1(\Gamma)$ of the variational problem (3.7) satisfying*

$$\|\Phi - \Phi_h\|_{H^{\frac{1}{2}}(\Gamma)} \leq c h^{s+\frac{1}{2}} (|\Phi|_{H^{s+1}(\Gamma)} + |S_1 \Phi|_{H^s_{\mathrm{pw}}(\Gamma)} + |S_0 \Phi|_{H^s_{\mathrm{pw}}(\Gamma)}).$$

If furthermore $S_i : H^{s+1}(\Gamma) \to H^s(\Gamma)$ is bounded then

$$\|\Phi - \Phi_h\|_{H^{\frac{1}{2}}(\Gamma)} \leq c h^{s+\frac{1}{2}} \|\Phi\|_{H^{s+1}(\Gamma)}.$$

Proof. Since $\widetilde{A}$ is $H^{\frac{1}{2}}(\Gamma)$-elliptic by Corollary 3.2 we can use the Strang Lemma, see, e.g., [34, p. 192] to obtain unique solvability and

$$\|\Phi - \Phi_h\|_{H^{\frac{1}{2}}(\Gamma)} \leq c \left(\inf_{v_h \in S_h^1(\Gamma)} \|\Phi - v_h\|_{H^{\frac{1}{2}}(\Gamma)} + \|(A - \widetilde{A})\Phi\|_{H^{-\frac{1}{2}}(\Gamma)} \right).$$

We use the approximation property of $S_h^1(\Gamma)$, see, e.g., [34, p. 241], to obtain

$$\inf_{v_h \in S_h^1(\Gamma)} \|\Phi - v_h\|_{H^{\frac{1}{2}}(\Gamma)} \leq c h^{s+\frac{1}{2}} |\Phi|_{H^{s+1}(\Gamma)}.$$

The error estimate (3.13) together with the approximation property of $S_h^0(\Gamma)$, given in [34, p. 237], yields

$$\|\Phi - \Phi_h\|_{H^{\frac{1}{2}}(\Gamma)} \leq c\, h^{s+\frac{1}{2}} (|\Phi|_{H^{s+1}(\Gamma)} + |S_1\Phi|_{H^s_{\mathrm{pw}}(\Gamma)} + |S_0\Phi|_{H^s_{\mathrm{pw}}(\Gamma)}).$$

If $S_i : H^{s+1}(\Gamma) \to H^s(\Gamma)$ is bounded then $|S_i\Phi|_{H^s_{\mathrm{pw}}(\Gamma)} \leq \|\Phi\|_{H^{s+1}(\Gamma)}$ and therefore the second estimate follows. □

Using an Aubin–Nitsche trick [14] we are able to provide an error estimate for the operator approximation in $H^\mu(\Gamma)$ with $\mu \in [-2, -\frac{1}{2}]$.

Lemma 3.4. *For some $\mu \in [-2, -\frac{1}{2}]$ assume that $V : H^{-1-\mu}(\Gamma) \to H^{-\mu}(\Gamma)$ is continuous and bijective and $\left(\frac{1}{2}I \pm K'\right) : H^\mu(\Gamma) \to H^\mu(\Gamma)$ are continuous. Let $s \in [-\frac{1}{2}, 1]$ and let $v \in H^{s+1}(\Gamma)$ such that $S_i v \in H^s_{\mathrm{pw}}(\Gamma)$. Then there holds the error estimate*

$$\|(A - \widetilde{A})v\|_{H^\mu(\Gamma)} \leq c h^{s-\mu} (|S_1 v|_{H^s_{\mathrm{pw}}(\Gamma)} + |S_0 v|_{H^s_{\mathrm{pw}}(\Gamma)}).$$

If furthermore $S_i : H^{s+1}(\Gamma) \to H^s(\Gamma)$ is bounded then

$$\|(A - \widetilde{A})v\|_{H^\mu(\Gamma)} \leq c h^{s-\mu} \|v\|_{H^{s+1}(\Gamma)}.$$

Proof. We consider the error of $\widetilde{S}_1$, the exterior case is analogous. By definition (3.5) and boundedness of $\left(\frac{1}{2}I + K'\right)$ we have got

$$\|(S_1 - \widetilde{S}_1)v\|_{H^\mu(\Gamma)} = \left\| \left(\frac{1}{2}I + K'\right)(w_1 - w_{1,h}) \right\|_{H^\mu(\Gamma)} \leq \|w_1 - w_{1,h}\|_{H^\mu(\Gamma)}.$$

By an Aubin–Nitsche trick [34, Theorem 12.3] for the auxiliary problem (3.6) we have an error estimate for $w_{1,h}$ given by

$$\|w_1 - w_{1,h}\|_{H^\mu(\Gamma)} \leq c h^{s-\mu} |w_1|_{H^s_{\mathrm{pw}}(\Gamma)}.$$

By using the identity $w_1 = V^{-1}\left(\frac{1}{2}I + K\right)v = S_1 v$ we obtain

$$\|(\widetilde{S}_1 - S_1)v\|_{H^\mu(\Gamma)} \leq c h^{s-\mu} |S_1 v|_{H^s_{\mathrm{pw}}(\Gamma)}.$$

Therefore we can conclude

$$\begin{aligned}\|(A-\widetilde{A})v\|_{H^\mu(\Gamma)} &\leq \varepsilon_0\|(\widetilde{S}_0-S_0)v\|_{H^\mu(\Gamma)}+\varepsilon_1\|(\widetilde{S}_1-S_1)v\|_{H^\mu(\Gamma)}\\ &\leq ch^{s-\mu}(|S_1v|_{H^s_{\mathrm{pw}}(\Gamma)}+|S_0v|_{H^s_{\mathrm{pw}}(\Gamma)}).\end{aligned}$$

By using boundedness of S_i the second result follows. □

Our next goal is to obtain an $H^\mu(\Gamma)$-error estimate of the potential Φ for $\mu\in[-1,\frac{1}{2}]$. For this purpose we will use the $H^{\frac{1}{2}}(\Gamma)$-projection $Q_h^{\frac{1}{2}}$ to $S_h^1(\Gamma)$ and its properties, which we will provide in the following lemma:

Lemma 3.5 ([34, p. 241])**.** *Let $u\in H^s(\Gamma)$, $s\in[\frac{1}{2},2]$. We define the $H^{\frac{1}{2}}(\Gamma)$-projection $Q_h^{\frac{1}{2}}: H^s(\Gamma)\to S_h^1(\Gamma)$ by*

$$\langle Q_h^{\frac{1}{2}}u, v_h\rangle_{H^{\frac{1}{2}}(\Gamma)} = \langle u, v_h\rangle_{H^{\frac{1}{2}}(\Gamma)} \quad \text{for all } v_h\in S_h^1(\Gamma). \tag{3.14}$$

Then there holds

$$\|u-Q_h^{\frac{1}{2}}u\|_{H^{\frac{1}{2}}(\Gamma)} \leq ch^{s-\frac{1}{2}}|u|_{H^s(\Gamma)}.$$

Now we are able to prove an $H^\mu(\Gamma)$-error of the potential, using the ideas given by [10] and [34].

Theorem 3.6. *For some $s\in[\frac{1}{2},2]$ let $\Phi\in H^s(\Gamma)$ be the unique solution of the continuous variational problem* (3.4) *and let $\Phi_h\in S_h^1(\Gamma)$ be the unique solution of the discrete variational problem* (3.7)*. Let the assumptions of Lemma 3.3 and Lemma 3.4 hold true. Assume that $A:=(\varepsilon_1S_1+\varepsilon_0S_0): H^{1-\mu}(\Gamma)\to H^{-\mu}(\Gamma)$ is bounded and bijective for $\mu\in[-1,\frac{1}{2}]$. Then there holds the error estimate*

$$\|\Phi-\Phi_h\|_{H^\mu(\Gamma)} \leq ch^{s-\mu}\|\Phi\|_{H^s(\Gamma)}.$$

Proof. We start by using duality and the bijectivity of A

$$\begin{aligned}\|\Phi-\Phi_h\|_{H^\mu(\Gamma)} &= \sup_{0\neq w\in H^{-\mu}(\Gamma)}\frac{\langle\Phi-\Phi_h,w\rangle_\Gamma}{\|w\|_{H^{-\mu}(\Gamma)}} = \sup_{0\neq v\in H^{1-\mu}(\Gamma)}\frac{\langle A(\Phi-\Phi_h),v\rangle_\Gamma}{\|Av\|_{H^{-\mu}(\Gamma)}}\\ &\leq c\left(\sup_{0\neq v\in H^{1-\mu}(\Gamma)}\frac{\langle A(\Phi-\Phi_h),v\rangle_\Gamma}{\|v\|_{H^{1-\mu}(\Gamma)}}\right).\end{aligned}$$

From the variational problems (3.4) and (3.7) we can conclude that for $v_h\in S_h^1(\Gamma)$ there holds $\langle A\Phi,v_h\rangle_\Gamma=\langle\widetilde{A}\Phi_h,v_h\rangle_\Gamma$. It follows that

$$\langle A(\Phi-\Phi_h),v_h\rangle_\Gamma = \langle(\widetilde{A}-A)\Phi_h,v_h\rangle_\Gamma.$$

Therefore we can add in the $H^{\frac{1}{2}}(\Gamma)$-projection $Q_h^{\frac{1}{2}} v$ and obtain

$$\begin{aligned}
\langle A(\Phi - \Phi_h), v\rangle_\Gamma &= \langle A(\Phi - \Phi_h), v - Q_h^{\frac{1}{2}} v\rangle_\Gamma + \langle A(\Phi - \Phi_h), Q_h^{\frac{1}{2}} v\rangle_\Gamma \\
&= \langle A(\Phi - \Phi_h), v - Q_h^{\frac{1}{2}} v\rangle_\Gamma + \langle (\widetilde{A} - A)\Phi_h, Q_h^{\frac{1}{2}} v\rangle_\Gamma \\
&= \underbrace{\langle A(\Phi - \Phi_h), v - Q_h^{\frac{1}{2}} v\rangle_\Gamma}_{=:I} + \underbrace{\langle (\widetilde{A} - A)(\Phi_h - \Phi), Q_h^{\frac{1}{2}} v\rangle_\Gamma}_{=:II} \\
&\quad + \underbrace{\langle (\widetilde{A} - A)\Phi, Q_h^{\frac{1}{2}} v\rangle_\Gamma}_{=:III}.
\end{aligned}$$

We estimate term I by using boundedness of A, Lemma 3.3, and Lemma 3.5:

$$\begin{aligned}
|\langle A(\Phi - \Phi_h), v - Q_h^{\frac{1}{2}} v\rangle_\Gamma| &\leq \|A(\Phi - \Phi_h)\|_{H^{-\frac{1}{2}}(\Gamma)} \|v - Q_h^{\frac{1}{2}} v\|_{H^{\frac{1}{2}}(\Gamma)} \\
&\leq c\|\Phi - \Phi_h\|_{H^{\frac{1}{2}}(\Gamma)} h^{\frac{1}{2}-\mu} \|v\|_{H^{1-\mu}(\Gamma)} \\
&\leq c h^{s-\mu} \|\Phi\|_{H^s(\Gamma)} \|v\|_{H^{1-\mu}(\Gamma)}.
\end{aligned}$$

For the second term II we first use the energy error of the potential Φ given in Lemma 3.3 and selfadjointness of A and $\widetilde{A}$:

$$\begin{aligned}
|\langle (\widetilde{A} - A)(\Phi_h - \Phi), Q_h^{\frac{1}{2}} v\rangle_\Gamma| &= |\langle \Phi_h - \Phi, (\widetilde{A} - A) Q_h^{\frac{1}{2}} v\rangle_\Gamma| \\
&\leq \|\Phi - \Phi_h\|_{H^{\frac{1}{2}}(\Gamma)} \|(\widetilde{A} - A) Q_h^{\frac{1}{2}} v\|_{H^{-\frac{1}{2}}(\Gamma)} \\
&\leq c h^{s-\frac{1}{2}} \|\Phi\|_{H^s(\Gamma)} \|(\widetilde{A} - A) Q_h^{\frac{1}{2}} v\|_{H^{-\frac{1}{2}}(\Gamma)}.
\end{aligned}$$

We estimate $\|(\widetilde{A} - A) Q_h^{\frac{1}{2}} v\|_{H^{-\frac{1}{2}}(\Gamma)}$ by using duality and the selfadjointness of A and $\widetilde{A}$:

$$\|(\widetilde{A} - A) Q_h^{\frac{1}{2}} v\|_{H^{-\frac{1}{2}}(\Gamma)} = \sup_{0 \neq u \in H^{\frac{1}{2}}(\Gamma)} \frac{\langle (\widetilde{A} - A) Q_h^{\frac{1}{2}} v, u\rangle_\Gamma}{\|u\|_{H^{\frac{1}{2}}(\Gamma)}} = \sup_{0 \neq u \in H^{\frac{1}{2}}(\Gamma)} \frac{\langle Q_h^{\frac{1}{2}} v, (\widetilde{A} - A) u\rangle_\Gamma}{\|u\|_{H^{\frac{1}{2}}(\Gamma)}}.$$

Now we use again the error estimate of the projection from Lemma 3.5 and the approximation error of $\widetilde{A}$ from Lemma 3.4 to estimate the denominator:

$$\begin{aligned}
|\langle Q_h^{\frac{1}{2}} v, (\widetilde{A} - A) u\rangle_\Gamma| &\leq |\langle Q_h^{\frac{1}{2}} v - v, (\widetilde{A} - A) u\rangle_\Gamma| + |\langle v, (\widetilde{A} - A) u\rangle_\Gamma| \\
&\leq \|Q_h^{\frac{1}{2}} v - v\|_{H^{\frac{1}{2}}(\Gamma)} \|(\widetilde{A} - A) u\|_{H^{-\frac{1}{2}}(\Gamma)} \\
&\quad + \|v\|_{H^{1-\mu}(\Gamma)} \|(\widetilde{A} - A) u\|_{H^{-1+\mu}(\Gamma)} \\
&\leq c h^{\frac{1}{2}-\mu} \|v\|_{H^{1-\mu}(\Gamma)} \|u\|_{H^{\frac{1}{2}}(\Gamma)}.
\end{aligned}$$

Altogether we now have

$$|\langle (\widetilde{A} - A)(\Phi_h - \Phi), Q_h^{\frac{1}{2}} v\rangle_\Gamma| \leq c h^{s-\mu} \|\Phi\|_{H^s(\Gamma)} \|v\|_{H^{1-\mu}(\Gamma)}.$$

The third term III is estimated analogously to the second one

$$\begin{aligned}|\langle(\widetilde{A}-A)\Phi, Q_h^{\frac{1}{2}}v\rangle_\Gamma| &\leq |\langle(\widetilde{A}-A)\Phi, Q_h^{\frac{1}{2}}v - v\rangle_\Gamma| + |\langle(\widetilde{A}-A)\Phi, v\rangle_\Gamma| \\ &\leq \|(\widetilde{A}-A)\Phi\|_{H^{-\frac{1}{2}}(\Gamma)}\|Q_h^{\frac{1}{2}}v - v\|_{H^{\frac{1}{2}}(\Gamma)} \\ &\quad + \|(\widetilde{A}-A)\Phi\|_{H^{-1+\mu}(\Gamma)}\|v\|_{H^{1-\mu}(\Gamma)} \\ &\leq ch^{s-\mu}\|\Phi\|_{H^s(\Gamma)}\|v\|_{H^{1-\mu}(\Gamma)}.\end{aligned}$$

The assertion follows by summation of the terms I, II, and part III. □

We will now consider errors for the approximate Neumann data $t_{1,h}$ and $t_{0,h}$ given by (3.10).

Lemma 3.7. *For $i \in \{0,1\}$ let $t_i \in H^{-\frac{1}{2}}(\Gamma)$ be the unique solution of*

$$\langle Vt_i, \tau\rangle_\Gamma = \left\langle \left(\frac{1}{2}I \pm K\right)\Phi, \tau\right\rangle_\Gamma \quad \text{for all } \tau \in H^{-\frac{1}{2}}(\Gamma).$$

There exists a unique solution $t_{i,h} \in S_h^0(\Gamma)$ with

$$\langle Vt_{i,h}, \tau_h\rangle_\Gamma = \left\langle \left(\frac{1}{2}I \pm K\right)\Phi_h, \tau_h\right\rangle_\Gamma \quad \text{for all } \tau_h \in S_h^0(\Gamma).$$

If the assumptions of Lemma 3.3 are satisfied then there holds the error estimate

$$\|t_i - t_{i,h}\|_{H^{-\frac{1}{2}}(\Gamma)} \leq ch^{s+\frac{1}{2}}\|\Phi\|_{H^{s+1}(\Gamma)}.$$

Proof. Since V is $H^{\frac{1}{2}}(\Gamma)$-elliptic we can use the Strang Lemma [34, Th. 8.3] to obtain unique solvability and the error estimate

$$\|t_i - t_{i,h}\|_{H^{-\frac{1}{2}}(\Gamma)} \leq c\left(\inf_{w_h \in S_h^0(\Gamma)}\|t_i - w_h\|_{H^{-\frac{1}{2}}(\Gamma)} + c_2^K\|(\Phi - \Phi_h)\|_{H^{\frac{1}{2}}(\Gamma)}\right).$$

By the approximation error of $S_h^0(\Gamma)$ [34, Th.10.4] and the identity $S_i\Phi = t_i$ we obtain

$$\inf_{w_h \in S_h^0(\Gamma)}\|t_i - w_h\|_{H^{-\frac{1}{2}}(\Gamma)} \leq ch^{s+\frac{1}{2}}|S_i\Phi|_{H^s_{\mathrm{pw}}(\Gamma)} \leq ch^{s+\frac{1}{2}}\|\Phi\|_{H^{s+1}(\Gamma)}.$$

Together with the boundedness of $\left(\frac{1}{2}I \pm K\right)$ and the $H^{\frac{1}{2}}(\Gamma)$-error for the potential Φ_h from Lemma 3.3 the assertion follows. □

Theorem 3.8. *Let the assumptions of Theorem 3.6 and Lemma 3.7 hold true. Assume that for $\mu \in [-2, -\frac{1}{2}]$ the operators $\left(\frac{1}{2}I \pm K\right) : H^{1+\mu}(\Gamma) \to H^{1+\mu}(\Gamma)$ are bounded. Then there holds that*

$$\|t_i - t_{i,h}\|_{H^\mu(\Gamma)} \leq ch^{s-\mu}\|\Phi\|_{H^{s+1}(\Gamma)}.$$

Proof. We use the bijectivity and boundedness of $V : H^{-1-\mu}(\Gamma) \to H^{-\mu}(\Gamma)$ to obtain

$$\|t_i - t_{i,h}\|_{H^\mu(\Gamma)} = \sup_{0\neq v\in H^{-\mu}(\Gamma)} \frac{\langle t_i - t_{i,h}, v\rangle_\Gamma}{\|v\|_{H^{-\mu}(\Gamma)}} \leq c \sup_{0\neq w\in H^{-1-\mu}(\Gamma)} \frac{\langle V(t_i - t_{i,h}), w\rangle_\Gamma}{\|w\|_{H^{-1-\mu}(\Gamma)}}.$$

Now we add and subtract the $L^2(\Gamma)$-projection $Q_h : H^s(\Gamma) \to S_h^0(\Gamma)$ with the property [34, Cor.10.3]

$$\|w - Q_h w\|_{H^{-\frac{1}{2}}(\Gamma)} \leq c h^{-\frac{1}{2}-\mu} \|w\|_{H^{-1-\mu}(\Gamma)}, \tag{3.15}$$

to get

$$\begin{aligned}\|t_i - t_{i,h}\|_{H^\mu(\Gamma)} \leq & \sup_{0\neq w\in H^{-1-\mu}(\Gamma)} \frac{\langle V(t_i - t_{i,h}), w - Q_h w\rangle_\Gamma}{\|w\|_{H^{-1-\mu}(\Gamma)}} \\ & + \sup_{0\neq w\in H^{-1-\mu}(\Gamma)} \frac{\langle V(t_i - t_{i,h}), Q_h w\rangle_\Gamma}{\|w\|_{H^{-1-\mu}(\Gamma)}}.\end{aligned}$$

We note that

$$\langle V(t_i - t_{i,h}), w_h\rangle_\Gamma = \left\langle \left(\frac{1}{2} I \pm K\right)(\Phi - \Phi_h), w_h \right\rangle_\Gamma \quad \text{for all } w_h \in S_h^0(\Gamma),$$

and thus

$$\begin{aligned}\|t_i - t_{i,h}\|_{H^\mu(\Gamma)} \leq & \sup_{0\neq w\in H^{-1-\mu}(\Gamma)} \frac{\langle V(t_i - t_{i,h}), w - Q_h w\rangle_\Gamma}{\|w\|_{H^{-1-\mu}(\Gamma)}} \\ & + \sup_{0\neq w\in H^{-1-\mu}(\Gamma)} \frac{\left\langle \left(\frac{1}{2} I \pm K\right)(\Phi - \Phi_h), Q_h w\right\rangle_\Gamma}{\|w\|_{H^{-1-\mu}(\Gamma)}}.\end{aligned}$$

For the first term we have by boundedness of V, Lemma 3.7, and the above projection property (3.15)

$$\begin{aligned}|\langle V(t_i - t_{i,h}), w - Q_h w\rangle_\Gamma| &\leq \|t_i - t_{i,h}\|_{H^{-\frac{1}{2}}(\Gamma)} \|w - Q_h w\|_{H^{-\frac{1}{2}}(\Gamma)} \\ &\leq c h^{s-\mu} \|\Phi\|_{H^{s+1}(\Gamma)} \|w\|_{H^{-1-\mu}(\Gamma)}.\end{aligned}$$

For the second term we use the boundedness of $(\frac{1}{2} I \pm K)$, the projection property (3.15), the $H^{1+\mu}(\Gamma)$-error estimate of Φ_h in Theorem 3.6, and Lemma 3.3

$$\begin{aligned}&\left|\left\langle \left(\frac{1}{2} I \pm K\right)(\Phi - \Phi_h), Q_h w\right\rangle_\Gamma\right| \\ &\qquad \leq \left|\left\langle \left(\frac{1}{2} I \pm K\right)(\Phi - \Phi_h), w\right\rangle_\Gamma\right| + \left|\left\langle \left(\frac{1}{2} I \pm K\right)(\Phi - \Phi_h), Q_h w - w\right\rangle_\Gamma\right| \\ &\qquad \leq c\left(\|\Phi - \Phi_h\|_{H^{1+\mu}(\Gamma)} \|w\|_{H^{-1-\mu}(\Gamma)} + h^{-\frac{1}{2}-\mu} \|\Phi - \Phi_h\|_{H^{\frac{1}{2}}(\Gamma)} \|w\|_{H^{-1-\mu}(\Gamma)}\right) \\ &\qquad \leq c h^{s-\mu} \|\Phi\|_{H^{s+1}(\Gamma)} \|w\|_{H^{-1-\mu}(\Gamma)}.\end{aligned}$$

By summation we obtain the assertion. □

3.3 Double Layer Potential Formulation

For the double layer potential formulation (2.24) we first compute a discrete approximation $\widetilde{\psi}_h \in S_h^1(\Gamma)$ of $\widetilde{\psi} \in H^{\frac{1}{2}}(\Gamma)$, which we need for the computation of $v \in H^{\frac{1}{2}}(\Gamma)$. We use piecewiese linear and globally continuous basis functions $\{\psi_m^1\}_{m=1}^M$ in the Galerkin variational formulation of (2.16) to obtain the linear system

$$\left(\frac{1}{2}\widehat{M}_h + \widehat{K}_h + \underline{b}\,\underline{b}^\top\right)\underline{\widetilde{\psi}} = \widehat{V}_h \underline{g},$$

where for $m, n = 1, \ldots, M, \ell = 1, \ldots, N$

$$\widehat{M}_h[m,n] = \langle \psi_n^1, \psi_m^1 \rangle_\Gamma, \qquad \widehat{K}_h[m,n] = \langle K\psi_n^1, \psi_m^1 \rangle_\Gamma,$$
$$\widehat{V}_h[m,\ell] = \langle V\psi_\ell^0, \psi_m^1 \rangle_\Gamma, \qquad b_m = \langle \psi_m^1, 1 \rangle_\Gamma,$$

and $\underline{g} \in \mathbb{R}^M$ is the vector of the $L^2(\Gamma)$-projections $g_h \in S_h^0(\Gamma)$ of $-\gamma_1^{\text{int}}\Phi_{\text{part}}$ onto $S_h^0(\Gamma)$. Now we consider the discrete version of (2.24), which is to find $v_h \in S_h^1(\Gamma)$ such that

$$\left(\frac{1}{2}\frac{\varepsilon_1 + \varepsilon_0}{\varepsilon_1 - \varepsilon_0}\widehat{M}_h + \widehat{K}_h\right)\underline{v} = -\varepsilon_0 \widehat{M}_h \underline{\widetilde{\psi}}. \tag{3.16}$$

Finally, we use v_h and $\widetilde{\psi}_h$ to compute approximations of the electric field by the evaluation (2.28):

$$\begin{aligned}\widetilde{\mathbf{E}}(x) = -\nabla\Phi_{\text{part}}(x) &+ \frac{1}{\varepsilon_1}\nabla(Wv_h)(x) \\ &- \frac{\varepsilon_1 - \varepsilon_0}{\varepsilon_1}(\nabla(\widetilde{V}g_h)(x) - \nabla(W\widetilde{\psi}_h)(x)) \quad \text{for } x \in \Omega, \\ \widetilde{\mathbf{E}}(x) = -\nabla\Phi_{\text{part}}(x) &+ \frac{1}{\varepsilon_0}\nabla(Wv_h)(x) \qquad\qquad\qquad\qquad \text{for } x \in \Omega^{\text{ext}}.\end{aligned} \tag{3.17}$$

In the case of a simply connected domain the evaluation of the electric field changes as given in the modified evaluation (2.33) to

$$\widetilde{\mathbf{E}}(x) = -\frac{\varepsilon_0}{\varepsilon_1}\nabla\Phi_{\text{part}}(x) + \frac{1}{\varepsilon_1}\nabla(Wv_h)(x) \quad \text{for } x \in \Omega. \tag{3.18}$$

4 Numerical Examples

In this chapter we will consider two applications for the given formulations, the unit sphere and a cube with side length a. The quantities, which we had beforehand, i.e. the densities of the single layer potential and double layer potential formulations computed by (2.2) and (2.24), the potential obtained from the three formulations (3.7), (4.10), (4.11) and the electric field calculated by the standard evaluations (3.2), (3.11), (3.17) and the modified evaluations (3.3), (3.12) and (3.18) will be computed numerically and compared with respect to errors and computational times. Furthermore we will introduce two additional physical quantities.

We consider ε_0 to be the vacuum permittivity, i.e. $\varepsilon_0 = 8.8541878... \times 10^{-12} \frac{\mathrm{A}^2\,\mathrm{s}^4}{\mathrm{kg}\,\mathrm{m}^3}$, and $\varepsilon_1 = \varepsilon_0\varepsilon_r$ with different values of the relative permittivity ε_r. We restrict ourselves to incoming waves of the form

$$\mathbf{E}^{\mathrm{inc}}(x) = \mathbf{E}_0 e^{i\omega\sqrt{\varepsilon_0\mu_0}d\cdot x} \quad \text{for } x \in \mathbb{R}^3,$$

with $\|d\|_2 = 1$, which corresponds to $-\nabla\Phi_{\mathrm{part}}$ in Section 1.2 and $\mu_0 = 4\pi \times 10^{-7} \frac{\mathrm{V\,s}}{\mathrm{A\,m}}$ is the vacuum permeability. In the quasi-static case we can approximate the incoming wave by $\mathbf{E}^{\mathrm{inc}}_{\mathrm{qs}}(x) \equiv \mathbf{E}_0$.

Throughout this chapter we also use the modified evaluations (2.29), (2.32) and (2.33) in the case of a simply connected domain, since we will only consider domains with this property. For the linear systems we will use the fast multipole method, see, e.g., [11, 27], with a maximal level of 6 or 7, a polynomial degree of 6 or 7 and a nearfield parameter of 3.5.

For our error computations we use the $L^2(\Gamma)$-norm and the norm $\|\cdot\|_V$, which is given by

$$\|w\|_V^2 = \frac{1}{4\pi} \int_\Gamma w(x) \int_\Gamma \frac{1}{|x-y|} w(y) ds_y ds_x, \tag{4.1}$$

to calculate a relative error in $H^{-\frac{1}{2}}(\Gamma)$, as the single layer boundary integral operator V induces an equivalent norm. We calculate the norms on the finest refinement level and the integrals by a seven-point approximation.

4.1 Dipole Moment and Scattering Cross Section

Before we discuss some numerical examples we introduce two additional quantities. We are interested in their computation and possible error estimates for the numerical approximations.

The first quantity of interest is the electric dipole moment $p = \|\mathbf{p}\|_2$,

$$\mathbf{p}[j] := \varepsilon_0 \int_\Gamma x_j \sigma(x) ds_x, \qquad j = 1, 2, 3, \tag{4.2}$$

which is "a measure of the separation of positive and negative electrical charges within a system" ([38]). The occurring σ is the surface charge density, which can be computed by

$$\sigma := \mathbf{E}_0^s\big|_{\partial\Omega^{\text{ext}}} \cdot \mathbf{n} - \mathbf{E}_1^s\big|_{\partial\Omega} \cdot \mathbf{n}, \tag{4.3}$$

where $\mathbf{E}^s := \mathbf{E} - \mathbf{E}_{\text{qs}}^{\text{inc}}$ is the scattered electric field. It corresponds to the density function w in the single layer potential formulation (2.2).

In our setting it is possible to calculate an approximation for (4.2) by

$$\widetilde{\mathbf{p}} = \varepsilon_0 \int_\Gamma x\, \sigma_h(x) ds_x = \varepsilon_0 \sum_{\ell=1}^{N} \int_{\tau_\ell} x\, \sigma_h(x) ds_x = \varepsilon_0 \sum_{\ell=1}^{N} \sigma_\ell |\tau_\ell| x_\ell^s, \tag{4.4}$$

where σ_ℓ is the constant $\sigma_h(x)$ for $x \in \tau_\ell$ and x_ℓ^s is the center of τ_ℓ.

For the numerical computation of σ in the single layer potential approach we solve the system of linear equations (3.1), which yields an approximation of σ by

$$\sigma_h^{SL} = w_h. \tag{4.5}$$

For the Steklov–Poincaré interface equation we plug the evaluation of the electric field (2.27) into (4.3) to obtain

$$\sigma = \gamma_1^{\text{int}} \Phi_1 - \gamma_1^{\text{ext}} \Phi_0,$$

which corresponds to a numerical approximation by

$$\sigma_h^{SP} = t_{1,h} - t_{0,h}. \tag{4.6}$$

For the double layer formulation we use the computed internal and external electric fields $\widetilde{\mathbf{E}}_1$ and $\widetilde{\mathbf{E}}_0$ in the centers of the elements to obtain

$$\sigma_h^{DL} = (\widetilde{\mathbf{E}}_0 - \widetilde{\mathbf{E}}_1) \cdot \mathbf{n}. \tag{4.7}$$

Lemma 4.1. *Let $\sigma, \sigma_h \in H^\mu(\Gamma)$ for some $\mu \in \mathbb{R}$ and let $\widetilde{p} := \|\widetilde{\mathbf{p}}\|_2$, where $\widetilde{\mathbf{p}}$ is the approximation given by (4.4). Then there holds that*

$$|p - \widetilde{p}| \leq c\|\sigma - \sigma_h\|_{H^\mu(\Gamma)}.$$

Remark 4.1. *In fact μ is restricted by the given error estimates for σ and σ_h. In the case of the Steklov–Poincaré formulation we will see that we are able to give an estimate for $\mu \geq -2$.*

Proof. We start by using triangle inequality to obtain

$$|p - \widetilde{p}| = |\|\mathbf{p}\|_2 - \|\widetilde{\mathbf{p}}\|_2| \leq \|\mathbf{p} - \widetilde{\mathbf{p}}\|_2 = \sqrt{\sum_{j=1}^{3} (\mathbf{p}[j] - \widetilde{\mathbf{p}}[j])^2}.$$

For $j \in \{1, 2, 3\}$ we have

$$\begin{aligned} |\mathbf{p}[j] - \widetilde{\mathbf{p}}[j]| &= \left| \varepsilon_0 \int_\Gamma x_j \, \sigma(x) ds_x - \varepsilon_0 \int_\Gamma x_j \, \sigma_h(x) ds_x \right| \\ &= \varepsilon_0 \left| \int_\Gamma x_j (\sigma(x) - \sigma_h(x)) ds_x \right| = \varepsilon_0 |\langle x_j, \sigma - \sigma_h \rangle_\Gamma|. \end{aligned}$$

Since x_j is a linear function of $x \in \mathbb{R}^3$ it is arbitrarily smooth and we obtain by using duality

$$|\mathbf{p}[j] - \widetilde{\mathbf{p}}[j]| \leq \varepsilon_0 \|x_j\|_{H^{-\mu}(\Gamma)} \|\sigma - \sigma_h\|_{H^\mu(\Gamma)}.$$

Hence we have

$$|p - \widetilde{p}| \leq \varepsilon_0 \|\sigma - \sigma_h\|_{H^\mu(\Gamma)} \sqrt{\sum_{j=1}^{3} \|x_j\|^2_{H^{-\mu}(\Gamma)}} \leq c\|\sigma - \sigma_h\|_{H^\mu(\Gamma)}$$

□

The second physical quantity, which we would like to discuss is the scattering cross section, which is given by

$$C_{sca} = \frac{1}{6\pi} \omega^4 \mu_0^2 p^2 \tag{4.8}$$

in the quasi-static case. We will show that the error convergence is asymptotically equal to the error behavior of the dipole moment.

Lemma 4.2 ([25]). *For the approximation*

$$\widetilde{C}_{sca} = \frac{1}{6\pi}\omega^4\mu_0^2\widetilde{p}^2$$

of the scattering cross section C_{sca} there holds

$$|C_{sca} - \widetilde{C}_{sca}| = \mathcal{O}(|p - \widetilde{p}|).$$

Proof. We define $\delta := p - \widetilde{p}$ and therefore $\widetilde{p} = p - \delta$. We have

$$|p^2 - \widetilde{p}^2| = |(p + \widetilde{p})(p - \widetilde{p})| = |2p - \delta||\delta|$$

and hence

$$\begin{aligned}\lim_{\sigma_h \to \sigma} \left| \frac{|C_{sca} - \widetilde{C}_{sca}|}{|p - \widetilde{p}|} \right| &= \frac{1}{6\pi}\omega^4\mu_0^2 \lim_{\delta \to 0} \frac{|p^2 - \widetilde{p}^2|}{|p - \widetilde{p}|} = \frac{1}{6\pi}\omega^4\mu_0^2 \lim_{\delta \to 0} \frac{|2p - \delta||\delta|}{|\delta|} \\ &= \frac{1}{6\pi}\omega^4\mu_0^2 \lim_{\delta \to 0} |2p - \delta| < \infty\end{aligned}$$

□

Using (4.16) and Lemma 4.2 we obtain for $\Phi \in H^s(\Gamma)$, $s \in [\frac{1}{2}, 2]$:

$$|C_{sca} - \widetilde{C}_{sca}| = \mathcal{O}(h^{s-\mu}). \tag{4.9}$$

4.2 Sphere

Our first example is a sphere with radius $r = 1$, incoming wave $\mathbf{E}_0 = (0, 0, 1)^\top$ and relative permittivity $\varepsilon_r = 5$. We discretize the geometry with different uniformly refined levels $L = 0, \ldots, 7$ by $8 \cdot 4^L$ plane triangles with nodes on the sphere surface, where the corresponding number of panels and nodes are given by Table 4.1.

For the sphere we have analytical solutions for all occurring quantities, see, e.g., [16, p. 114]. We will start with the density of the single layer potential ansatz w_h, which is computed by (3.1), and the double layer density v_h, which is calculated by (3.16). For the Steklov–Poincaré formulation we observe the errors of the Neumann data t_h.

Densities and Neumann data

For the densities of the single layer potential and double layer potential approaches we have analytical solutions given by

$$w(x) = 3 \left| \frac{\varepsilon_r - 1}{\varepsilon_r + 2} \right| \|\mathbf{E}_0\|_2 x_3$$

Level	Panels	Nodes
0	8	6
1	32	18
2	128	66
3	512	258
4	2048	1026
5	8192	4098
6	32768	16386
7	131072	65538

Table 4.1: Number of nodes and panels of the sphere

and

$$v(x) = -3\varepsilon_0 \left| \frac{\varepsilon_r - 1}{\varepsilon_r + 2} \right| \|\mathbf{E}_0\|_2 x_3.$$

For the Neumann data we have

$$t_1(x) = \left| \frac{\varepsilon_r - 1}{\varepsilon_r + 2} \right| \|\mathbf{E}_0\|_2 n(x)_3,$$

where $n(x)$ is the normal vector in x and

$$t_0(x) = -3 \left| \frac{\varepsilon_r - 1}{\varepsilon_r + 2} \right| \|\mathbf{E}_0\|_2 \left(x_3 - \frac{n(x)_3}{3} \right).$$

We denote by v_L, w_L, and $t_{1,L}$ for $L = 0, \ldots, 7$ the approximate solutions of the single layer density, the double layer density, and the interior Neumann data of the Steklov–Poincaré formulation on the corresponding levels. The relative errors for w_L in $\|\cdot\|_V$ and the relative errors of v_L, w_L, and $t_{1,L}$ in $\|\cdot\|_{L^2(\Gamma)}$, as well as the estimate orders of convergence are given in Table 4.2. We observe that the convergence rate of the double layer density is approximately 2.00, which corresponds to the highest order expected by the approximation property of $S_h^1(\Gamma)$. The convergence rate of the single layer density is about 1.85, where we would expect only 1.5 by the approximation property of $S_h^0(\Gamma)$. The convergence order of the interior Neumann data is approximately 1.00, which is the highest order that could be obtained by Theorem 3.8. Note that we do not consider the effects of the approximation of the sphere in our error analysis. It can be shown that this additional approximation does not reduce the order of convergence [23, 24].

Potential

In this section we will study the errors made by the different approaches, when computing the potential Φ. For the single layer and double layer formulation we obtain

L	$\frac{\|w_L-w\|_V}{\|w\|_V}$	eoc	$\frac{\|v_L-v\|_{L^2(\Gamma)}}{\|v\|_{L^2(\Gamma)}}$	eoc	$\frac{\|t_{1,L}-t_1\|_{L^2(\Gamma)}}{\|t_1\|_{L^2(\Gamma)}}$	eoc
0	2.20e-1		7.70e-2		2.05e-3	
1	7.94e-2	1.47	3.12e-2	1.31	3.62e-2	−4.14
2	2.24e-2	1.82	8.47e-3	1.88	1.52e-2	1.25
3	6.11e-3	1.88	1.74e-3	2.28	5.87e-3	1.37
4	1.66e-3	1.88	4.11e-4	2.09	2.51e-3	1.23
5	4.54e-4	1.87	9.97e-5	2.04	1.07e-3	1.24
6	1.28e-4	1.82	2.61e-5	1.93	4.97e-4	1.10
7	3.76e-5	1.77	6.15e-6	2.09	2.77e-4	0.84

Table 4.2: Sphere with $\varepsilon_r = 5.0$, Errors of the densities

the potentials from the densities by using the single layer ansatz (2.1) and the double layer ansatz (2.23). Therefore we have

$$\Phi_h^{SL} := \widetilde{V} w_h \tag{4.10}$$

and

$$\Phi_h^{DL} := -W v_h. \tag{4.11}$$

For the Steklov–Poincaré interface equation the potential Φ_h^{SP} is computed directly by (3.7). We compare the relative errors with respect to the $L^2(\Gamma)$-norm to the analytical solution

$$\Phi(x) = -\left(\frac{3}{\varepsilon_r + 2}\right) \|\mathbf{E}_0\|_2 x_3. \tag{4.12}$$

The numerical results are given in Table 4.3. The $L^2(\Gamma)$-errors are computed on every level by seven point integration. We observe quadratic convergence for all three formulations. For the Steklov–Poincaré formulation this is what we expect by Theorem 3.6. In the two other cases it corresponds to the order in the approximation property of $S_h^1(\Gamma)$.

For the double layer potential we have

$$\|\Phi_h^{DL} - \Phi\|_{L^2(\Gamma)} = \frac{1}{\varepsilon_0} \|\widetilde{\Phi}_{0,h}^{DL} - \widetilde{\Phi}_0\|_{L^2(\Gamma)} \leq c \|v_h - v\|_{L^2(\Gamma)}. \tag{4.13}$$

Hence we expect the same convergence rates for potential and density, which corresponds to our observation of both having quadratic convergence, see Table 4.2.

If we assume that there holds

$$\|w_h - w\|_{H^{-1}(\Gamma)} \leq c h^{\frac{1}{2}} \|w_h - w\|_{H^{-\frac{1}{2}}(\Gamma)},$$

L	$\frac{\|\Phi_L^{SL}-\Phi\|_{L^2(\Gamma)}}{\|\Phi\|_{L^2(\Gamma)}}$	eoc	$\frac{\|\Phi_L^{DL}-\Phi\|_{L^2(\Gamma)}}{\|\Phi\|_{L^2(\Gamma)}}$	eoc	$\frac{\|\Phi_L^{SP}-\Phi\|_{L^2(\Gamma)}}{\|\Phi\|_{L^2(\Gamma)}}$	eoc
0	3.61e-1		2.45e-1		2.05e-3	
1	1.09e-1	1.73	7.80e-2	1.65	1.50e-2	−2.87
2	2.78e-2	1.97	1.93e-2	2.02	4.27e-3	1.81
3	6.89e-3	2.01	4.89e-3	1.98	1.14e-3	1.91
4	1.70e-3	2.02	1.22e-3	2.01	2.98e-4	1.93
5	4.23e-4	2.01	3.03e-4	2.01	7.63e-5	1.96
6	1.05e-4	2.01	7.56e-5	2.00	1.93e-5	1.98
7	2.62e-5	2.00	1.89e-5	2.00	4.89e-6	1.98

Table 4.3: Sphere with $\varepsilon_r = 5.0$, Errors of the potentials

then we obtain a similar estimate for the single layer potential by linearity and boundedness of $V : H^{-1}(\Gamma) \to L^2(\Gamma)$, see [4]:

$$\begin{aligned} \|\Phi_h^{SL} - \Phi\|_{L^2(\Gamma)} &= \|V(w_h - w)\|_{L^2(\Gamma)} \\ &\leq c\|w_h - w\|_{H^{-1}(\Gamma)} \leq ch^{\frac{1}{2}}\|w_h - w\|_{H^{-\frac{1}{2}}(\Gamma)}. \end{aligned} \tag{4.14}$$

Therefore we would expect that the convergence rate of the potential is half an order higher as the one given by the density, but actually the rates are 2.00 and 1.85.

Furthermore we see that we obtain the smallest errors on every level, if we use the Steklov–Poincaré interface equation and the largest errors by using the single layer formulation. The Steklov–Poincaré solution is roughly one level better than the other two solutions.

Electric field

Next we consider the electric field. We use the calculations given in Chapter 3, i.e. for the single layer potential formulation we compute the electric field by (3.2), for the Steklov–Poincaré approach by (3.11) and for the double layer potential formulation by (3.17). The analytical solution for the electric field on the sphere is given by

$$\mathbf{E} = \left(0, 0, \frac{3}{\varepsilon_r + 2}\right)^\top.$$

The numerical results for the standard calculation are given in Table 4.4. In Table 4.5 one can find results for the adapted calculation for a simply connected domain, i.e. computing the electric field for the single layer approach by (3.3), for the Steklov–Poincaré formulation by (3.12) and for the double layer potential approach by (3.18).

For the electric fields given by the single layer and double layer approach we obtain linear convergence of the errors, for the Steklov–Poincaré formulation the order of

L	$\frac{\|\mathbf{E}_L^{SL}-\mathbf{E}\|_V}{\|\mathbf{E}\|_V}$	eoc	$\frac{\|\mathbf{E}_L^{DL}-\mathbf{E}\|_V}{\|\mathbf{E}\|_V}$	eoc	$\frac{\|\mathbf{E}_L^{SP}-\mathbf{E}\|_V}{\|\mathbf{E}\|_V}$	eoc
0	3.35e-1		6.08e-2		2.74e-3	
1	1.59e-1	1.07	3.34e-2	0.86	2.28e-2	−3.06
2	8.26e-2	0.95	1.74e-2	0.94	7.14e-3	1.68
3	4.39e-2	0.91	9.01e-3	0.95	2.10e-3	1.76
4	2.28e-2	0.94	4.62e-3	0.96	6.14e-4	1.77
5	1.16e-2	0.97	2.35e-3	0.98	1.75e-4	1.81
6	5.87e-3	0.99	1.18e-3	0.99	5.04e-5	1.80
7	2.95e-3	0.99	5.94e-4	0.99	1.52e-5	1.73

Table 4.4: Sphere with $\varepsilon_r = 5.0$, Errors of the electric field

L	$\frac{\|\mathbf{E}_L^{SL}-\mathbf{E}\|_V}{\|\mathbf{E}\|_V}$	eoc	$\frac{\|\mathbf{E}_L^{DL}-\mathbf{E}\|_V}{\|\mathbf{E}\|_V}$	eoc	$\frac{\|\mathbf{E}_L^{SP}-\mathbf{E}\|_V}{\|\mathbf{E}\|_V}$	eoc
0	4.86e-1		6.08e-2		8.36e-3	
1	1.98e-1	1.30	3.43e-2	0.83	2.22e-2	−1.41
2	7.55e-2	1.39	1.75e-2	0.97	7.06e-3	1.65
3	3.43e-2	1.14	9.02e-3	0.96	2.07e-3	1.77
4	1.71e-2	1.00	4.63e-3	0.96	5.95e-4	1.80
5	8.66e-3	0.98	2.35e-3	0.98	1.65e-4	1.85
6	4.37e-3	0.99	1.18e-3	0.99	4.52e-5	1.87
7	2.20e-3	0.99	5.94e-4	0.99	1.25e-5	1.85

Table 4.5: Sphere with $\varepsilon_r = 5.0$, Errors of the electric field, simply connected

convergence is approximately 1.8. The errors of the Steklov–Poincaré formulation are by far the lowest ones. By comparing Table 4.4 and Table 4.5 we see that the single layer approach and the Steklov–Poincaré formulation perform slightly better, when calculating the electric field by the modified computation in the simply connected case. If we assume that that the convergence rate of the electric field is similar to the one of $\mathbf{E} \cdot n$ we are able to provide some estimates for the electric field.

For the single layer potential formulation we obtain, in the case of calculation for simply connected domains, with (3.3) the estimate:

$$\begin{aligned}
&\|\mathbf{E}^{SL}\cdot n - \mathbf{E}\cdot n\|_{H^{-\frac{1}{2}}(\Gamma)} \\
&\quad = \|\nabla\widetilde{V}(w_{j,h} - w_h)\cdot n - (-\nabla\Phi_{\text{part}} - \nabla(\widetilde{V}w))\cdot n\|_{H^{-\frac{1}{2}}(\Gamma)} \\
&\quad \leq \|\nabla(\widetilde{V}w_{j,h})\cdot n - (-\nabla\Phi_{\text{part}})\cdot n\|_{H^{-\frac{1}{2}}(\Gamma)} + \|\nabla(\widetilde{V}(w - w_h))\cdot n\|_{H^{-\frac{1}{2}}(\Gamma)},
\end{aligned}$$

and hence we have

$$\begin{aligned}&\|\mathbf{E}^{SL}\cdot n-\mathbf{E}\cdot n\|_{H^{-\frac{1}{2}}(\Gamma)}\\&\quad\leq\underbrace{\|\nabla(\widetilde{V}w_{j,h})\cdot n-(-\nabla\Phi_{\text{part}})\cdot n\|_{H^{-\frac{1}{2}}(\Gamma)}}_{(*)}+c\|w-w_h\|_{H^{-\frac{1}{2}}(\Gamma)}.\end{aligned}\tag{4.15}$$

We will study the term $(*)$ later. In the general case we obtain by using (3.2)

$$\begin{aligned}\|\mathbf{E}^{SL}\cdot n-\mathbf{E}\cdot n\|_{H^{-\frac{1}{2}}(\Gamma)}&\leq\|\nabla(\widetilde{V}(w-w_h))\cdot n\|_{H^{-\frac{1}{2}}(\Gamma)}\\&\leq c\|w-w_h\|_{H^{-\frac{1}{2}}(\Gamma)}.\end{aligned}$$

Hence we could assume that the convergence rate for the error of the electric field computed by the single layer approach behaves like the error of the single layer density, which is not the case, since we have only 1.0, the expected maximal convergence rate by the approximation property is 1.5 and the actual observed convergence rate in Table 4.2 was 1.85.

For the double layer approach by similar calculations using the evaluations (3.17) and (3.18) and assuming

$$\|v_h-v\|_{H^{\frac{1}{2}}(\Gamma)}\leq ch^{-\frac{1}{2}}\|v_h-v\|_{L^2(\Gamma)},$$

we obtain

$$\begin{aligned}&\|\mathbf{E}^{DL}\cdot n-\mathbf{E}\cdot n\|_{H^{-\frac{1}{2}}(\Gamma)}\\&\quad\leq\begin{cases}ch^{-\frac{1}{2}}\|v-v_h\|_{L^2(\Gamma)} & \text{simply conn.,}\\ c\left(h^{-\frac{1}{2}}\|v-v_h\|_{L^2(\Gamma)}+\|g-g_h\|_{H^{-\frac{1}{2}}(\Gamma)}+\|\widetilde{\psi}-\widetilde{\psi}_h\|_{H^{\frac{1}{2}}(\Gamma)}\right) & \text{else.}\end{cases}\end{aligned}$$

This means the convergence rate should be half an order lower than the one obtained by the double layer density in the $L^2(\Gamma)$-norm, which is not the observed result, since we see 1.00 for the electric field and 2.00 for the density.

For the Steklov–Poincaré operator formulation we have by evaluation (3.11)

$$\|\mathbf{E}^{SP}\cdot n-\mathbf{E}\cdot n\|_{H^{-\frac{1}{2}}(\Gamma)}\leq\|t_{i,h}-t_i\|_{H^{-\frac{1}{2}}(\Gamma)}$$

for the standard calculation, where t_i corresponds to the respective Neumann datum, and by evaluation (3.12)

$$\begin{aligned}&\|\mathbf{E}^{SP}\cdot n-\mathbf{E}\cdot n\|_{H^{-\frac{1}{2}}(\Gamma)}\\&\quad\leq\left(\|(-\nabla\Phi_{part}-(\nabla(\widetilde{V}(S_1\widetilde{\psi}_h))-\nabla(W\widetilde{\psi}_h)))\cdot n\|_{H^{-\frac{1}{2}}(\Gamma)}+\|t_{1,h}-t_1\|_{H^{-\frac{1}{2}}(\Gamma)}\right)\end{aligned}$$

L	$\frac{\lvert p_L^{SL}-p\rvert}{p}$	eoc	$\frac{\lvert p_L^{DL}-p\rvert}{p}$	eoc	$\frac{\lvert p_L^{SP}-p\rvert}{p}$	eoc
0	7.52e-1		7.25e-1		6.84e-1	
1	3.45e-1	1.12	3.60e-1	1.01	2.97e-1	1.21
2	1.05e-1	1.71	1.36e-1	1.40	8.84e-2	1.75
3	2.77e-2	1.93	5.04e-2	1.43	2.32e-2	1.93
4	7.00e-3	1.98	2.03e-2	1.32	5.87e-3	1.98
5	1.75e-3	2.00	8.85e-3	1.20	1.47e-3	2.00
6	4.39e-4	2.00	4.10e-3	1.11	3.68e-4	2.00
7	1.10e-4	2.00	1.97e-3	1.06	9.21e-5	2.00

Table 4.6: Sphere with $\varepsilon_r = 5.0$, Errors of the dipole moment

for the adapted calculation in case of a simply connected domain. Therefore we would expect a convergence rate, which is lower or equal to the convergence rate of the Neumann data in the $H^{\frac{1}{2}}(\Gamma)$-norm. By Theorem 3.8 we expect an order of convergence of 1.5. In Table 4.5 we observe an order of 1.85, which is higher than the expected 1.5. Note that we have not taken into account the boundary approximation in these considerations.

Dipole moment and scattering cross section

The analytical value of the electric dipole moment is given by

$$p = 4\pi\varepsilon_0 \left|\frac{\varepsilon_r - 1}{\varepsilon_r + 2}\right| \|\mathbf{E}_0\|_2.$$

We calculate approximations $\widetilde{p}$ of the dipole moment as shown in Section 4.1 and we investigate the relative error $\frac{|\widetilde{p}-p|}{p}$. Thus we obtain the errors in Table 4.6.

For the single layer approach we observe quadratic convergence. By Lemma 4.1 we have

$$|p - p^{SL}| \leq c\|w - w_h\|_{H^\mu(\Gamma)},$$

for some $\mu \leq -\frac{1}{2}$. Hence we also have that the convergence order of the dipole should be greater equal to the one obtained by the single layer density. This is satisfied by the quadratic order, since the convergence rate obtained by the single layer density was only 1.8.

We also observe quadratic convergence for the Steklov–Poincaré formulation. With Lemma 4.1 we obtain, since $\sigma \in H^{-\frac{1}{2}}(\Gamma), \sigma_h^{SP} \in L^2(\Gamma)$ and therefore $\sigma, \sigma_h^{SP} \in H^\mu(\Gamma)$, that there holds

$$|p - p^{SP}| \leq c\|\sigma - \sigma_h^{SP}\|_{H^\mu(\Gamma)} \leq c\left(\|t_0 - t_{0,h}\|_{H^\mu(\Gamma)} + \|t_1 - t_{1,h}\|_{H^\mu(\Gamma)}\right).$$

L	$\frac{\lvert C^{SL}_{sca,L}-C_{sca}\rvert}{C_{sca}}$	eoc	$\frac{\lvert C^{DL}_{sca,L}-C_{sca}\rvert}{C_{sca}}$	eoc	$\frac{\lvert C^{SP}_{sca,L}-C_{sca}\rvert}{C_{sca}}$	eoc
0	9.38e-1		9.24e-1		9.00e-1	
1	5.71e-1	0.72	5.90e-1	0.65	5.05e-1	0.83
2	1.99e-1	1.52	2.53e-1	1.22	1.69e-1	1.58
3	5.46e-2	1.87	9.84e-2	1.36	4.58e-2	1.88
4	1.40e-2	1.97	4.01e-2	1.29	1.17e-2	1.97
5	3.51e-3	1.99	1.76e-2	1.19	2.94e-3	1.99
6	8.77e-4	2.00	8.18e-3	1.11	7.36e-4	2.00
7	2.19e-4	2.00	3.93e-3	1.06	1.84e-4	2.00

Table 4.7: Sphere with $\varepsilon_r = 5.0$, Errors of the scattering cross section

We now restrict $\mu \geq -2$, since then Theorem 3.8 is applicable if we additionally assume that the operators $\left(\frac{1}{2}I \pm K\right) : H^{-1}(\Gamma) \to H^{-1}(\Gamma)$ are bounded. This holds true for the sphere by [4]. By using Theorem 3.8 there holds the error estimate

$$|p - p^{SP}| \leq ch^{s+2}\|\Phi\|_{H^{s+1}(\Gamma)}, \tag{4.16}$$

for $s \in [-\frac{1}{2}, 1]$. This error analysis neglects the approximation of the sphere by plane triangles. This additional error was investigated in [23, 24] and an error estimate for the potential with quadratic order was proven. Similarly, we observe only quadratic convergence in Table 4.6. A quadratic convergence rate was observed for two and three dimensions in a similar setting of a transmission problem in [22].

For the double layer potential we obtain linear convergence of the dipole moment, which is plausible, since by

$$|p - p^{DL}| \leq c\left(\|\mathbf{E}_0^{DL} - \mathbf{E}_0\|_{H^\mu(\Gamma)} + \|\mathbf{E}_1^{DL} - \mathbf{E}_1\|_{H^\mu(\Gamma)}\right), \tag{4.17}$$

the convergence rate is greater or equal than the order of convergence of the electric field, for which we observed 1.0 in Table 4.5.

The errors for the scattering cross section (4.8) are given in Table 4.7. We see that the errors behaves like the errors of the dipole moments at higher levels, which we expect by Lemma 4.2. We also observe that for the higher levels the scattering cross section error is approximately twice the error of the dipole for all three formulations. Therefore it suffices to consider the dipole error for the comparison of computational times, which is our next task.

Comparison of computational times

In Tables 4.8 and 4.9 the single layer potential ansatz, the double layer potential formulation, and the Steklov–Poincaré operator formulation are compared with respect

L	$\frac{\|\mathbf{E}_L^{SL}-\mathbf{E}\|_V}{\|\mathbf{E}\|_V}$	Time(sec.)	$\frac{\|\mathbf{E}_L^{DL}-\mathbf{E}\|_V}{\|\mathbf{E}\|_V}$	Time(sec.)	$\frac{\|\mathbf{E}_L^{SP}-\mathbf{E}\|_V}{\|\mathbf{E}\|_V}$	Time(sec.)
0	4.86e-1	0	6.08e-2	0	8.36e-3	0
1	1.98e-1	0	3.43e-2	0	2.22e-2	0
2	7.55e-2	0	1.75e-2	0	7.06e-3	0
3	3.43e-2	0	9.02e-3	3	2.07e-3	5
4	1.71e-2	3	4.63e-3	15	5.95e-4	72
5	8.66e-3	14	2.35e-3	83	1.65e-4	184
6	4.37e-3	76	1.18e-3	365	4.52e-5	927
7	2.20e-3	240	5.94e-4	1087	1.25e-5	3205

Table 4.8: Sphere with $\varepsilon_r = 5.0$, Errors of the electric field with times

L	$\frac{\|p_L^{SL}-p\|}{p}$	Time(sec.)	$\frac{\|p_L^{DL}-p\|}{p}$	Time(sec.)	$\frac{\|p_L^{SP}-p\|}{p}$	Time(sec.)
0	0.75	0	0.73	0	0.68	0
1	0.35	0	0.36	0	0.30	0
2	0.11	0	0.14	0	8.84e-2	0
3	2.77e-2	0	5.04e-2	3	2.32e-2	5
4	7.00e-3	3	2.03e-2	15	5.87e-3	72
5	1.75e-3	14	8.85e-3	83	1.47e-3	184
6	4.39e-4	76	4.10e-3	365	3.68e-4	927
7	1.10e-4	240	1.97e-3	1087	9.21e-5	3205

Table 4.9: Sphere with $\varepsilon_r = 5.0$, Errors of the dipole moment with times

to the computational times (without the postprocessing time needed for the error computation) and the accuracy of the dipole moment and the electric field.

When computing the electric field, we observe, that, with respect to the computational times on the same mesh, the single layer approach is the fastest one. The Steklov–Poincaré formulation has the longest computational times. But the observed order of convergence for the electric field is highest for the Steklov–Poincaré formulation and about the same for the other two formulations. We see that the Steklov–Poincaré formulation at refinement level 3 yields an error for the electric field, which is comparable to the error of the single layer approach on level 7 and the error of the double layer approach on level 5. With respect to the computational time for this error value the Steklov–Poincaré formulation outperforms the other two formulations. On the other hand the double layer approach performs better than the single layer approach.

However, if we take a look at the dipole errors, the errors of the single layer approach are comparable to the errors of the Steklov–Poincaré approach on every level,

but the single layer approach is much faster than the other two formulations. The Steklov–Poincaré formulation performs better than the double layer approach, since the error on level 4 is comparable to the error of the double layer formulation on level 7. This could be caused by the different approximations used for the computation of the dipole moment, where we do not have to do an extra computation for the single layer to obtain the surface charge density. The convergence orders of the errors of the single layer and Steklov–Poincaré formulations are very similar, whereas the convergence order for the double layer approach is not as high.

4.3 Cube

In this example we consider a microscopic particle in the form of a cube $\Omega = [0, a]^3$, where $a = 1\,\text{nm}$, with $\varepsilon_r = 2.25$ (glas), $\mathbf{E}_0 = (0, 0, 1)^\top$, and wavelength $\nu = 400\,\text{nm}$ in Ω^{ext} ($\omega = 4.7091 \cdot 10^{15}[\text{rad/s}]$). We discretize the geometry with refinement steps $L \in \{0, \ldots, 7\}$ by $24 \cdot 4^L$ plane triangles, where the corresponding number of panels and nodes are given in Table 4.10. We also consider $\varepsilon_r = 50000$ to test the numerical stability of the approaches. For the cube we do not have analytical solutions at hand. Therefore we use approximations of the best versions on the finest level as reference solutions. The formulation, which is used as reference may differ for various considered quantities.

In the computation we use a grid of the cube $[0, 1]^3$, hence a scaling of the input data and output data is necessary.

4.3.1 Scaling

Let $\varphi : \Omega = [0, a]^3 \to [0, 1]^3 = \Omega_*$, $x \mapsto \frac{1}{a} \cdot x =: x^*$. We define $\Omega_* := \varphi(\Omega)$ and also $\Omega_*^{\text{ext}} := \varphi(\Omega^{\text{ext}})$ and $\Gamma_* := \varphi(\Gamma)$. For a function $f : \Omega \to \mathbb{R}$ we define $f^* : \Omega_* \to \mathbb{R}$ as $f^*(x^*) := f(x)$, where $x = \varphi^{-1}(x^*)$. For the gradient of a function there holds

$$a \cdot \nabla f(\varphi^{-1}(x^*)) = \nabla^* f^*(x^*) \quad \text{for } x^* \in \Omega_*.$$

When we use this properties on (1.5) we obtain the dimensionless problem

$$-\Delta^* \Phi_1^*(x^*) = 0 \qquad \text{for } x^* \in \Omega_*, \tag{4.18a}$$

$$-\Delta^* \Phi_0^*(x^*) = 0 \qquad \text{for } x^* \in \Omega_*^{\text{ext}}, \tag{4.18b}$$

$$\Phi_1^*(x^*) = \Phi_0^*(x^*) \qquad \text{for } x^* \in \Gamma_*, \tag{4.18c}$$

$$\varepsilon_r \left(\frac{\partial^*}{\partial n} \Phi_1^*(x^*) \right) - \left(\frac{\partial^*}{\partial n} \Phi_0^*(x^*) \right) = (1 - \varepsilon_r)(0, 0, a)^\top \cdot \mathbf{n} \qquad \text{for } x^* \in \Gamma_*, \tag{4.18d}$$

$$\Phi_0^*(x^*) = \mathcal{O}\left(\frac{1}{|x^*|} \right) \qquad \text{as } |x^*| \to \infty. \tag{4.18e}$$

Level	Panels	Nodes
0	24	14
1	96	50
2	384	194
3	1536	770
4	6144	3074
5	24576	12290
6	98304	49154
7	393216	196610

Table 4.10: Number of nodes and panels of the cube

A surface integral on Γ_* can be computed as

$$a^2 \cdot \int_{\Gamma_*} f(x^*) ds_{x^*} = \int_{\Gamma} f(x) ds_x.$$

The transformation of the fundamental solution U^* is

$$U^*(\varphi(x), \varphi(y)) = \frac{1}{4\pi|\varphi(x) - \varphi(y)|} = \frac{a}{4\pi|x-y|} = a \cdot U^*(x, y).$$

With the mentioned properties it can be easily seen that the boundary integral operators transform in the following way for $w^* \in H^{-\frac{1}{2}}(\Gamma_*)$, $v^* \in H^{\frac{1}{2}}(\Gamma_*)$, $x^* \in \Omega_*$:

$$(\widetilde{V}^* w^*)(x^*) = \frac{1}{a} \cdot (\widetilde{V}(w^* \circ \varphi))(\varphi^{-1}(x^*)), \tag{4.19a}$$
$$(V^* w^*)(x^*) = \frac{1}{a} \cdot (V(w^* \circ \varphi))(\varphi^{-1}(x^*)), \tag{4.19b}$$
$$(K'^* w^*)(x^*) = (K'(w^* \circ \varphi))(\varphi^{-1}(x^*)), \tag{4.19c}$$
$$(K^* v^*)(x^*) = (K(v^* \circ \varphi))(\varphi^{-1}(x^*)), \tag{4.19d}$$
$$(W^* v^*)(x^*) = (W(v^* \circ \varphi))(\varphi^{-1}(x^*)), \tag{4.19e}$$
$$(D^* v^*)(x^*) = a \cdot (D(v^* \circ \varphi))(\varphi^{-1}(x^*)). \tag{4.19f}$$

The single layer formulation (2.2) of the transformed problem (4.18) is

$$\left(\frac{1}{2}\frac{\varepsilon_1 + \varepsilon_0}{\varepsilon_1 - \varepsilon_0} I + K'^*\right) w^* = (0, 0, a)^\top \cdot \mathbf{n} \quad \text{on } \Gamma_*,$$

which can be transformed using (4.19) to obtain

$$\left(\frac{1}{2}\frac{\varepsilon_1 + \varepsilon_0}{\varepsilon_1 - \varepsilon_0} I + K'\right) (\frac{1}{a} w^* \circ \varphi) = (0, 0, 1)^\top \cdot \mathbf{n} \quad \text{on } \Gamma.$$

If we compare this to the single layer formulation of the original problem (1.5) we obtain that

$$w_h = \frac{1}{a} w_h^* \circ \varphi,$$

where w_h is the solution of the single layer formulation (2.2) and not the direct transformation of w_h^*. Using the evaluation of the single layer potential formulation (2.26) we get

$$\widetilde{\mathbf{E}}(x) = (0,0,1)^\top - \frac{1}{a} \nabla^*(\widetilde{V}^* w_h^*)(\varphi(x)) \quad \text{for } x \in \mathbb{R}^3.$$

In the same manner we can transform the Steklov–Poincaré operator formulation (2.9) by $S_i^* v^*(x^*) = a \cdot (S_i(v^* \circ \varphi))(\varphi^{-1}(x^*))$ for $v^* \in H^{\frac{1}{2}}(\Gamma_*)$ to obtain

$$\begin{aligned} t_{i,h} &= \frac{1}{a} t_{i,h}^* \circ \varphi \quad \text{for } i = 1,2, \\ \Phi_h &= \Phi_h^* \circ \varphi, \end{aligned}$$

and by using the evaluation (2.27)

$$\begin{aligned} \widetilde{\mathbf{E}}(x) &= (0,0,1)^\top - \frac{1}{a} \left(\nabla^*(\widetilde{V}^* t_{1,h}^*)(\varphi(x)) - \nabla^*(W^* \Phi_h^*)(\varphi(x)) \right) && \text{for } x \in \Omega, \\ \widetilde{\mathbf{E}}(x) &= (0,0,1)^\top + \frac{1}{a} \left(\nabla^*(\widetilde{V}^* t_{0,h}^*)(\varphi(x)) - \nabla^*(W^* \Phi_h^*)(\varphi(x)) \right) && \text{for } x \in \Omega^{\text{ext}}. \end{aligned}$$

If we do the same for the double layer formulation (2.24) we observe

$$\begin{aligned} v_h &= v_h^* \circ \varphi, \\ \widetilde{\psi}_h &= \widetilde{\psi}_h^* \circ \varphi, \end{aligned}$$

and hence the electric field can be evaluated as in (2.28) by

$$\begin{aligned} \widetilde{\mathbf{E}}(x) &= (0,0,1)^\top + \frac{1}{a} \left(\frac{1}{\varepsilon_1} \nabla^*(W^* v_h^*)(\varphi(x)) - \frac{\varepsilon_1 - \varepsilon_0}{\varepsilon_1} \nabla^* \widetilde{\psi}_h^*(\varphi(x)) \right) && \text{for } x \in \Omega, \\ \widetilde{\mathbf{E}}(x) &= (0,0,1)^\top + \frac{1}{a} \left(\frac{1}{\varepsilon_0} \nabla^*(W^* v_h^*)(\varphi(x)) \right) && \text{for } x \in \Omega^{\text{ext}}. \end{aligned}$$

4.3.2 Error Convergence Study for $\varepsilon_r = 2.25$

Now we study the errors and convergence rates of the occurring quantities for the cube with relative permittivity $\varepsilon_r = 2.25$.

L	$\frac{\|w_L - w_7\|_V}{\|w_7\|_V}$	eoc	$\frac{\|v_L - v_7\|_{L^2(\Gamma)}}{\|v_7\|_{L^2(\Gamma)}}$	eoc
0	8.49e-2		2.59e-2	
1	4.12e-2	1.04	9.31e-3	1.47
2	2.13e-2	0.95	3.00e-3	1.63
3	1.12e-2	0.93	1.00e-3	1.58
4	5.86e-3	0.94	3.58e-4	1.48
5	2.94e-3	1.00	1.43e-4	1.32
6	1.28e-3	1.20	6.26e-5	1.19
7	0.00		0.00	

Table 4.11: Cube with $\varepsilon_r = 2.25$, Errors of the densities

L	$\frac{\|\Phi_L^{SL} - \Phi_7^{DL}\|_{L^2(\Gamma)}}{\|\Phi_7^{DL}\|_{L^2(\Gamma)}}$	eoc	$\frac{\|\Phi_L^{DL} - \Phi_7^{DL}\|_{L^2(\Gamma)}}{\|\Phi_7^{DL}\|_{L^2(\Gamma)}}$	eoc	$\frac{\|\Phi_L^{SP} - \Phi_7^{DL}\|_{L^2(\Gamma)}}{\|\Phi_7^{DL}\|_{L^2(\Gamma)}}$	eoc
0	6.08e-2		3.58e-2		8.78e-2	
1	1.99e-2	1.61	1.52e-2	1.24	2.96e-2	1.57
2	6.83e-3	1.54	5.19e-3	1.55	9.38e-3	1.66
3	2.45e-3	1.48	1.73e-3	1.59	3.09e-3	1.60
4	9.11e-4	1.43	5.84e-4	1.57	1.06e-3	1.54
5	3.48e-4	1.39	2.01e-4	1.54	3.77e-4	1.49
6	1.36e-4	1.36	6.81e-5	1.56	1.43e-4	1.40
7	5.29e-5	1.36	0.00e0		6.98e-5	1.03

Table 4.12: Cube with $\varepsilon_r = 2.25$, Errors of the potentials

Densities

For the single layer and double layer density we use the respective solutions on the seventh level for computing the relative errors. In Table 4.11 we see, that the convergence rate of the double layer density is approximately 1.45, whereas the convergence rate of the single layer density is about 0.95. Both convergence rates are lower than the ones obtained for the sphere, which is reasonable, since the sphere is the domain with smoother boundary. For a transmission problem with jumping coefficients we expect reduced regularity by [5].

Potential

Since the potential of the double layer approach on level 7 seems to be the best approximation we choose it as reference solution of the potential. The $L^2(\Gamma)$-errors are computed by prolongation to the finest level and 7 point integration. In Table 4.12

we observe that the estimated convergence rate of the single layer potential is about 1.4, therefore the convergence rate is approximately half an order higher as the convergence rate of the density, which is the expected outcome, see (4.14).

For the double layer potential we observe that the order of convergence is about 1.55, which is similar to the convergence rate of the double layer density in $L^2(\Gamma)$, and therefore also as expected by (4.13).

For the Steklov–Poincaré operator formulation we obtain an order of 1.5.

Electric field

We use the approximation $\mathbf{E}_7^{DL}$ of the double layer approach at level 7 as reference solution for the relative approximate $H^{-\frac{1}{2}}(\Gamma)$-errors of the electric field, as it is approximately of the same accuracy as the Steklov–Poincaré formulation, but faster and therefore more convenient in practice. The numerical results based on the standard approach and the simply connected version are given in Tables 4.13 and 4.14. In Table 4.13 we observe linear convergence for all three formulations. Based on the error tables the choice of the solution obtained from the double layer approach as reference solution seems appropriate. Both other formulations converge up to the seventh refinement level to this solution. The error on the seventh level of the Steklov–Poincaré formulation is smaller than the error of the double layer approach on level 6, which is why it is hard to say, if it is still meaningful, since at this point the two approaches are comparable.

In all three approaches we observe a lower convergence rate than for the sphere in Tables 4.4 and 4.5, which is expected by the reduced regularity of the solution [5]. If we compare the standard computation to the adapted one for simply connected domains, we observe that the double layer approach yields similar errors with a convergence rate of 1.0. The same holds true for the Steklov–Poincaré operator formulation. Concerning the single layer approach we obtain a discrepancy between the two variants, where the

L	$\frac{\|\mathbf{E}_L^{SL}-\mathbf{E}_7^{DL}\|_V}{\|\mathbf{E}_7^{DL}\|_V}$	eoc	$\frac{\|\mathbf{E}_L^{DL}-\mathbf{E}_7^{DL}\|_V}{\|\mathbf{E}_7^{DL}\|_V}$	eoc	$\frac{\|\mathbf{E}_L^{SP}-\mathbf{E}_7^{DL}\|_V}{\|\mathbf{E}_7^{DL}\|_V}$	eoc
0	5.07e-2		4.40e-2		4.25e-2	
1	2.63e-2	0.94	2.32e-2	0.93	2.36e-2	0.85
2	1.37e-2	0.94	1.22e-2	0.93	1.26e-2	0.91
3	7.08e-3	0.95	6.38e-3	0.93	6.66e-3	0.92
4	3.61e-3	0.97	3.26e-3	0.97	3.46e-3	0.95
5	1.79e-3	1.01	1.55e-3	1.07	1.69e-3	1.03
6	8.67e-4	1.04	5.96e-4	1.38	7.17e-4	1.24
7	5.01e-4	0.79	0.00e0		2.13e-4	1.75

Table 4.13: Cube with $\varepsilon_r = 2.25$, Errors of the electric field

L	$\frac{\|\mathbf{E}_L^{SL}-\mathbf{E}_7^{DL}\|_V}{\|\mathbf{E}_7^{DL}\|_V}$	eoc	$\frac{\|\mathbf{E}_L^{DL}-\mathbf{E}_7^{DL}\|_V}{\|\mathbf{E}_7^{DL}\|_V}$	eoc	$\frac{\|\mathbf{E}_L^{SP}-\mathbf{E}_7^{DL}\|_V}{\|\mathbf{E}_7^{DL}\|_V}$	eoc
0	3.44e-1		4.40e-2		4.32e-2	
1	2.13e-1	0.69	2.32e-2	0.93	2.39e-2	0.86
2	1.35e-1	0.66	1.22e-2	0.93	1.27e-2	0.91
3	8.67e-2	0.63	6.38e-3	0.93	6.72e-3	0.92
4	5.66e-2	0.62	3.26e-3	0.97	3.49e-3	0.94
5	3.71e-2	0.61	1.55e-3	1.07	1.71e-3	1.03
6	2.44e-2	0.61	5.96e-4	1.38	7.28e-4	1.24
7	1.59e-2	0.61	0.00e0		2.18e-4	1.74

Table 4.14: Cube with $\varepsilon_r = 2.25$, Errors of the electric field, simply connected

L	$\frac{\|\nabla(\widetilde{V}w_{j,h})\cdot n-(-\nabla\Phi_{\text{part}})\cdot n\|_V}{\|(-\nabla\Phi_{\text{part}})\cdot n\|_V}$	eoc
0	2.62e-1	
1	1.60e-1	0.71
2	1.00e-1	0.68
3	6.43e-2	0.64
4	4.19e-2	0.62
5	2.75e-2	0.61
6	1.81e-2	0.60
7	1.19e-2	0.60

Table 4.15: Cube, Errors of the particular solution

convergence rate of the standard computation is 1.0 and the order for the adapted computation is 0.6. We can explain this difference by the term $(*)$ occurring in the estimate (4.15). In Table 4.15 we see that this part causes the lower convergence rate of the electric field, since its order of convergence is 0.6. Therefore we can assume linear convergence of the electric field.

We now make the same assumptions on the electric field as in Section 4.2. Hence we expect the same convergence rate for the single layer density in $H^{-\frac{1}{2}}(\Gamma)$ and the electric field in $H^{-\frac{1}{2}}(\Gamma)$, which corresponds to the observed behavior. For the double layer formulation linear convergence is the expected outcome, since the density has approximately an order of 1.5 in $L^2(\Gamma)$. The errors of the electric field, obtained by the Steklov–Poincaré formulation, also show linear convergence. The considerations in Section 4.2 show that this corresponds to the expectation, as we guess that $\Phi \in H^{\frac{3}{2}}(\Gamma)$, since the convergence rate in Table 4.12 is 1.5.

L	$\frac{\lvert p_L^{SL}-p_7^{SP}\rvert}{p_7^{SP}}$	eoc	$\frac{\lvert p_L^{DL}-p_7^{SP}\rvert}{p_7^{SP}}$	eoc	$\frac{\lvert p_L^{SP}-p_7^{SP}\rvert}{p_7^{SP}}$	eoc
0	6.11e-2		5.41e-2		4.64e-3	
1	1.95e-2	1.65	2.37e-2	1.19	2.23e-3	1.06
2	5.86e-3	1.73	9.47e-3	1.32	5.93e-4	1.91
3	1.72e-3	1.76	3.59e-3	1.40	1.76e-4	1.76
4	5.04e-4	1.77	1.26e-3	1.51	5.57e-5	1.66
5	1.48e-4	1.77	3.73e-4	1.75	1.76e-5	1.66
6	4.47e-5	1.73	5.90e-5	2.66	4.59e-6	1.94
7	1.47e-5	1.60	3.60e-5	0.71	0.00	

Table 4.16: Cube with $\varepsilon_r = 2.25$, Errors of the dipole moment

L	$\frac{\lvert C_{sca,L}^{SL}-C_{sca,7}^{SP}\rvert}{C_{sca,7}^{SP}}$	eoc	$\frac{\lvert C_{sca,L}^{DL}-C_{sca,7}^{SP}\rvert}{C_{sca,7}^{SP}}$	eoc	$\frac{\lvert C_{sca,L}^{SP}-C_{sca,7}^{SP}\rvert}{C_{sca,7}^{SP}}$	eoc
0	1.18e-1		1.05e-1		9.31e-3	
1	3.85e-2	1.62	4.68e-2	1.17	4.47e-3	1.06
2	1.17e-2	1.72	1.89e-2	1.31	1.19e-3	1.91
3	3.45e-3	1.76	7.16e-3	1.40	3.51e-4	1.76
4	1.01e-3	1.77	2.52e-3	1.51	1.11e-4	1.66
5	2.96e-4	1.77	7.47e-4	1.75	3.52e-5	1.66
6	8.95e-5	1.73	1.18e-4	2.66	9.19e-6	1.94
7	2.95e-5	1.60	7.20e-5	0.71	1.21e-16	36.14

Table 4.17: Cube with $\varepsilon_r = 2.25$, Errors of the scattering cross section

.

Dipole moment and scattering cross section

We use the approximations given by the Steklov–Poincaré formulation on the seventh refinement level as reference solutions for the dipole moment and the scattering cross section. The results are shown in Tables 4.16 and 4.17. For the single layer approach we observe an estimated order of convergence of approximately 1.77, which is as expected to be higher than the convergence order of 1.0 in Table 4.11 of the single layer density. For the errors of the dipole moment obtained by the double layer approach we would expect a rate higher than the one obtained for the errors of the electric field of the double layer approach, see (4.17). This holds true, since we observe an estimated order of 1.6, while the order of the electric field in Table 4.14 is 1.0. In the case of computing the errors of the Steklov–Poincaré operator formulation the order of convergence is approximately 1.7. This is slightly lower than the convergence rate for the sphere in Table 4.6, which is 2.0. In Table 4.17 we observe again that the errors of the scattering

L	$\frac{\|\mathbf{E}_L^{SL}-\mathbf{E}_7^{DL}\|_V}{\|\mathbf{E}_7^{DL}\|_V}$	Time(sec.)	$\frac{\|\mathbf{E}_L^{DL}-\mathbf{E}_7^{DL}\|_V}{\|\mathbf{E}_7^{DL}\|_V}$	Time(sec.)	$\frac{\|\mathbf{E}_L^{SP}-\mathbf{E}_7^{DL}\|_V}{\|\mathbf{E}_7^{DL}\|_V}$	Time(sec.)
0	3.44e-1	0	4.40e-2	0	4.32e-2	0
1	2.13e-1	1	2.32e-2	0	2.39e-2	0
2	1.35e-1	1	1.22e-2	3	1.27e-2	3
3	8.67e-2	5	6.38e-3	21	6.72e-3	62
4	5.66e-2	12	3.26e-3	69	3.49e-3	177
5	3.71e-2	30	1.55e-3	173	1.71e-3	582
6	2.44e-2	84	5.96e-4	482	7.28e-4	2045
7	1.59e-2	293	0.00e0	1477	2.18e-4	8420

Table 4.18: Cube with $\varepsilon_r = 2.25$, Errors of the electric field with times

cross section behaves like the errors of the dipole moments at higher levels. We also see that for the higher levels the scattering cross section error is approximately twice the error of the dipole for all three formulations. Therefore it suffices also for this case to consider only the dipole moment for comparison of computational times.

Comparison of computational times

In Tables 4.18 and 4.19 the modified versions (3.3), (3.12), and (3.18) for simply connected domains for the single layer potential ansatz, the Steklov–Poincaré operator formulation, and the double layer potential formulation are compared with respect to the computational times (without the postprocessing time needed for the error computation) and the accuracy of the dipole moment and the electric field.

In Table 4.18 the accuracy of the electric field of the single layer approach is not as good as the observed accuracy in the other two formulations. The double layer approach is much faster than the Steklov–Poincaré formulation, if we aim for the

L	$\frac{\|p_L^{SL}-p_7^{SP}\|}{p_7^{SP}}$	Time(sec.)	$\frac{\|p_L^{DL}-p_7^{SP}\|}{p_7^{SP}}$	Time(sec.)	$\frac{\|p_L^{SP}-p_7^{SP}\|}{p_7^{SP}}$	Time(sec.)
0	6.11e-2	0	5.41e-2	0	4.64e-3	0
1	1.95e-2	1	2.37e-2	0	2.23e-3	0
2	5.86e-3	1	9.47e-3	3	5.93e-4	3
3	1.72e-3	5	3.59e-3	21	1.76e-4	62
4	5.04e-4	12	1.26e-3	69	5.57e-5	177
5	1.48e-4	30	3.73e-4	173	1.76e-5	582
6	4.47e-5	84	5.90e-5	482	4.59e-6	2045
7	1.47e-5	293	3.60e-5	1477	0.00e0	8420

Table 4.19: Cube with $\varepsilon_r = 2.25$, Errors of the dipole with times

same accuracy of the electric field.

In Table 4.19 one can observe for the dipole moment that the single layer formulation is far better with respect to computational performance than the other two formulations. The error of the sixth level is lower than the error of the double layer approach on level 6 and the error of the Steklov–Poincaré formulation on level 4. On the other hand the computational time needed is half the time of the Steklov–Poincaré formulation and less than a fifth of the double layer's computational time. We can also conclude that the double layer performs worst.

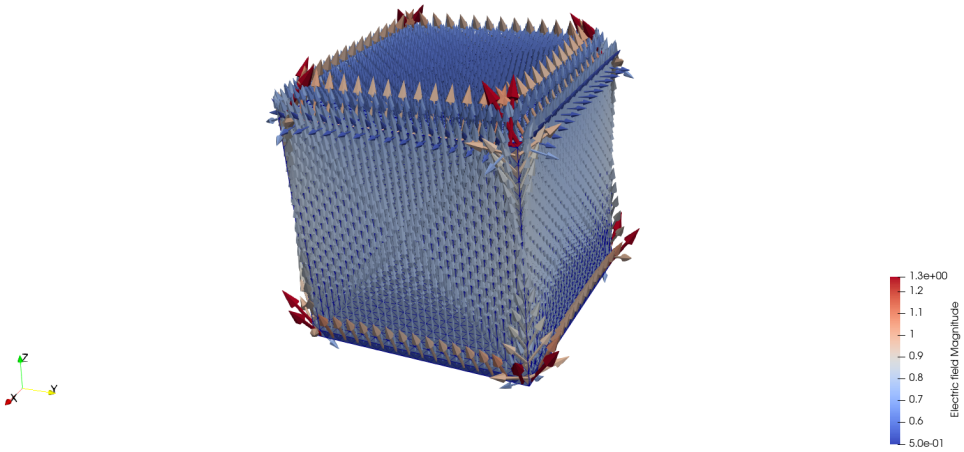

Figure 4.1: Electric field of the cube, single layer approach, $\varepsilon_r = 2.25$

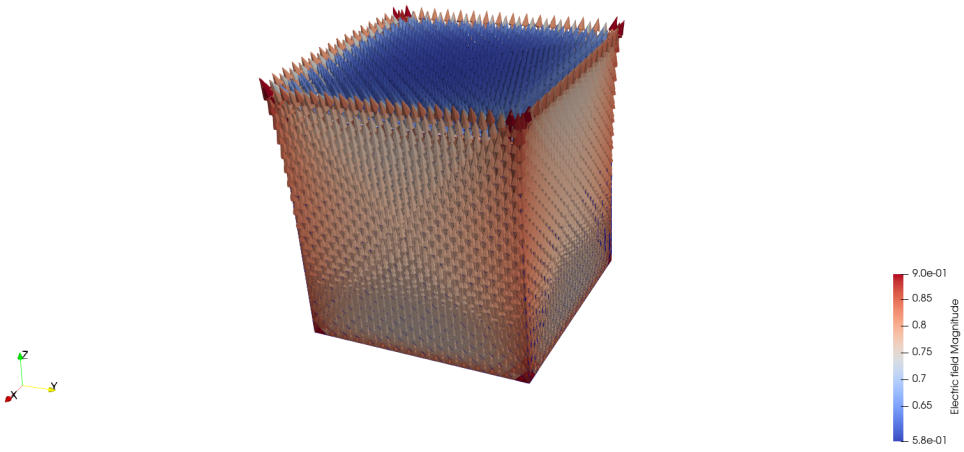

Figure 4.2: Electric field of the cube, Steklov–Poincaré formulation, $\varepsilon_r = 2.25$

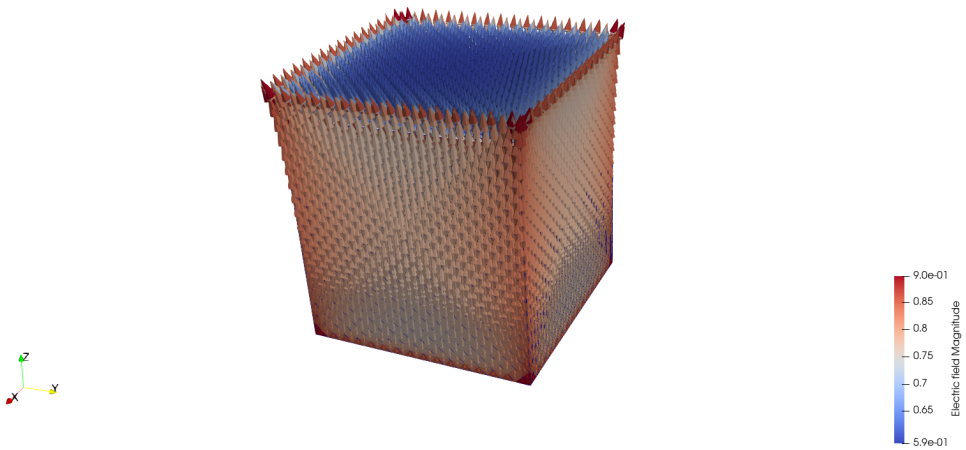

Figure 4.3: Electric field of the cube, double layer approach, $\varepsilon_r = 2.25$

In Figures 4.1–4.3 plots of the electric fields, computed by the different formulations with the modified variant in the simply connected case, are given. We see that the fields for the Steklov–Poincaré and double layer formulations are similar, only the electric field of the single layer approach seems to be inaccurate at edges and corners.

4.3.3 Error Convergence Study for $\varepsilon_r = 50000$

Densities

For the single layer and double layer density we use the respective solutions on the seventh level for computing the relative errors in Table 4.20.

The observed convergence rate for the double layer density is approximately 1.2,

L	$\frac{\|w_L - w_7\|_V}{\|w_7\|_V}$	eoc	$\frac{\|v_L - v_7\|_{L^2(\Gamma)}}{\|v_7\|_{L^2(\Gamma)}}$	eoc
0	3.34e-1		1.11e-1	
1	1.83e-1	0.87	3.96e-2	1.49
2	1.05e-1	0.80	1.44e-2	1.46
3	6.20e-2	0.77	5.67e-3	1.35
4	3.61e-2	0.78	2.38e-3	1.25
5	1.98e-2	0.87	1.07e-3	1.15
6	9.14e-3	1.12	4.88e-4	1.13
7	0.00e0		0.00e0	

Table 4.20: Cube with $\varepsilon_r = 50000$, Errors of the densities

L	$\frac{\|\Phi_L^{SL}-\Phi_7^{DL}\|_{L^2(\Gamma)}}{\|\Phi_7^{DL}\|_{L^2(\Gamma)}}$	eoc	$\frac{\|\Phi_L^{DL}-\Phi_7^{DL}\|_{L^2(\Gamma)}}{\|\Phi_7^{DL}\|_{L^2(\Gamma)}}$	eoc	$\frac{\|\Phi_L^{SP}-\Phi_7^{DL}\|_{L^2(\Gamma)}}{\|\Phi_7^{DL}\|_{L^2(\Gamma)}}$	eoc
0	2.52e-1		1.18e-1		1.72e-3	
1	1.01e-1	1.32	4.99e-2	1.24	4.65e-4	1.89
2	4.04e-2	1.32	1.77e-2	1.50	1.27e-4	1.88
3	1.65e-2	1.29	6.75e-3	1.39	3.70e-5	1.77
4	6.89e-3	1.26	2.76e-3	1.29	1.13e-5	1.71
5	2.93e-3	1.23	1.17e-3	1.23	3.53e-6	1.68
6	1.26e-3	1.21	5.05e-4	1.21	1.04e-6	1.76
7	5.46e-4	1.21	2.10e-4	1.26	0.00e0	

Table 4.21: Cube with $\varepsilon_r = 50000$, Errors of the potentials

whereas the convergence rate of the single layer density is about 0.8. Both convergence rates are lower than the ones obtained for a lower relative permittivity, where we observed 1.45 and 0.95, respectively. The reduced regularity is again as expected by [5].

Potential

For the relative permittivity $\varepsilon_r = 50000$ the potential of the Steklov–Poincare formulation on level 7 seems to be the best approximation, therefore we choose it as the reference solution for error computation of the potentials in Table 4.21. The $L^2(\Gamma)$-errors are computed by prolongation to the finest level and seven point integration. In Table 4.21 the estimated convergence rate of the single layer potential is 1.25. Therefore the convergence rate is approximately half an order higher as the convergence rate of the single layer density, which is the expected outcome, see (4.14). For the double layer potential we observe that the order of convergence is 1.25, which is similar to the convergence rate of the density, see (4.13). We obtain an order of 1.7 for the Steklov–Poincaré operator formulation. This order is surprisingly higher than the convergence rate of the potential in Table 4.12 for $\varepsilon_r = 2.25$, which was linear.

Electric field

We use the approximation $\mathbf{E}_7^{DL}$ of the double layer approach at level 7, which was obtained by the simply connected version (3.18), as reference solution for the relative $H^{-\frac{1}{2}}(\Gamma)$-errors of the electric field, as it is approximately of the same accuracy as the Steklov–Poincaré formulation, but faster and thus more convenient in practice. In Table 4.22 we see that for higher permittivities the standard calculations of the single layer and double layer electric fields do not converge. Only the Steklov–Poincaré solution converges, but the errors are high. With the adapted calculations (3.3),

L	$\frac{\|\mathbf{E}_L^{SL}-\mathbf{E}_7^{DL}\|_V}{\|\mathbf{E}_7^{DL}\|_V}$	eoc	$\frac{\|\mathbf{E}_L^{DL}-\mathbf{E}_7^{DL}\|_V}{\|\mathbf{E}_7^{DL}\|_V}$	eoc	$\frac{\|\mathbf{E}_L^{SP}-\mathbf{E}_7^{DL}\|_V}{\|\mathbf{E}_7^{DL}\|_V}$	eoc
0	2.91e3		3.72e-1		1.99e1	
1	1.62e3	0.84	3.46e-1	0.10	8.07e0	1.30
2	1.23e3	0.40	4.30e-1	−0.31	3.54e0	1.19
3	3.69e3	−1.59	8.60e-1	−1.00	1.65e0	1.10
4	4.98e3	−0.43	1.09e0	−0.34	7.97e-1	1.05
5	5.42e1	6.52	1.14e-1	3.26	3.97e-1	1.01
6	4.66e1	0.22	1.22e-1	−0.09	2.03e-1	0.97
7	2.43e1	0.94	0.00e0		1.03e-1	0.98

Table 4.22: Cube with $\varepsilon_r = 50000$, Errors of the electric field

L	$\frac{\|\mathbf{E}_L^{SL}-\mathbf{E}_7^{DL}\|_V}{\|\mathbf{E}_7^{DL}\|_V}$	eoc	$\frac{\|\mathbf{E}_L^{DL}-\mathbf{E}_7^{DL}\|_V}{\|\mathbf{E}_7^{DL}\|_V}$	eoc	$\frac{\|\mathbf{E}_L^{SP}-\mathbf{E}_7^{DL}\|_V}{\|\mathbf{E}_7^{DL}\|_V}$	eoc
0	5.57e-1		1.80e-1		2.13e-1	
1	3.75e-1	0.57	1.03e-1	0.81	1.23e-1	0.80
2	2.51e-1	0.58	6.02e-2	0.77	7.22e-2	0.77
3	1.68e-1	0.58	3.55e-2	0.76	4.33e-2	0.74
4	1.13e-1	0.58	2.03e-2	0.80	2.54e-2	0.77
5	7.52e-2	0.58	1.07e-2	0.92	1.43e-2	0.83
6	4.96e-2	0.60	4.51e-3	1.25	8.51e-3	0.75
7	3.20e-2	0.63	0.00e0		2.18e-3	1.97

Table 4.23: Cube with $\varepsilon_r = 50000$, Errors of the electric field, simply connected

(3.18), and (3.12) the result is by far better, all three formulations converge and the errors are reasonable small as we can observe in Table 4.23. The choice of the solution obtained from the double layer approach as reference solution seems appropriate. Both other formulations converge up to the seventh refinement level to this solution. The error on the seventh level of the Steklov–Poincaré formulation is smaller than the error of the double layer approach on level 6, therefore they are comparable on this level. We observe that the accuracy is not as high as in the case of $\varepsilon_r = 2.25$ for all three formulations. Only the single layer approach yields the same order of 0.6, which could be due to the fact that the convergence rate of the auxiliary calculation in Table 4.15 is the limiting factor, see (4.15). The error of the Steklov–Poincaré formulation on level 7 is close to the one on level 6, which indicates that level 7 is not relevant anymore, since it may be as close to the real value as the double layer solution of level 7. Both the double layer approach and the Steklov–Poincaré formulation have a convergence rate of about 0.8. This order seems appropriate for the double layer approach, since it is approximately half an order lower than the double layer density, see Table 4.20.

L	$\frac{\lvert p_L^{SL}-p_7^{SP}\rvert}{p_7^{SP}}$	eoc	$\frac{\lvert p_L^{DL}-p_7^{SP}\rvert}{p_7^{SP}}$	eoc	$\frac{\lvert p_L^{SP}-p_7^{SP}\rvert}{p_7^{SP}}$	eoc
0	2.49e-1		1.12e-1		8.00e-2	
1	9.96e-2	1.32	2.82e-2	1.98	2.64e-2	1.60
2	3.81e-2	1.39	3.69e-3	2.93	9.28e-3	1.51
3	1.43e-2	1.41	1.15e-2	−1.64	3.40e-3	1.45
4	5.37e-3	1.42	1.10e-2	0.07	1.25e-3	1.44
5	2.00e-3	1.43	8.45e-3	0.38	4.37e-4	1.52
6	7.17e-4	1.48	5.97e-3	0.50	1.23e-4	1.83
7	2.28e-4	1.65	4.05e-3	0.56	0.00e0	

Table 4.24: Cube with $\varepsilon_r = 50000$, Errors of the dipole moment

L	$\frac{\lvert C_{sca,L}^{SL}-C_{sca,7}^{SP}\rvert}{C_{sca,7}^{SP}}$	eoc	$\frac{\lvert C_{sca,L}^{DL}-C_{sca,7}^{SP}\rvert}{C_{sca,7}^{SP}}$	eoc	$\frac{\lvert C_{sca,L}^{SP}-C_{sca,7}^{SP}\rvert}{C_{sca,7}^{SP}}$	eoc
0	4.35e-1		2.11e-1		1.54e-1	
1	1.89e-1	1.20	5.56e-2	1.92	5.20e-2	1.56
2	7.47e-2	1.34	7.40e-3	2.91	1.85e-2	1.49
3	2.85e-2	1.39	2.32e-2	−1.65	6.80e-3	1.44
4	1.07e-2	1.41	2.21e-2	0.07	2.50e-3	1.44
5	3.99e-3	1.43	1.70e-2	0.38	8.74e-4	1.52
6	1.43e-3	1.48	1.20e-2	0.50	2.46e-4	1.83
7	4.57e-4	1.65	8.11e-3	0.56	1.18e-16	40.92

Table 4.25: Cube with $\varepsilon_r = 50000$, Errors of the scattering cross section

.

Dipole moment and scattering cross section

We use the approximations given by the Steklov–Poincaré formulation on the seventh refinement level as reference solutions for the dipole moment (4.2) and the scattering cross section (4.8). The results are given in Tables 4.24 and 4.25. The single layer approach yields an estimated order of convergence of approximately 1.4, which is higher than the convergence rate of the single layer density and therefore it seems to be plausible. For the errors of dipole moment obtained by the Steklov–Poincaré operator formulation the order of convergence is approximately 1.5. For the dipole moment generated by the double layer approach the determination of a convergence rate seems to be difficult and the errors on higher levels are larger than for the other two formulations. Again we observe that the errors of the scattering cross section in Table 4.25 behave like the errors of the dipole moments at higher levels. We also see that for the higher levels the scattering cross section error is approximately twice the

L	$\frac{\|\mathbf{E}_L^{SL}-\mathbf{E}_7^{DL}\|_V}{\|\mathbf{E}_7^{DL}\|_V}$	Time(sec.)	$\frac{\|\mathbf{E}_L^{DL}-\mathbf{E}_7^{DL}\|_V}{\|\mathbf{E}_7^{DL}\|_V}$	Time(sec.)	$\frac{\|\mathbf{E}_L^{SP}-\mathbf{E}_7^{DL}\|_V}{\|\mathbf{E}_7^{DL}\|_V}$	Time(sec.)
0	0.56	0	0.18	0	0.21	0
1	0.38	0	0.10	1	0.12	1
2	0.25	0	6.02e-2	5	7.22e-2	4
3	0.17	3	3.55e-2	16	4.33e-2	60
4	0.11	11	2.03e-2	54	2.54e-2	197
5	7.52e-2	29	1.07e-2	143	1.43e-2	614
6	4.96e-2	89	4.51e-3	441	8.51e-3	2259
7	3.20e-2	288	0.00	1517	2.18e-3	8834

Table 4.26: Cube with $\varepsilon_r = 50000$, Errors of the electric field with times

L	$\frac{\|p_L^{SL}-p_7^{SP}\|}{p_7^{SP}}$	Time(sec.)	$\frac{\|p_L^{DL}-p_7^{SP}\|}{p_7^{SP}}$	Time(sec.)	$\frac{\|p_L^{SP}-p_7^{SP}\|}{p_7^{SP}}$	Time(sec.)
0	2.49e-1	0	1.12e-1	0	8.00e-2	0
1	9.96e-2	0	2.82e-2	1	2.64e-2	1
2	3.81e-2	0	3.69e-3	5	9.28e-3	4
3	1.43e-2	3	1.15e-2	16	3.40e-3	60
4	5.37e-3	11	1.10e-2	54	1.25e-3	197
5	2.00e-3	29	8.45e-3	143	4.37e-4	614
6	7.17e-4	89	5.97e-3	441	1.23e-4	2259
7	2.28e-4	288	4.05e-3	1517	0.00e0	8834

Table 4.27: Cube with $\varepsilon_r = 50000$, Errors of the dipole with times

error of the dipole for all three formulations. Therefore it suffices once more to consider only the dipole moment for comparison of computational times. We can observe that overall convergence rates are lower with a difference of 0.2-0.3 to the lower permittivity $\varepsilon_r = 2.25$.

Comparison of computational times

In Tables 4.26 and 4.27 the single layer potential ansatz, the double layer potential formulation, and the Steklov–Poincaré operator formulation are compared with respect to the computational times (without the postprocessing time needed for the error computation) and the accuracy of the dipole moment and the electric field. The double layer approach is better than the single layer approach, as the error of the double layer approach on level 4 is lower than the error of the single layer formulation on level 7, and the computational time is significantly lower. We can also observe that the errors and computational times of the double layer approach are on every

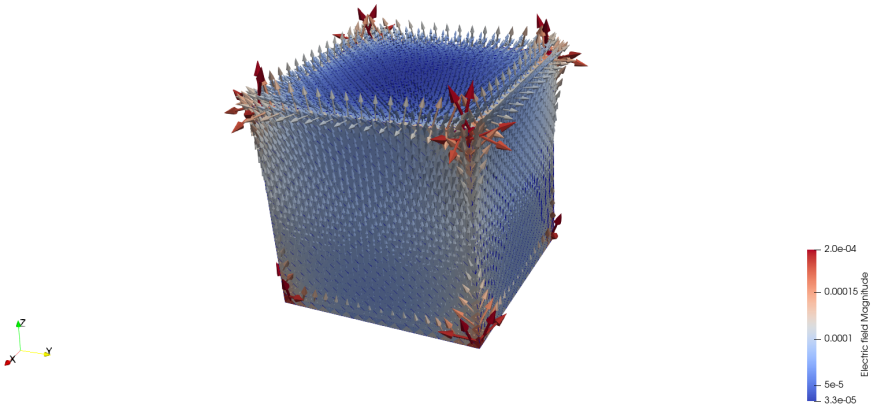

Figure 4.4: Electric field of the cube, single layer approach, $\varepsilon_r = 50000$

level smaller or similar to the errors and computational times of the Steklov–Poincaré formulation. The accuracy of the single layer approach is worse than the accuracy observed for the other two formulations, where the double layer approach is much faster than the Steklov–Poincaré formulation, if we aim for the same accuracy of the electric field. For the dipole moment we obtain a similar result as in the case of a smaller relative permittivity $\varepsilon_r = 2.25$ in Table 4.16. The Steklov–Poincaré formulation on level 5 yields an error that is comparable to the error of the single layer approach on level 7, where the single layer approach is much faster. On the other hand we see that the errors computed by the double layer approach differ on higher levels significantly to the ones given by the other two methods. We can conclude that the double layer approach is not as good as the other two methods for computing the dipole moment, when considering big relative permittivities.

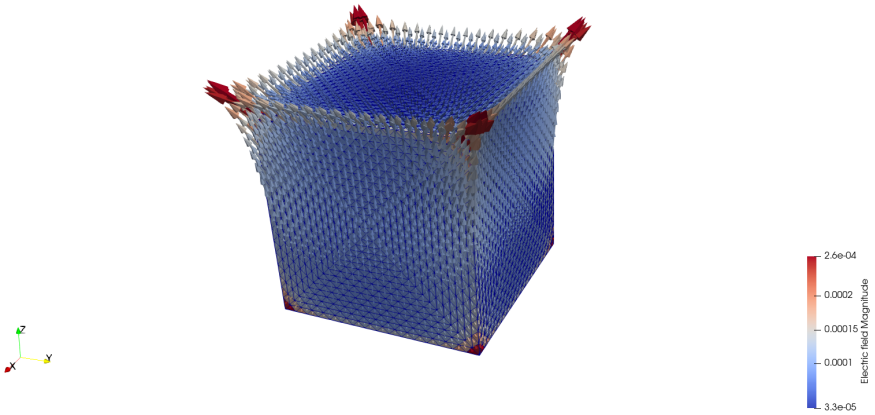

Figure 4.5: Electric field of the cube, Steklov–Poincaré formulation, $\varepsilon_r = 50000$

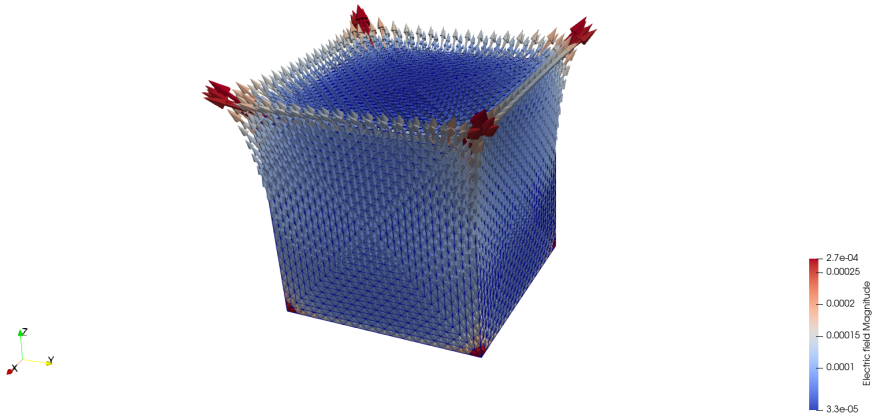

Figure 4.6: Electric field of the cube, double layer approach, $\varepsilon_r = 50000$

In the plots of the electric field in Figures 4.4 – 4.6 we can see that the electric field seems to be meaningful for physical applications, if computed by the double layer approach and the Steklov–Poincaré formulation, but the same is not quite true for the single layer approach close to corners and edges.

4.4 Summary

With our observations from Tables 4.22 and 4.23 in mind we see that, as expected beforehand, the modified versions (3.3), (3.12), and (3.18) for computing the electric field in simply connected domains are useful, if the relative permittivity ε_r is high. On the other hand, if ε_r is low, we see, by comparing Tables 4.13 and 4.14, that we should always consider if the modified version is needed, since it could cause an extra error. Depending on the quantity that we want to compute and the given geometry, all three formulations (2.2), (2.9), and (2.24) have their advantages and disadvantages. Different formulations may be the best approach with respect to the time needed to achieve the same accuracy. The single layer approach performs best in all considered examples, if we aim at computing the dipole moment. However the electric field computed by the single layer approach seems to be critical in the physical interpretation, since we observe unphysical fields in the layer of boundary elements along corners and edges. The double layer is most suitable for computing the electric field of the cube, but the errors for the dipole moment are high compared to the other two formulations. The Steklov–Poincaré formulation is best for computing the electric field of the sphere. It seems to be the most stable of all three formulations, since its performance is in all examples in the first or second place and it shows convergence, where the other two formulations do not, see Tables 4.22 and 4.23. On the other hand the Steklov-Poincaré formulation is also most demanding computationally.

5 Alternative Methods and Modifications

In this chapter various adaptions will be tested to find additional improvements for the numerical computations. We will test different discretization methods for the single layer potential formulation such as the collocation method in Section 5.1 or point sources as ansatz functions in Section 5.2. Furthermore we will change the discretization of the boundary by applying a graded mesh refinement in Section 5.3. Finally we will use a different approach for calculating the dipole moment for the double layer potential formulation in Section 5.4.

5.1 Collocation

Additionally to the three approaches (3.1), (3.7), and (3.16) where we used the Galerkin method, we test the single layer potential formulation (3.1) with the collocation method, where the collocation points are chosen to be the centers of the boundary elements. We use the fast multipole method with the same settings as for the Galerkin method. In Tables 5.1 – 5.3 we see the results for the sphere and the cube.

In the case of the sphere we compare the results to the results in Tables 4.5 and 4.6. We observe that, although the initial errors on the first levels for the electric field are higher, the order of convergence for both computations is linear. For the relative dipole error on the other hand the order of convergence is 1.0, which is not as high as for the Galerkin method, where we have approximately quadratic convergence. If we aim at the same accuracy the computational times are higher, when using the collocation method. This can be seen if we compare the sixth level of the collocation method, which takes 34 seconds to compute, to the fourth levels in Tables 4.8 and 4.9, where comparable errors are achieved in only 3 seconds.

We compare the collocation results for the cube to Tables 4.14, 4.16, 4.23 and 4.24. We observe higher initial errors of the electric field and the dipole moment. We also notice a slightly lower convergence rate for the electric field. The errors that we obtain for the dipole moment are higher than for the Galerkin method, therefore the Galerkin method seems to yield better approximations. Also the computational times for comparable accuracies are again higher for the collocation method, which can be seen in Tables 4.18, 4.26, 4.19, and 4.27.

L	$\frac{\|\mathbf{E}_L^{SL}-\mathbf{E}\|_V}{\|\mathbf{E}\|_V}$	eoc	$\frac{\|p_L^{SL}-p\|}{p}$	eoc	Time(sec.)
0	5.48e-1		7.64e-1		0
1	3.90e-1	0.49	4.14e-1	0.89	0
2	2.51e-1	0.64	1.80e-1	1.20	0
3	1.47e-1	0.77	7.80e-2	1.20	0
4	8.05e-2	0.87	3.56e-2	1.13	1
5	4.22e-2	0.93	1.68e-2	1.08	6
6	2.16e-2	0.96	8.16e-3	1.04	34
7	1.09e-2	0.98	4.02e-3	1.02	113

Table 5.1: Computational results of the single layer approach for the sphere by collocation, $\varepsilon_r = 5.0$

L	$\frac{\|\mathbf{E}_L^{SL}-\mathbf{E}_7^{DL}\|_V}{\|\mathbf{E}_7^{DL}\|_V}$	eoc	$\frac{\|p_L^{SL}-p_7^{SP}\|}{p_7^{SP}}$	eoc	Time(sec.)
0	4.36e-1		9.54e-2		0
1	3.37e-1	0.37	5.09e-2	0.91	0
2	2.51e-1	0.43	2.69e-2	0.92	0
3	1.82e-1	0.46	1.43e-2	0.91	2
4	1.30e-1	0.49	7.64e-3	0.90	7
5	9.12e-2	0.51	4.12e-3	0.89	18
6	6.34e-2	0.52	2.22e-3	0.89	67
7	4.37e-2	0.54	1.21e-3	0.88	222

Table 5.2: Computational results of the single layer approach for the cube by collocation, $\varepsilon_r = 2.25$

L	$\frac{\|\mathbf{E}_L^{SL}-\mathbf{E}_7^{DL}\|_V}{\|\mathbf{E}_7^{DL}\|_V}$	eoc	$\frac{\|p_L^{SL}-p_7^{SP}\|}{p_7^{SP}}$	eoc	Time(sec.)
0	6.63e-1		3.48e-1		0
1	5.48e-1	0.27	2.29e-1	0.60	0
2	4.34e-1	0.33	1.48e-1	0.63	1
3	3.37e-1	0.37	9.51e-2	0.64	2
4	2.53e-1	0.41	6.07e-2	0.65	6
5	1.85e-1	0.45	3.87e-2	0.65	28
6	1.34e-1	0.47	2.45e-2	0.66	66
7	9.48e-2	0.49	1.55e-2	0.66	231

Table 5.3: Computational results of the single layer approach for the cube with collocation, $\varepsilon_r = 50000$

5.2 Discretization Variants

Next we will consider two alternative discretizations of the single layer potential formulation (2.2). We choose Dirac like ansatz functions and matching test functions, following the ideas given in [9]. In particular we consider point sources in the centers of the elements and in the nodes. The errors of the approximations of the potentials will be investigated for different discretizations.

5.2.1 Point Sources in Centers of the Elements

We consider the ansatz function

$$\widetilde{w}_h(x) = \sum_{k=1}^{N} \widetilde{w}_k \delta(x - \hat{x}_k) \quad \text{for } x \in \Gamma,$$

where $\hat{x}_k$ is the center of the element τ_k and $\delta(\cdot)$ is the Dirac delta function. With the single layer formulation (2.2) and by using piecewise constant test functions we get

$$\left\langle \left(\frac{1}{2} \frac{\varepsilon_1 + \varepsilon_0}{\varepsilon_1 - \varepsilon_0} I + K' \right) \widetilde{w}_h, \psi_k^0 \right\rangle_\Gamma = \langle -\gamma_1^{\text{int}} \Phi_{\text{part}}, \psi_k^0 \rangle_\Gamma \quad \text{for } k = 1, \ldots, N.$$

By computing

$$\langle \widetilde{w}_h, \psi_k^0 \rangle_\Gamma = \sum_{\ell=1}^{N} \widetilde{w}_\ell \int_\Gamma \psi_k^0(x) \delta(x - \hat{x}_\ell) ds_x = \widetilde{w}_k$$

and

$$\begin{aligned} \langle K' \widetilde{w}_h, \psi_k^0 \rangle_\Gamma &= \int_\Gamma \psi_k^0(x) \int_\Gamma \gamma_{1,x}^{\text{int}} U^*(x,y) \sum_{\ell=1}^{N} \widetilde{w}_\ell \delta(y - \hat{y}_\ell) ds_y ds_x \\ &= \sum_{\ell=1}^{N} \widetilde{w}_\ell \int_\Gamma \psi_k^0(x) \gamma_{1,x}^{\text{int}} U^*(x, \hat{y}_\ell) ds_x = \sum_{\ell=1}^{N} \widetilde{w}_\ell (K \psi_k^0)(\hat{y}_\ell) \end{aligned}$$

we obtain

$$\left(\frac{1}{2} \frac{\varepsilon_1 + \varepsilon_0}{\varepsilon_1 - \varepsilon_0} I + \widetilde{K}_h^\top \right) \underline{\widetilde{w}} = \underline{f}^0, \tag{5.1}$$

where for $k, \ell = 1, \ldots, N$

$$\widetilde{K}_h[\ell, k] = (K \psi_k^0)(\hat{y}_\ell), \quad f_k^0 = \langle -\gamma_1^{\text{int}} \Phi_{\text{part}}, \psi_k^0 \rangle_\Gamma.$$

We denote by w_h the approximation of the density obtained by the standard single layer approach (3.1), i.e.,

$$w_h = \sum_{k=1}^{N} w_k \psi_k^0, \quad \text{on } \Gamma.$$

Since (3.1) is comparable to (5.1), if we approximate the integration by evaluation in the centers, we are tempted to demand $\int_{\tau_k}(w_h(x)-\widetilde{w}_h(x))ds_x = 0$. Thus we obtain for $k = 1,\dots,N$

$$\widetilde{w}_k \approx w_k|\tau_k|. \tag{5.2}$$

This corresponds to a scaling of the original coefficients. We can also evaluate the single layer potential for $\widetilde{w}_h$ by

$$\widetilde{\Phi}_h^{SL}(x) = V\widetilde{w}_h(x) = \sum_{k=1}^{N} \widetilde{w}_k U^*(x,\widetilde{y}_k) \quad \text{for } x \in \Gamma, \tag{5.3}$$

in contrast to the original computation

$$\Phi_h^{SL}(x) = Vw_h(x) = \sum_{k=1}^{N} w_k \int_{\tau_k} U^*(x,y)ds_y \quad \text{for } x \in \Gamma. \tag{5.4}$$

We denote by $\widetilde{\Phi}_L^{SL}$ and Φ_L^{SL} the corresponding numerical computations on level L and by Φ the analytic solution (4.12) for the sphere. For the computation of the $L^2(\Gamma)$-error of $\widetilde{\Phi}_h$ we have tested several approaches for the numerical integration to ensure the error computation is not a limiting factor for the observed order of convergence. The seven point formula used before cannot be used due to the singularities in the centers of the elements. In the first integration variant we start by using linear interpolation on $\widetilde{\Phi}_h$ in the vertices to obtain

$$I_h^1\widetilde{\Phi}_h(x) = \sum_{i=1}^{M} \psi_i^1(x)(V\widetilde{w}_h)(x_i) \quad \text{for } x \in \Gamma, \tag{5.5}$$

and afterwards compute the $L^2(\Gamma)$-error of the linear interpolation with the seven point formula. The second variant uses Gauß quadrature, avoiding the centers of the elements as evaluation points. For the third variant we refine every triangle to six triangles, such that the center is a node for every subtriangle and the other used nodes are the original triangle nodes and the midpoints of the edges. Now we can use the seven point formula on the six subtriangles.

All three variants yield linear convergence as can be seen in Table 5.4. Thus we conclude that linear convergence is characteristic for the method (5.1), whereas the original formulation had quadratic convergence in Table 4.3.

To better understand this discrepancy we also consider the potential computed by the $L^2(\Gamma)$-projection of the analytic density w onto S_h^0. We use transformation (5.2) to compute another approximation $\widehat{\Phi}_h$ with coefficients $\widehat{w}_k = w_k|\tau_k|$ by

$$\widehat{\Phi}_h(x) = \sum_{k=1}^{N} w_k|\tau_k|U^*(x,\widetilde{y}_k) \quad \text{for } x \in \Gamma. \tag{5.6}$$

L	$\frac{\|\widetilde{\Phi}_L^{SL,V1}-\Phi\|_{L^2(\Gamma)}}{\|\Phi\|_{L^2(\Gamma)}}$	eoc	$\frac{\|\widetilde{\Phi}_L^{SL,V2}-\Phi\|_{L^2(\Gamma)}}{\|\Phi\|_{L^2(\Gamma)}}$	eoc	$\frac{\|\widetilde{\Phi}_L^{SL,V3}-\Phi\|_{L^2(\Gamma)}}{\|\Phi\|_{L^2(\Gamma)}}$	eoc
0	8.11e-1		5.94e-1		6.38e-1	
1	4.57e-1	0.83	2.97e-1	1.00	2.65e-1	1.27
2	2.03e-1	1.17	1.44e-1	1.04	1.19e-1	1.16
3	9.01e-2	1.17	6.96e-2	1.05	5.40e-2	1.14
4	4.18e-2	1.11	3.41e-2	1.03	2.56e-2	1.07
5	2.00e-2	1.06	1.69e-2	1.01	1.26e-2	1.03

Table 5.4: Sphere with $\varepsilon_r = 5.0$, Errors of the potentials, evaluation (5.3), point sources in centers of elements (5.1)

L	$\frac{\|\widehat{\Phi}_L^{SL,V2}-\Phi\|_{L^2(\Gamma)}}{\|\Phi\|_{L^2(\Gamma)}}$	eoc
0	5.81e-1	
1	2.77e-1	1.07
2	1.16e-1	1.25
3	5.14e-2	1.17
4	2.40e-2	1.10
5	1.16e-2	1.05

Table 5.5: Sphere with $\varepsilon_r = 5.0$, Errors of the potential with the second variant for the error computation and $L^2(\Gamma)$-projection of the analytic density as input for evaluation (5.6), point sources in centers of elements

For all three integration variants we observe linear convergence. As an example the errors computed with the second variant are given in Table 5.5. Since the convergence is again linear we conclude that the reduced order of convergence is due to the different computation of the potentials.

By using relation (5.2) we are able to compute another approximation $\check{\Phi}_h$ from $\widetilde{w}_h$ by

$$\check{\Phi}_h(x) = \sum_{k=1}^{N} \frac{\widetilde{w}_k}{|\tau_k|} \int_{\tau_k} U^*(x,y) ds_y \quad \text{for } x \in \Gamma. \tag{5.7}$$

Now we observe quadratic convergence for all integration variants. For instance using the first integration variant we obtain Table 5.6.

Summary

For Φ_h based on $w_h \in S_h^0$, computed by (5.4), we observed quadratic convergence in several implementations of the $L^2(\Gamma)$-error. For various implementations of the $L^2(\Gamma)$-

L	$\frac{\|\check{\Phi}_L^{SL,V1}-\Phi\|_{L^2(\Gamma)}}{\|\Phi\|_{L^2(\Gamma)}}$	eoc
0	3.74e-1	
1	1.22e-1	1.62
2	3.30e-2	1.89
3	8.38e-3	1.97
4	2.10e-3	2.00

Table 5.6: Sphere with $\varepsilon_r = 5.0$, Errors of the potential with the first variant for the error computation and solution of (5.1) as input for evaluation (5.7), point sources in centers of elements

error only linear convergence for $\widetilde{\Phi}_h$, computed by (5.3), was obtained. If we use (5.2) to scale the coefficients of the $L^2(\Gamma)$-projection of the analytic solution $Q_h^0 w = w_h$ to $\widetilde{w}_h$ and compute $\widehat{\Phi}_h$ by (5.6) we observe only linear convergence. Vice versa the scaled coefficients of $\widetilde{w}_h$ plugged into $\check{\Phi}_h$, see (5.7), provide quadratic convergence. As we use the same error routines for both versions we may assume that these routines are correct. We assume reasonable quality of $\widetilde{w}_h$ as we observe quadratic convergence after scaling. We see two possible reasons for the reduced order. The first possibility is insufficient accuracy in the evaluation of the solution. As the interpolation of the solution by piecewise linear functions has reduced order we are tempted to exclude this case. The second possibility is a reduced approximation quality of the Dirac functions. We guess and observe that any transformation to $\widetilde{w}_h$ in the space of linear combinations of point sources in the centers of the elements implies the reduced order of convergence.

5.2.2 Point Sources in the Nodes

We consider the ansatz function

$$\widetilde{w}_h(x) = \sum_{k=1}^{M} \widetilde{w}_k \delta(x - x_k) \quad \text{for } x \in \Gamma,$$

where x_k is the k-th node of the mesh. Analogous to the derivation of (2.2) we have for the general jump term σ, that

$$\left(\left(\sigma + \frac{\varepsilon_0}{\varepsilon_1 - \varepsilon_0} \right) I + K' \right) w = -\gamma_1^{\text{int}} \Phi_{\text{part}} \quad \text{on } \Gamma. \tag{5.8}$$

Using piecewise linear, globally continuous test functions we get

$$\left\langle \left(\left(\sigma + \frac{\varepsilon_0}{\varepsilon_1 - \varepsilon_0} \right) I + K' \right) \widetilde{w}_h, \psi_k^1 \right\rangle_\Gamma = \left\langle -\gamma_1^{\text{int}} \Phi_{\text{part}}, \psi_k^1 \right\rangle_\Gamma \quad \text{for } k = 1, \ldots, M.$$

By computing

$$\left\langle \widetilde{w}_h, \psi_k^1 \right\rangle_\Gamma = \sum_{\ell=1}^{M} \widetilde{w}_\ell \int_\Gamma \psi_k^1(x)\delta(x - x_\ell) ds_x = \widetilde{w}_k$$

and

$$\begin{aligned}\left\langle K'\widetilde{w}_h, \psi_k^1 \right\rangle_\Gamma &= \int_\Gamma \psi_k^1(x) \int_\Gamma \gamma_{1,x}^{\text{int}} U^*(x,y) \sum_{\ell=1}^{M} \widetilde{w}_\ell \delta(y - y_\ell) ds_y ds_x \\ &= \sum_{\ell=1}^{M} \widetilde{w}_\ell \int_\Gamma \psi_k^1(x) \gamma_{1,x}^{\text{int}} U^*(x, y_\ell) ds_x = \sum_{\ell=1}^{M} \widetilde{w}_\ell (K\psi_k^1)(y_\ell)\end{aligned}$$

we obtain

$$\left(\left(\sigma + \frac{\varepsilon_0}{\varepsilon_1 - \varepsilon_0} \right) I + \widehat{K}_h^\top \right) \underline{\widetilde{w}} = \underline{f}^1, \tag{5.9}$$

where for $k, \ell = 1, \ldots, M$

$$\widehat{K}_h[\ell, k] = K\psi_k^1(y_\ell), \quad f_k^1 = \langle -\gamma_1^{\text{int}} \Phi_{\text{part}}, \psi_k^1 \rangle_\Gamma.$$

We denote by w_h the $L^2(\Gamma)$-projection of the analytic solution w onto S_h^1 and the related coefficients w_k, therefore

$$w_h = \sum_{k=1}^{M} w_k \psi_k^1, \quad \text{on } \Gamma. \tag{5.10}$$

We can also compute the potential with $\widetilde{w}_h$ by

$$\widetilde{\Phi}_h^{SL}(x) = V\widetilde{w}_h(x) = \sum_{k=1}^{M} \widetilde{w}_k U^*(x, y_k) \quad \text{for } x \in \Gamma \tag{5.11}$$

in contrast to the original computation

$$\Phi_h^{SL}(x) = Vw_h(x) = \sum_{k=1}^{M} w_k \sum_{\tau \subset \text{supp}(\psi_k^1)} \int_\tau U^*(x,y)\psi_k^1(y) ds_y \quad \text{for } x \in \Gamma. \tag{5.12}$$

We denote by $\widetilde{\Phi}_L^{SL}$ and Φ_L^{SL} the corresponding numerical computations and by Φ the analytic solution (4.12) for the sphere. In Table 5.7 we observe linear convergence for $\widetilde{\Phi}_h^{SL}$.

L	$\frac{\|\widetilde{\Phi}_L^{SL}-\Phi\|_{L^2(\Gamma)}}{\|\Phi\|_{L^2(\Gamma)}}$	eoc
0	4.50e-1	
1	2.74e-1	0.72
2	1.52e-1	0.85
3	7.82e-2	0.96
4	3.94e-2	0.99
5	1.97e-2	1.00

Table 5.7: Sphere with $\varepsilon_r = 5.0$, Errors of the potential computed by numerical integration with 7 point quadrature rule, evaluation (5.11), point sources in the nodes (5.9)

L	$\frac{\|\widehat{\Phi}_L^{SL}-\Phi\|_{L^2(\Gamma)}}{\|\Phi\|_{L^2(\Gamma)}}$	eoc
0	4.32e-1	
1	2.70e-1	0.68
2	1.51e-1	0.84
3	7.78e-2	0.95
4	3.92e-2	0.99
5	1.97e-2	1.00

Table 5.8: Sphere with $\varepsilon_r = 5.0$, Errors of the potential computed by numerical integration with 7 point quadrature rule with the $L^2(\Gamma)$-projection of the analytic density as input for evaluation (5.14), point sources in the nodes (5.9)

As for the point sources in the centers we try to map the function $\widetilde{w}_h$ into $S_h^1(\Gamma)$. Similar to relation (5.2) we find a scaling for $k = 1, \ldots, M$

$$\widetilde{w}_k \approx w_k \left(\sum_{\tau \subset \operatorname{supp}(\psi_k^1)} \int_\tau \psi_k^1(x) ds_x \right) = w_k \left(\sum_{\tau \subset \operatorname{supp}(\psi_k^1)} \frac{|\tau|}{3} \right). \tag{5.13}$$

By using relation (5.13) we are again able to compute another approximation $\widehat{\Phi}_h$ based on the coefficients of the $L^2(\Gamma)$-projection w_h by

$$\widehat{\Phi}_h(x) = \sum_{k=1}^{M} w_k \left(\sum_{\tau \subset \operatorname{supp}(\psi_k^1)} \frac{|\tau|}{3} \right) U^*(x, y_k) \quad \text{for } x \in \Gamma. \tag{5.14}$$

With this computation we obtain the results given in Table 5.8. We again observe linear convergence.

L	$\frac{\|\check{\Phi}_L^{SL}-\Phi\|_{L^2(\Gamma)}}{\|\Phi\|_{L^2(\Gamma)}}$	eoc
0	3.42e-1	
1	1.16e-1	1.57
2	3.27e-2	1.82
3	9.48e-3	1.79
4	2.58e-3	1.88

Table 5.9: Sphere with $\varepsilon_r = 5.0$, Errors of the potential computed by numerical integration with 7 point quadrature rule and solution of (5.9) as input for evaluation (5.15), point sources in the nodes

Analogous to Subsection 5.2.1 we use (5.13) to compute another approximation $\check{\Phi}_h$ by

$$\check{\Phi}_h(x) = \sum_{k=1}^{M} \frac{\widetilde{w}_k}{\sum\limits_{\tau\subset\mathrm{supp}(\psi_k^1)} \frac{|\tau|}{3}} \sum_{\tau\subset\mathrm{supp}(\psi_k^1)} \int_\tau U^*(x,y)\psi_k^1(y)ds_y \quad \text{for } x\in\Gamma. \tag{5.15}$$

This potential converges quadratically, as can be seen in Table 5.9.

Summary

For the approximation Φ_h, computed by (5.12), based on $w_h \in S_h^0$ given by (5.10) we observed quadratic convergence of the $L^2(\Gamma)$-error. On the other hand only linear convergence for $\widetilde{\Phi}_h^{SL}$ in (5.11) was obtained. If we use the relation of the densities (5.13) to scale the coefficients of the $L^2(\Gamma)$-projection of an analytic solution $Q_h^1 w = w_h$ to $\widetilde{w}_h$ and compute $\widehat{\Phi}_h$ by (5.14) we observe only linear convergence. Vice versa the scaled coefficients of $\widetilde{w}_h$ plugged into $\check{\Phi}_h$, computed by (5.15), provide quadratic convergence. As we use the same error routines for both versions we may assume that this routines are correct. We assume reasonable quality of $\widetilde{w}_h$ as we observe quadratic convergence in Table 5.9. We guess and observe that any transformation to $\widetilde{w}_h$ in the space of linear combinations of point sources in the nodes implies the reduced order of convergence.

5.3 Graded Meshes for the Cube

Additionally to the uniform refinement of the cube we will consider an adaptive refinement of the mesh. As we expect corner and edge singularities in the solution of the transmission problem, we refine the meshes towards edges and corners. Remember that h was defined by $h := \max\limits_{\ell\in\{1,\dots,N\}} h_\ell$, with $h_\ell := \operatorname{diam}\tau_\ell$. We approximate the distance of the triangle τ_ℓ to a corner $x^{(j)}$ of the cube, $j = 1,\dots,8$, by $r_{\ell,j} := |x_\ell^s - x^{(j)}|$,

where x_ℓ^s is the center of the ℓ-th element. The distance to an edge $E \in \mathcal{E}_h$, where $\mathcal{E}_h$ is the set of all edges of the cube, is $r_{\ell,E} := \inf_{x \in E} |x - x_\ell^s|$. Additionally to the uniform refinement steps, which we had before, we use refinement conditions for a graded mesh analogous to the ones given in [17, 29, 30] to further refine triangles close to edges and corners. We refine until there holds for all $\ell = 1, \dots, N$:

$$\begin{aligned} h_\ell &\leq h \left(\frac{r_{\ell,j}}{c_1} \right)^{1-\mu_1} \quad \text{for } j = 1, \dots, 8, \\ h_\ell &\leq h \left(\frac{r_{\ell,E}}{c_2} \right)^{1-\mu_2} \quad \text{for } E \in \mathcal{E}_h, \\ h_\ell &\leq 2^{-L}, \end{aligned} \tag{5.16}$$

where $\mu_1, \mu_2 \in (0, 1]$ and $c_1, c_2 \in (0, 1]$. Note that the refinement happens after scaling to the unit cube, hence the level L in the third condition corresponds to the number of uniform refinement steps, as before. In contrast to the prior refinement strategy we now use newest vertex bisection. For the choice of the parameters we did some testing until we found suitable values. No theoretical investigation was done, only a numerical case study to evaluate the possible improvement by graded meshes. The estimated order of convergence was calculated with respect to the number of panels N_L for a level $L \in \{0, \dots, 7\}$ by

$$\mathrm{eoc}_L = \frac{\log(\mathrm{err}_L / \mathrm{err}_{L-1})}{\log(\sqrt{N_{L-1}} / \sqrt{N_L})}.$$

For a uniform refinement we have $\sqrt{N_{L-1}}/\sqrt{N_L} = \frac{1}{2}$ and therefore this corresponds to the eoc that we had before. We evaluate the errors of the dipole moment. The chosen reference solution is the approximation obtained by computation of the Steklov–Poincaré formulation on the finest graded mesh.

5.3.1 Cube with $\varepsilon_r = 2.25$

For the relative permittivity $\varepsilon_r = 2.25$ we first tuned the parameter μ_2 of the grading with respect to the edges. After finding a good choice for μ_2 the second parameter μ_1, which indicates the grading in the direction of corners was adjusted, such that we obtained a slightly better approximation than we would have had without doing this extra grading. The other constants are chosen similar to [29]. The explicit choice of the parameters for this relative permittivity is

$$c_1 = 0.2, \quad \mu_1 = 0.6, \quad c_2 = 0.1, \quad \mu_2 = 0.8.$$

The corresponding numbers of panels and nodes of the graded meshes as well as the mesh widths h_{max} are given in Table 5.10. Note that the seventh level is technically

Level	Panels	Nodes	h_{max}
0	24	14	1.0000
1	144	74	0.5000
2	480	242	0.2500
3	2160	1082	0.1250
4	10464	5234	0.0625
5	39504	19754	0.0313
6	154416	77210	0.0156
7	318912	159458	0.0110

Table 5.10: Number of nodes, panels and mesh widths of the graded meshes for relative permittivity $\varepsilon = 2.25$

only a "half" level better than the sixth level since no full uniform refinement step was done from the sixth to the seventh level. Instead just one bisection of the triangles was done, which results in h_{max} on the sixth level being only a factor $\sqrt{2}$ smaller than the next level. The graded mesh on the fifth level is shown in Figure 5.1. On this

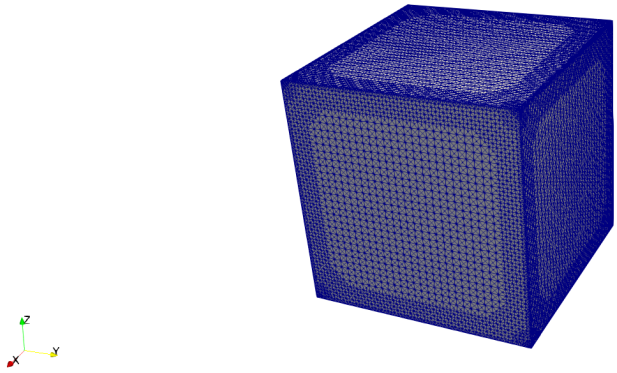

Figure 5.1: Graded mesh on the fifth level obtained by refinement conditions (5.16) for $\varepsilon = 2.25$

level there are one and a half additional refinement steps towards the edge and three additional refinement steps towards the corner. As reference solutions we select the solutions obtained by computation of the Steklov–Poincaré formulation on the seventh level on the graded mesh, since this seems to yield a better solution than the reference solutions, which we had before.

L	$\frac{\lvert p_L^{SL}-p_7^{SP}\rvert}{p_7^{SP}}$	eoc	$\frac{\lvert p_L^{DL}-p_7^{SP}\rvert}{p_7^{SP}}$	eoc	$\frac{\lvert p_L^{SP}-p_7^{SP}\rvert}{p_7^{SP}}$	eoc
0	6.11e-2		5.41e-2		4.64e-3	
1	1.79e-2	1.37	2.64e-2	0.80	1.82e-3	1.04
2	6.34e-3	1.72	1.27e-2	1.22	5.98e-4	1.85
3	1.51e-3	1.91	3.97e-3	1.54	1.20e-4	2.14
4	3.32e-4	1.92	1.56e-5	7.02	2.71e-5	1.89
5	1.02e-4	1.77	2.51e-4	−4.18	5.63e-6	2.37
6	2.93e-5	1.84	2.56e-4	−0.03	1.21e-6	2.26
7	1.43e-5	1.97	3.79e-4	−1.08	0.00	

Table 5.11: Cube with graded mesh, $\varepsilon_r = 2.25$, Errors of the dipole moment

L	N	$\frac{\lvert p_L^{SL-A}-p_7^{SP}\rvert}{p_7^{SP}}$	eoc	Time	N	$\frac{\lvert p_L^{SL}-p_7^{SP}\rvert}{p_7^{SP}}$	eoc	Time
0	24	6.11e-2		0	24	6.11e-2		0
1	144	1.79e-2	1.37	0	96	2.12e-2	1.53	0
2	480	6.34e-3	1.72	0	384	6.87e-3	1.63	0
3	2160	1.51e-3	1.91	2	1536	2.15e-3	1.68	3
4	10464	3.32e-4	1.92	7	6144	6.59e-4	1.70	3
5	39504	1.02e-4	1.77	21	24576	2.01e-4	1.71	9
6	154416	2.93e-5	1.84	71	98304	6.11e-5	1.72	46
7	318912	1.43e-5	1.97	130	393216	1.96e-5	1.64	172

Table 5.12: Cube with graded mesh, $\varepsilon_r = 2.25$, Comparison of single layer errors for adaptive and uniform refinement

We obtain the errors of the dipole moment given in Table 5.11. We observe higher orders of convergence for the single layer approach and the Steklov–Poincaré formulation, compared to uniform refinement. The double layer approach yields a good approximation and a surprisingly good fourth level, the fifth level again matches the expectation, but afterwards the errors only get worse.

In Table 5.12 we compare the results of the adaptive refinement p^{SL-A} to the results obtained by the uniform refinement with newest vertex bisection. We observe an improved order of convergence of approximately 1.9, where the uniform refinement only yields 1.7. On the seventh level the adaptive refinement has a smaller error and the computational time is lower than for the uniform refinement.

Level	Panels	Nodes	h_{max}
0	24	14	1.0000
1	144	74	0.5000
2	960	482	0.2500
3	3360	1682	0.1250
4	18864	9434	0.0625
5	79920	39962	0.0313
6	285888	142946	0.0156

Table 5.13: Number of nodes, panels and mesh widths of the graded meshes for relative permittivity $\varepsilon = 50000$

5.3.2 Cube with $\varepsilon_r = 50000$

For a relative permittivity $\varepsilon_r = 50000$ we again first tuned the parameter μ_2 of the grading with respect to the edges. After finding a good choice for μ_2 the second parameter μ_1 for grading in the direction of corners was set to $\mu_1 = \mu_2 - 0.2$ as for the first case in Section 5.3.1. The explicit choice of the parameters for this relative permittivity is

$$c_1 = 0.2, \quad \mu_1 = 0.4, \quad c_2 = 0.1, \quad \mu_2 = 0.6.$$

The corresponding numbers of panels and nodes of the graded meshes as well as the mesh widths h_{max} are given in Table 5.13. The parameters provide meshes with a stronger grading.

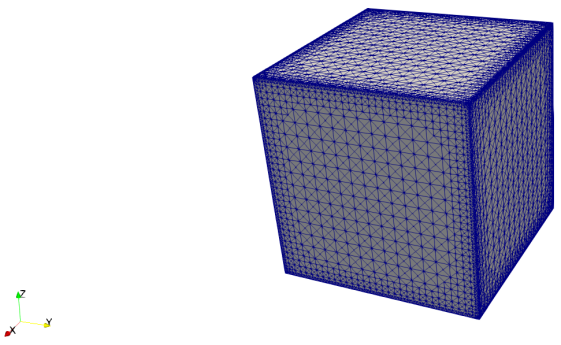

Figure 5.2: Graded mesh on the fourth level obtained by refinement conditions (5.16) for $\varepsilon = 50000$

L	$\frac{\lvert p_L^{SL}-p_6^{SP}\rvert}{p_6^{SP}}$	eoc	$\frac{\lvert p_L^{DL}-p_6^{SP}\rvert}{p_6^{SP}}$	eoc	$\frac{\lvert p_L^{SP}-p_6^{SP}\rvert}{p_6^{SP}}$	eoc
0	0.25		0.11		8.01e-2	
1	8.79e-2	1.16	4.41e-2	1.04	2.39e-2	1.35
2	2.01e-2	1.55	1.16e-2	1.41	3.74e-3	1.96
3	7.64e-3	1.55	1.52e-2	−0.43	1.18e-3	1.84
4	1.76e-3	1.70	1.58e-2	−0.05	1.86e-4	2.14
5	4.74e-4	1.81	1.29e-2	0.28	2.16e-5	2.99
6	1.40e-4	1.91	7.72e-3	0.81	0.00	

Table 5.14: Cube with graded mesh, $\varepsilon_r = 50000$, Errors of the dipole moment

L	N	$\frac{\lvert p_L^{SL-A}-p_6^{SP}\rvert}{p_6^{SP}}$	eoc	Time	N	$\frac{\lvert p_L^{SL}-p_6^{SP}\rvert}{p_6^{SP}}$	eoc	Time
0	24	0.25		0	24	0.25		1
1	144	8.79e-2	1.16	0	96	0.10	1.27	0
2	960	2.01e-2	1.55	4	384	4.13e-2	1.31	2
3	3360	7.64e-3	1.55	17	1536	1.65e-2	1.33	2
4	18864	1.76e-3	1.70	50	6144	6.52e-3	1.34	5
5	79920	4.74e-4	1.81	71	24576	2.58e-3	1.34	11
6	285888	1.40e-4	1.91	242	98304	1.01e-3	1.35	49

Table 5.15: Cube with graded mesh, $\varepsilon_r = 50000$, Comparison of single layer errors for adaptive and uniform refinement

The graded mesh on the fourth level is shown in Figure 5.2. As reference solutions we choose the solutions obtained by the Steklov–Poincaré formulation on the sixth level on the graded mesh, since this seems to yield a better solution than the reference solutions, which we had before. We obtain the errors of the dipole moment given in Table 5.14. We observe higher order of convergence for the single layer approach and the Steklov–Poincaré formulation, compared to the uniform refinement. The double layer approach again performs worse with no observable convergence order, but reasonable approximations. In Table 5.15 we compare the results of the adaptive refinement p^{SL-A} to the results obtained by the uniform refinement. We observe an improved order of convergence of approximately 1.8, where the uniform refinement only yields 1.35. In terms of computational times for the same accuracy uniform refinement seems to be better, since the computational time of its sixth level is comparable to the time needed by the computation with graded meshes on the fourth level, but the error is lower. As we would expect, the singularities of the electric field computed on the graded meshes are easier to identify at the corners than for the electric field computed on the uniform mesh, as can be seen in Figures 5.3–5.5.

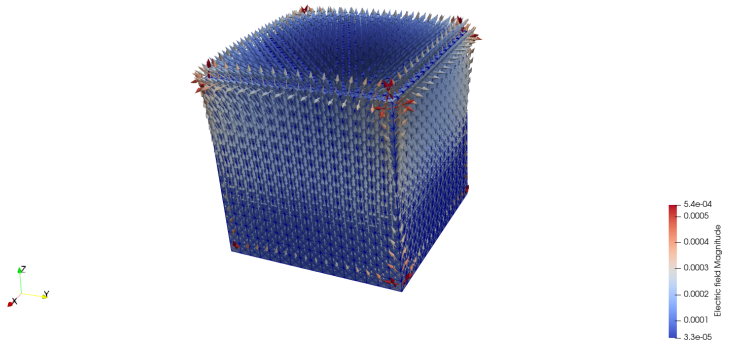

Figure 5.3: Electric field computed by the single layer formulation on the graded mesh for $\varepsilon = 50000$

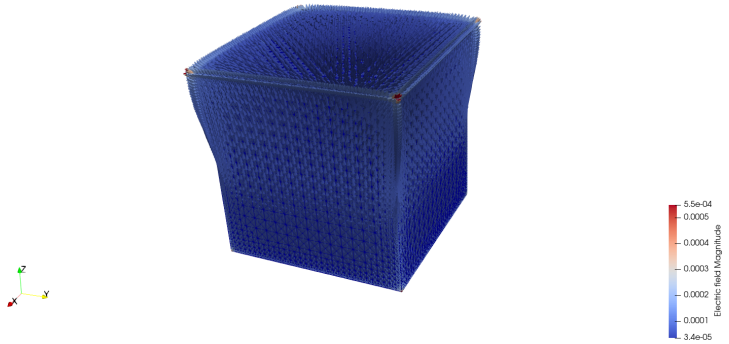

Figure 5.4: Electric field computed by the double layer formulation on the graded mesh for $\varepsilon = 50000$

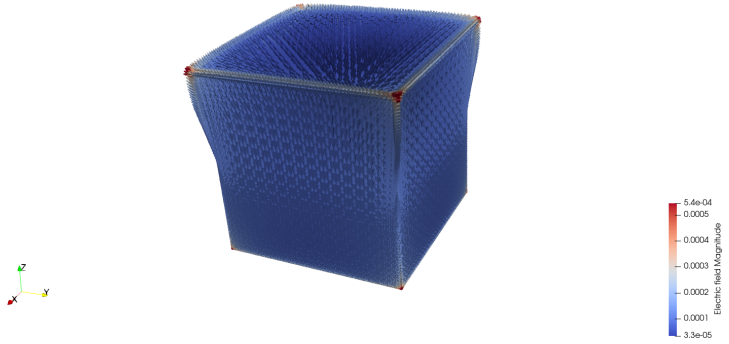

Figure 5.5: Electric field computed by the Steklov–Poincaré formulation on the graded mesh for $\varepsilon = 50000$

5.4 Improved Dipole Moment for the Double Layer Formulation

As we observed in previous numerical experiments, see, e.g. Tables 4.6, 4.16, and 4.24, the performance of the double layer formulation is rather unsatisfactory when it comes to computing the dipole moment. For this reason we are interested in an alternative calculation of the surface charge density σ_h^{DL} instead of (4.7). We plug the evaluation of the interior electric field (3.18) and exterior electric field (3.17) into (4.7) to obtain

$$\sigma_h^{DL} = -\frac{\varepsilon_1 - \varepsilon_0}{\varepsilon_1}\gamma_1^{\text{int}}\Phi_{\text{part}} + \frac{\varepsilon_1 - \varepsilon_0}{\varepsilon_1\varepsilon_0} Dv_h \quad \text{on } \Gamma.$$

Since Dv_h is in $H^{-\frac{1}{2}}(\Gamma)$ we want to test with piecewise linear and globally continuous basis functions $\{\psi_m^1\}_{m=1}^M$. The question is, which ansatz functions we should choose to be the basis functions of σ_h^{DL}. We know that $\sigma \in H^{-\frac{1}{2}}(\Gamma)$, hence piecewise constant basis functions $\{\psi_\ell^0\}_{\ell=1}^N$ seem to be appropriate. But the problem is, that we would obtain a mass matrix, which is not invertible. Thus we use the dual boundary space, see, e.g., [33], and introduce

$$W_h := \operatorname{span}\{\widetilde{\psi}_k\}_{k=1}^M,$$

where the $\widetilde{\psi}_k$ are piecewise constant functions on the dual boundary elements $\tilde{\tau}_k$ associated with the interior nodes x_k. The dual boundary element $\tilde{\tau}_k$ is defined by the centers x_ℓ^s of $\tau_\ell \subset \operatorname{supp}\psi_k^1$ and the midpoints of the related element edges. The resulting Galerkin–Petrov variational problem is to find $\sigma_h^{DL} \in W_h$ such that

$$\left\langle \sigma_h^{DL}, \psi_m^1 \right\rangle_\Gamma = \frac{\varepsilon_1 - \varepsilon_0}{\varepsilon_1}\left\langle -\gamma_1^{\text{int}}\Phi_{\text{part}}, \psi_m^1 \right\rangle_\Gamma + \frac{\varepsilon_1 - \varepsilon_0}{\varepsilon_1\varepsilon_0}\left\langle Dv_h, \psi_m^1 \right\rangle_\Gamma,$$

for $m = 1, \ldots, M$. This variational problem yields the linear system

$$\widetilde{G}_h \underline{\sigma}^{DL} = \frac{\varepsilon_1 - \varepsilon_0}{\varepsilon_1}\underline{f}^1 + \frac{\varepsilon_1 - \varepsilon_0}{\varepsilon_1\varepsilon_0} D_h \underline{v},$$

where

$$D_h[m,n] = \langle D\psi_n^1, \psi_m^1\rangle_\Gamma, \qquad \widetilde{G}_h[m,k] = \langle \widetilde{\psi}_k^0, \psi_m^1\rangle_\Gamma,$$
$$f_m^1 = \left\langle -\gamma_1^{\text{int}}\Phi_{\text{part}}, \psi_m^1 \right\rangle_\Gamma,$$

for $m, n, k = 1, \ldots, M$ and

$$\sigma_h^{DL} = \sum_{k=1}^M \sigma_k^{DL}\widetilde{\psi}_k^0.$$

L	N	$\frac{\lvert\widetilde{p}_L^{DL}-p\rvert}{p}$	eoc	Time	$\frac{\lvert p_L^{DL}-p\rvert}{p}$	eoc	Time	$\frac{\lvert p_L^{SP}-p\rvert}{p}$	eoc	Time
0	8	0.67		0	0.73		1	0.68		0
1	32	0.29	1.19	0	0.36	1.01	0	0.30	1.21	0
2	128	8.78e-2	1.74	0	0.14	1.40	1	8.84e-2	1.75	0
3	512	2.31e-2	1.93	1	5.05e-2	1.43	4	2.32e-2	1.93	6
4	2048	5.86e-3	1.98	6	2.03e-2	1.32	8	5.87e-3	1.98	75
5	8192	1.47e-3	1.99	39	8.85e-3	1.20	71	1.47e-3	2.00	196
6	32768	3.69e-4	1.99	215	4.10e-3	1.11	348	3.68e-4	2.00	1008
7	131072	9.21e-5	2.00	877	1.97e-3	1.06	1168	9.21e-5	2.00	3446

Table 5.16: Sphere with $\varepsilon_r = 5.0$, Comparison of double layer dipole moment errors for standard computation (4.7) and computation on the dual mesh (5.17)

The quadratic matrix $\widetilde{G}_h$ is invertible by [33] and therefore we are able to solve this linear system. Since σ_h^{DL} now has different basis functions we also have to change the calculation of the dipole moment (4.4) to

$$\widetilde{\mathbf{p}}^{DL} = \varepsilon_0 \int_\Gamma x\, \sigma_h^{DL}(x) ds_x = \varepsilon_0 \sum_{k=1}^{M} \int_{\tilde{\tau}_k} x\, \sigma_h^{DL}(x) ds_x = \varepsilon_0 \sum_{k=1}^{M} \sigma_k^{DL} |\tilde{\tau}_k| \tilde{x}_k^s, \tag{5.17}$$

where $\tilde{x}_k^s$ is the center of the k-th dual element. We compare the errors of the new results, where we denote the approximation of the dipole moment computed by (5.17) on the L-th level by $\widetilde{p}_L^{DL}$, to the previous errors, where we denote the approximation of the dipole moment computed by (4.7) on the L-th level by p_L^{DL}.

The comparison for the sphere can be found in Table 5.16. Additionally we have added the performance of the dipole moment calculated by the Steklov–Poincaré operator formulation, since we observed the lowest errors for the computation of the dipole moment for this formulation. The error of the dipole moment obtained by the original calculation (4.7) on the seventh level is comparable to the error of the adapted computation's (5.17) dipole moment on the fifth level, but the original computation took 1168 seconds for this task, whereas the new calculation only took 39 seconds. We conclude that the performance has increased drastically in comparison to the original calculation (4.7). Additionally the errors of the dipole moment computed by the double layer approach are now as small as the errors of the dipole moment computed by the Steklov–Poincaré operator formulation, but with much lower computational times. Also the convergence rate has increased to the expected quadratic convergence.

With this observations in mind it seems to be appropriate to use the dipole moment generated by the double layer formulation as reference solution for the following comparisons on the cube.

L	N	$\frac{\lvert\widetilde{p}_L^{DL}-\widetilde{p}_7^{DL}\rvert}{\widetilde{p}_7^{DL}}$	eoc	Time	$\frac{\lvert p_L^{DL}-\widetilde{p}_7^{DL}\rvert}{\widetilde{p}_7^{DL}}$	eoc	Time
0	24	6.73e-4		1	5.41e-2		2
1	96	9.37e-6	6.17	1	2.37e-2	1.19	1
2	384	8.46e-5	−3.17	8	9.47e-3	1.32	8
3	1536	3.67e-5	1.20	17	3.59e-3	1.40	13
4	6144	1.21e-5	1.60	21	1.26e-3	1.51	82
5	24576	3.40e-6	1.83	37	3.70e-4	1.76	166
6	98304	6.34e-7	2.42	145	5.54e-5	2.74	103
7	393216	0.00		440	3.87e-5	0.52	439

Table 5.17: Cube with $\varepsilon_r = 2.25$, Comparison of double layer dipole moment errors for standard computation (4.7) and computation on the dual mesh (5.17)

L	N	$\frac{\lvert\widetilde{p}_L^{DL}-\widetilde{p}_7^{DL}\rvert}{\widetilde{p}_7^{DL}}$	eoc	Time	$\frac{\lvert p_L^{DL}-\widetilde{p}_7^{DL}\rvert}{\widetilde{p}_7^{DL}}$	eoc	Time
0	24	2.44e-2		0	0.11		0
1	96	8.82e-3	1.47	2	2.82e-2	1.98	1
2	384	3.60e-3	1.29	8	3.65e-3	2.95	4
3	1536	1.40e-3	1.36	13	1.15e-2	−1.65	31
4	6144	5.37e-4	1.39	23	1.09e-2	0.07	40
5	24576	1.92e-4	1.48	45	8.41e-3	0.38	50
6	98304	5.46e-5	1.82	142	5.93e-3	0.50	150
7	393216	0.00		467	4.01e-3	0.57	510

Table 5.18: Cube with $\varepsilon_r = 50000$, Comparison of double layer dipole moment errors for standard computation (4.7) and computation on the dual mesh (5.17)

In Table 5.17 we compared the old and the new dipole moments for the cube with $\varepsilon_r = 2.25$. The error of the new dipole moment computed by (5.17) on the first level is already smaller than the error of the dipole moment computed by (4.7) on the finest level, but it is unusually small. The second level is what we would expect by an approximate convergence order of 1.5. The error of the new dipole moment on the third level is again smaller than the error of the old dipole moment on the finest level. Comparing computational times yields that the performance has increased. The observed order of convergence is approximately the same for both variants.

In Table 5.18 we compared the dipole moment for the cube with $\varepsilon_r = 50000$. In contrast to the standard computation of the dipole moment in Table 4.24 we are able to observe convergence. Furthermore the error on the second level is already smaller than every error of the dipole moment computed by (4.7), and again the difference in computational times is immense.

L	N	$\frac{\lvert\widetilde{p}_L^{DL-A}-\widetilde{p}_7^{DL-A}\rvert}{\widetilde{p}_7^{DL-A}}$	eoc	Time	$\frac{\lvert p_L^{DL-A}-\widetilde{p}_7^{DL-A}\rvert}{\widetilde{p}_7^{DL-A}}$	eoc	Time
0	24	6.77e-4		0	5.41e-2		0
1	144	1.84e-4	1.45	2	2.64e-2	0.80	1
2	480	1.23e-4	0.66	3	1.27e-2	1.22	7
3	2160	1.18e-5	3.12	7	3.96e-3	1.54	16
4	10464	4.01e-5	−1.55	23	9.40e-6	7.66	78
5	39504	1.13e-6	5.38	74	2.57e-4	−4.98	88
6	154416	1.06e-6	0.10	217	2.63e-4	−0.03	267
7	318912	0.00		407	3.86e-4	−1.06	470

Table 5.19: Cube with $\varepsilon_r = 2.25$, Comparison of double layer dipole moment errors for standard computation (4.7) and computation on the dual mesh (5.17)

L	N	$\frac{\lvert\widetilde{p}_L^{DL-A}-\widetilde{p}_7^{DL-A}\rvert}{\widetilde{p}_7^{DL-A}}$	eoc	Time	$\frac{\lvert p_L^{DL-A}-\widetilde{p}_7^{DL-A}\rvert}{\widetilde{p}_7^{DL-A}}$	eoc	Time
0	24	2.39e-2		0	0.11		0
1	144	9.89e-3	0.99	1	4.37e-2	1.04	1
2	960	1.44e-3	2.03	19	1.21e-2	1.36	6
3	3360	1.34e-4	3.79	38	1.56e-2	−0.42	20
4	18864	1.39e-4	−0.04	69	1.63e-2	−0.04	64
5	79920	6.95e-4	−2.23	218	1.34e-2	0.27	249
6	285888	0.00		809	8.19e-3	0.77	866

Table 5.20: Cube with $\varepsilon_r = 50000$, Comparison of double layer dipole moment errors for standard computation (4.7) and computation on the dual mesh (5.17)

We have also tested the new calculation of the dipole for the graded meshes of Section 5.3. The obtained errors for the cube with $\varepsilon_r = 2.25$ are given in Table 5.19. We observe that the errors are significantly lower on almost all levels. Both variants seem to have some outliers, but if we compare the error of the new calculation (5.17) on the third level to the lowest error of the standard computation (4.7), we observe an improvement from 78 seconds to only 7 seconds for the same accuracy. For both variants the convergence order, if there even is one, is hard to determine.

In Table 5.20 we compared the errors of the original calculation (4.7) and the new computation (5.17) for the cube with $\varepsilon_r = 50000$ and adaptive refinement. Again no convergence order seems to be appropriate for both computations. The difference in computational performance is huge, the error of the new calculation on the first level is comparable to the error of the old calculation on the finest level, where we observe computational times of only one second and 866 seconds, respectively.

6 Conclusions

In the first part of this thesis we reviewed important details of the previous work [1, 2, 19] to obtain necessary mathematical tools to further deepen our understanding of using boundary element methods for the electrostatic transmission problem.

We started on the continuous level, where we derived three boundary integral formulations: the single layer potential formulation (2.2), the Steklov–Poincaré interface equation (2.9), and the double layer potential formulation (2.24). With these boundary integral equations we were able to compute various quantities analytically, such as the potential of the electric field, densities for single layer and double layer formulations, and Neumann data. The equivalence of these three formulations, their unique solvability, as well as the standard evaluation of the electric field and the evaluation in the special case of a simply connected domain were discussed. We stated related Galerkin variational formulations and the corresponding linear systems (3.1), (3.9), and (3.16). We also showed how to compute approximations of several physical quantities on the discrete level.

As important extension of [1] we were able to perform an error analysis for the Steklov–Poincaré interface equation in Section 3.2.1, which provides us with theoretical orders of convergence for the errors of the numerical approximations of the potential and the Neumann data in weaker norms. We also found that, additionally to the continuous formulation, the discrete Steklov–Poincaré operator formulation is uniquely solvable.

We tested the proposed methods for three test cases relevant in the study on plasmon resonances of metallic nanoparticles, see, e.g., [7, 13, 37]. We started in Section 4.2 with the unit sphere and a relative permittivity of $\varepsilon_r = 5.00$. In comparison to [2] we increased the number of considered quantities for the numerical computations to obtain a better insight, how this quantities are connected and to understand the underlying theoretical behaviors to a greater degree. From the experiments we learned, that it depends on the considered quantity, which formulation one should prefer. For the computation of the potential the Steklov–Poincaré formulation yields the smallest error. It also performs better than the single layer and the double layer approach, when computing the electric field. If someone is interested in the dipole moment or scattering cross section the single layer potential formulation should be chosen for the numerical computation.

For the cube with a relative permittivity of $\varepsilon_r = 2.25$ we found that, compared to the sphere, the convergence orders were lower and the errors higher, which was to be expected. We observed that the electric field given by the single layer potential was

worse than the electric field obtained with the standard calculation, if it was computed by the modified version (3.3) for simply connected domains. After a detailed investigation we found that the approximation of the particular solution yields an additional error. Therefore it is in general recommendable to make sure if the modified version provides the better results. When considering the cube, not the Steklov–Poincaré formulation, but the double layer formulation is most advisable for computing the potential and the electric field. For a high relative permittivity of $\varepsilon_r = 50000$ we observed lower convergence rates and higher errors for all three approaches compared to the sphere and the cube with lower permittivity. The double layer approach turned out to be the most stable formulation for the electric field. The approximation of the electric field for high relative permittivity by the single layer potential seems to be inappropriate for physical applications. We also found that the modified version for simply connected domains indeed increases the computational performance of all three formulations, which was to be expected by the higher relative permittivity.

Finally, we tested several approaches to improve the numerical performance of the considered formulations in Chapter 5. We evaluated alternative discretization variants, including the popular collocation method. This method turned out not to be competitive to the Galerkin method with respect to postprocessing quantities like the dipole moment. Alternative ansatz functions with Dirac like point sources were tested, but the results showed that this approach was also inferior to the standard computation. On the other hand we achieved very good results by using graded meshes. Such meshes, adaptively refined towards corners and edges, help to realize higher orders of convergence for non-smooth solutions. At last, we suggested an alternative evaluation of the dipole moment for the double layer formulation, as the standard evaluation provided linear convergence only. The proposed projection of the surface charge density to piecewise constants on the dual mesh yields quadratic convergence and very accurate approximations of the dipole moment and therefore it should be used customarily for the computation of the dipole moment with the double layer formulation.

Bibliography

[1] Z. Andjelic, G. Of, O. Steinbach, and P. Urthaler. Boundary element methods for magnetostatic field problems: a critical view. *Comput. Vis. Sci.*, 14(3):117–130, 2011.

[2] Z. Andjelic, G. Of, O. Steinbach, and P. Urthaler. Fast boundary element methods for industrial applications in magnetostatics. In *Fast boundary element methods in engineering and industrial applications*, volume 63 of *Lect. Notes Appl. Comput. Mech.*, pages 111–143. Springer, Heidelberg, 2012.

[3] P. G. Ciarlet. *The finite element method for elliptic problems*. North-Holland Publishing Co., Amsterdam-New York-Oxford, 1978. Studies in Mathematics and its Applications, Vol. 4.

[4] M. Costabel. Boundary integral operators on Lipschitz domains: elementary results. *SIAM J. Math. Anal.*, 19(3):613–626, 1988.

[5] M. Costabel and E. Stephan. Boundary integral equations for mixed boundary value problems in polygonal domains and Galerkin approximation. In *Mathematical models and methods in mechanics*, volume 15 of *Banach Center Publ.*, pages 175–251. PWN, Warsaw, 1985.

[6] J.-L. Coulomb. Finite elements three dimensional magnetic field computation. *IEEE Trans. Magn.*, 17(6):3241–3246, 1981.

[7] F.J. García de Abajo and A. Howie. Retarded field calculation of electron energy loss in inhomogeneous dielectrics. *Phys. Rev. B*, 65(115418):1–17, 2002.

[8] L. Demkowicz, J. Kurtz, D. Pardo, M. Paszyński, W. Rachowicz, and A. Zdunek. *Computing with hp-adaptive finite elements. Vol. 2.* Chapman & Hall/CRC Applied Mathematics and Nonlinear Science Series. Chapman & Hall/CRC, Boca Raton, FL, 2008.

[9] Of G. and Steinbach O. Notes for alternative ansatz functions. Personal communication, 2019.

[10] Of G. and Steinbach O. Notes for the $L^2(\Gamma)$-error of the Steklov–Poincaré potential. Personal communication, 2019.

[11] L. Greengard and V. Rokhlin. A fast algorithm for particle simulations. *J. Comput. Phys.*, 73(2):325–348, 1987.

[12] J. Gwinner and E. P. Stephan. *Advanced boundary element methods*, volume 52 of *Springer Series in Computational Mathematics*. Springer, Cham, 2018.

[13] U. Hohenester and J. Krenn. Surface plasmon resonances of single and coupled metallic nanoparticles: A boundary integral method approach. *Phys. Rev. B*, 72:195429, 2005.

[14] G. C. Hsiao and W. L. Wendland. The Aubin-Nitsche lemma for integral equations. *J. Integral Equations*, 3(4):299–315, 1981.

[15] K. Ishibashi and Z. Andjelic. Nonlinear magnetostatic BEM formulation using one unknown double layer charge. *COMPEL*, 30(6):1870–1884, 2011.

[16] J. D. Jackson. *Classical electrodynamics*. John Wiley & Sons, Inc., New York-London-Sydney, second edition, 1975.

[17] B. Khoromskij and J. M. Melenk. Boundary concentrated finite element methods. *SIAM J. Numerical Analysis*, 41:1–36, 2003.

[18] B. Krstajic, Z. Andelic, S. Milojkovic, S. Babic, and S. Salon. Nonlinear 3d magnetostatic field calculation by the integral equation method with surface and volume magnetic charges. *IEEE Transactions on Magnetics*, 28(2):1088–1091, 1992.

[19] D. Lang. Boundary Element Methods for the Electrostatic Transmission Problem. Project Technomathematics, Institut für Angewandte Mathematik, Technische Universität Graz, WS 2017/18.

[20] D. Lindholm. Notes on boundary integral equations for three-dimensional magnetostatics. *IEEE Transactions on Magnetics*, 16(6):1409–1413, 1980.

[21] L. V. Lorenz. On the identity of the vibrations of light with electrical currents. *Phil. Mag.*, 34:287–301, 1867.

[22] D. Lukáš, G. Of, J. Zapletal, and J. Bouchala. A boundary element method for homogenization of periodic structures. *Math. Models Methods Appl. Sci.*, 2019. accepted.

[23] J.-C. Nédélec. Curved finite element methods for the solution of singular integral equations on surfaces in $\mathbb{R}^3$. *Comput. Methods Appl. Mech. and Engrg.*, 8(1):61–80, 1976.

[24] J.-C. Nédélec. Numerical approximations for some singular integral equations. In *The use of finite element method and finite difference method in geophysics (Proc. Summer School, Liblice, 1977)*, pages 207–227. Česk. Akad. Věd, Prague, 1978.

[25] G. Of. Notes for scattering cross section. Personal communication, 2019.

[26] G. Of. Advanced boundary elements method. Institut für Numerische Mathematik, Technische Universität Graz, WS 2015/16.

[27] G. Of, O. Steinbach, and W. L. Wendland. The fast multipole method for the symmetric boundary integral formulation. *IMA J. Numer. Anal.*, 26(2):272–296, 2006.

[28] C. Pechstein. *Finite and Boundary Element Tearing and Interconnecting Solvers for Multiscale Problems*. Lecture Notes in Computational Science and Engineering. Springer Berlin Heidelberg, 2012.

[29] J.T. Pfefferer. Numerical analysis for elliptic Neumann boundary control problems on polygonal domains. Dissertation, Fakultät für Bauingenieurwesen und Umweltwissenschaften der Universität der Bundeswehr München, 2014.

[30] J.T. Pfefferer and M. Winkler. Finite element error estimates for normal derivatives on boundary concentrated meshes. *arXiv 1804.05723*, 2018.

[31] R. Russell and L. Shampine. A collocation method for boundary value problems. *Numer. Math.*, 19:1–28, 1972.

[32] S. A. Sauter and C. Schwab. *Boundary element methods*, volume 39 of *Springer Series in Computational Mathematics*. Springer-Verlag, Berlin, 2011.

[33] O. Steinbach. *Stability estimates for hybrid coupled domain decomposition methods*, volume 1809 of *Lecture Notes in Mathematics*. Springer-Verlag, Berlin, 2003.

[34] O. Steinbach. *Numerical Approximation Methods for Elliptic Boundary Value Problems. Finite and Boundary Elements*. Springer, New York, 2008.

[35] O. Steinbach and W. L. Wendland. On C. Neumann's method for second-order elliptic systems in domains with non-smooth boundaries. *J. Math. Anal. Appl.*, 262(2):733–748, 2001.

[36] G. Strang and G. J. Fix. *An analysis of the finite element method*. Prentice-Hall, Inc., Englewood Cliffs, N. J., 1973.

[37] A. Trügler. Optical properties of metallic nanoparticles. Dissertation, Institut für Physik, Fachbereich Theoretische Phik, Karl–Franzens–Universität Graz, 2011.

[38] Wikipedia. Electric dipole moment — wikipedia, the free encyclopedia. `https://en.wikipedia.org/wiki/Electric_dipole_moment`, 2019. [Online; accessed 07-August-2019].

Affidavit

I declare that I have authored this thesis independently, that I have not used other than the declared sources/resources, and that I have explicitely indicated all material which has been quoted either literally or by content from the sources used. The text document uploaded to TUGRAZonline is identical to the present master‘s thesis.

Date	Signature